UNIVERSITY OF TECHNOLOGY SYDNEY
FACULTY OF ENGINEERING AND IT
SCHOOL OF ELECTRICAL AND DATA ENGINEERING

AN IMPROVED FINITE CONTROL SET MODEL PREDICTIVE CONTROL FOR POWER CONVERTERS IN DISTRIBUTED GENERATIONS/MICROGRIDS

A thesis submitted to the University of Technology Sydney for the Degree of Doctor of Philosophy

By Mahlagha MAHDAVI AGHDAM

03 February 2019

Title of Thesis:

An Improved Finite Control Set Model Predictive Control for Power Converters in Distributed Generations/Microgrids

PhD Candidate:

Mahlagha MAHDAVI AGHDAM

Mahlagha.MAHDAVIAGHDAM@uts.edu.au

Faculty of Engineering and IT, University of Technology Sydney, Australia

Principal Supervisor:

Associate Professor Li Li

Li.Li@uts.edu.au

Faculty of Engineering and IT, University of Technology Sydney, Australia

Co-Supervisors:

Dr. Ricardo Aguilera Echeverria

Ricardo.Aguilera@uts.edu.au

Faculty of Engineering and IT, University of Technology Sydney, Australia

Professor Jianguo Zhu

Jianguo.Zhu@syd.edu.au

Faculty of Engineering and IT, The University of Sydney, Australia

Certificate of original authorship

I, Mahlagha MAHDAVI AGHDAM declare that this thesis, is submitted in fulfillment of the requirements for the award of Doctor of Philosophy in Electrical Engineering, in the Faculty of Engineering and Information Technology at the University of Technology Sydney.

This thesis is wholly my own work unless otherwise reference or acknowledged. In addition, I certify that all information sources and literature used are indicated in the thesis.

This document has not been submitted for qualifications at any other academic institution.

This research is supported by the Australian Government Research Training Program.

Production Note:

SIGNATURE: Signature removed prior to publication.

MAHLAGHA MAHDAVI AGHDAM

03 FEBRUARY 2019

ACKNOWLEDGMENT

I am grateful to all of those with whom I have had the pleasure to work during my PhD at University of Technology Sydney (UTS). Each has provided me extensive personal and professional guidance and taught me a great deal about both scientific research and life in general. I would especially like to express sincere gratitude and appreciation to my supervisor Associate Professor Li Li, for his invaluable guidance, motivation, inspiring discussions, and consistent encouragement throughout the entire research. I am also thankful to Professor Jianguo Zhu for his inspiring discussions, and advice. Dr. Ricardo Aguilera Echeverria has been a constant source of insightful thoughts, inspiration, and guidance. I have benefited greatly from his timely advice, continuous encouragement, and generous support especially with the experimental test. I am also grateful to the support and guidance from Dr. Ha Pham and engineers Russell Nicholson and Jiang Chen.

I acknowledge the financial support provided by the Australian Government Research Training Program Scholarship.

Most importantly, I would like to thank my family: my parents and my brothers, whose love, inspiration and guidance are with me in whatever I pursue.

Last but not the least, I would like to thank all my other friends in the School of Electrical and Data Engineering for their kind support and care during my study. I am also grateful to my close friends who reminded me that there is a life beyond the lab and supported me along the way.

DEDICATION

To my FATHER.

For believing in me no matter what,
and for making me believe in myself.

RIP

Contents

List of Figures

List of Tables

List of Acronyms

ADC Analog to Digital Conversion

APF Active Power Filter

CHB Cascade H-bridge

CCS-MPC Continuous set based Model Predictive Control

DMC Direct Matrix Converter

DG Distributed Generation

DPC Direct Power Control

DTC Direct Torque Control

DSP Digital Signal Processor

ESS Energy Storage System

EV Electric Vehicle

FC Flying-capacitor

FCS-MPC Finite set based Model Predictive Control

FLC Fuzzy Logic Controller

FPGA Field Programming Gate Array

HVDC High Voltage DC

ILS Integer Least Square

MF Membership Function

MI Mutual Interference

MIPS Million Instructions per Second

MPC Model Predictive Control

NPC Neutral Point Clamped

PMSM Permanent Magnet Synchronous Motor

PV Photovoltaic

PWM Pulse Width Modulation

rL-sPh r-Level s-Phase

RTI Real-time Implementation

SAPF Shunt Active Power Filter

SHE Selective Harmonic Elimination

SSE Steady State Error

STATCOM Static Synchronous Compensator

THD Total Harmonic Distortion

UPS Uninterruptable power supply

VSI Voltage Source Inverter

VSR Voltage Source Rectifier

Abstract

This thesis focuses on finite control set model predictive control (FCS-MPC) of power converters in distributed generation (DG) and microgrids. In any network with an adequately high number of DG units, a hierarchy of control is one of the approaches to coordinate the system. Developments in the control of microgrids increase their potential to interact more efficiently with the main grid. Hierarchical control of the microgrid includes four levels: the component (zero) level, primary, secondary, and tertiary controls.

The FCS-MPC uses an internal model of the plant to predict the future progress of the controlled variables over the next prediction interval. An objective function is minimized via an exhaustive search to acquire the optimal control input sequence. While FCS-MPC carries some benefits, the algorithm needs to be reformed for various applications, mostly due to the variety of the plant characteristics that cause some challenges for the design.

The thesis is divided into two parts: The first part is devoted to theory and algorithms of FCS-MPC for power converters in DGs at the component (zero) level of the grid-connected microgrid, whereas the second part tackles power sharing, at the primary control level of microgrid, among DGs in the grid-connected microgrid.

The first part, Chapters 3, 4, and 5, investigate the main concerns of FCS-MPC algorithm with respect to implementation in terms of delay time compensation, computational burden in longer horizon, and weighting factor design. A time-delayed model with an advanced and flexible control algorithm is developed. As a result, the system is reliable in terms of applying the optimal sequence at the right interval. In order to decrease the computational burden and consequently prediction horizon, a simplified MPC can be utilized. To achieve robustness of the MPC technique under different operating conditions, a self-tuning MPC for power flowcontrol and power quality improvement in grid-connected power converters is proposed.

The second part of this thesis, Chapter 6, employs MPC scheme for the power sharing problem of parallel DGs in a grid-connected microgrid, to attain autonomous power sharing and power quality improvement. Generally, the droop control is used as the conventional control method of parallel inverters for regulating active power and reactive power in microgrids. The proposed scheme is modeled mathematically and simulated via MATLAB SIMULINK for two case studies. Case 1 consists of two parallel 2L-3Ph VSIs, whereas in case 2, a 2L-3Ph VSI and a 3L-3Ph neutral point clamped VSI are paralleled. The MPC algorithm shows a better performance than the droop control in terms of power sharing between two parallel grid-connected inverters. The measurements show that although the active and reactive power ripples are not compensated much by the MPC approach, the rise time and settling time are reduced considerably. As a result, the MPC scheme provides a better transient dynamics than the droop control scheme.

Chapter 1

INTRODUCTION

1.1 Motivation

In the last decade, microgrids have brought significant advantages for power system operators and consumers. The benefits of microgrid deployments are classified as economic, environmental, and technical points of view [1–4]. The microgrids are able to operate in the islanded and grid-connected mode, and therefore the implementation of a microgrid in the conventional electric power system will improve the overall resilience, reliability, and sustainability of the power system [5, 6].

Regardless of the type, a microgrid increases the complexity of the power system, which brings many challenges in generating, storing, controlling, and managing the energy. Therefore, for the effective integration, a hierarchical control structure for microgrids is employed to implement a coordinated interaction with management and controller units of the main grid. Hierarchical control of the microgrid includes four levels: the component (zero) level, primary, secondary, and tertiary controls, as shown in Fig. 1.1. The speed of response, operating time frame, and infrastructure requirements of these levels are varied [7, 8].

Advances in power switches alongside with digital control platforms have conveyed a rapid development in control of power converters. Power converters are one of the main components of microgrids utilized in distributed generations (DGs), electric vehicles, uninterruptible power supplies, energy storage systems, and electrical drives. The increasing numbers of such applications at the consumer side impose new challenges for setup, control, operation, management, and supervision of the microgrids and the main power grid [9–11].

Control approaches applied in power converters have been the research focus for decades. A power converter in the microgrid is broadly categorized into grid-forming, grid-feeding, and grid supporting converters. The controller in grid-forming power converters is responsible for setting the voltage amplitude and the frequency of the islanded microgrid. Therefore, this converter acts as the reference machine for the rest of the other power converters within the islanded microgrid. The controller in grid-feeding and gird-supporting power converters is aimed to meet the active and reactive power demand and improve the voltage profile of the microgrid in both operation modes, respectively [12].

In a three-phase system, power converters can be controlled in natural (ABC), stationary ($\alpha\beta$), or synchronous (dq) reference frame. Employment of the control algorithm in dq-frame is widely applied in different applications of three-phase sys-

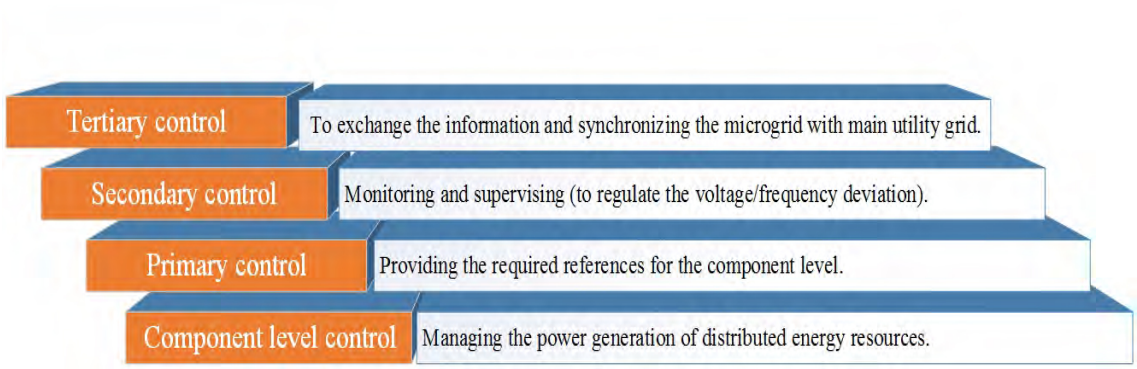

Figure 1.1: Hierarchical control of microgrids

tems. Although these scheme brings certain advantages like use of the simple the proportional integral (PI) controller, two stage coordinate transformations, decoupling network, and regulation efforts are essential to assure the stability and efficiency [13]. Yet, under unbalanced circumstances, PI controller is incapable to adjust the appeared fluctuations in current [14]. On the other hand, with the progress of faster, more accurate, and more powerful microprocessors, utilizing digital control platforms has revealed a new horizon for more flexible, consistent and effective approaches [15].

Over the years, model predictive control (MPC) has gained much attention among researchers as an alternative modern control for power converters in power system applications [16–20]. In spite of time-consuming calculation, the power electronics industries are able to employ it via digital control platform in practice. MPC is a well-established method and its concepts, operating principles [21], and technology readiness for real-time implementation [22] are well studied.

In particular, finite control set MPC (FCS-MPC) has been verified to be a very effective substitute for traditional control algorithms for power converters which are controlled with pulse width modulation (PWM) techniques [23, 24]. As power electronics applications are commonly controlled by using digital platforms, the system model is fitted in the state space form of the discrete-time domain. The FCS-MPC has been an intuitive and potent digital approach to controlling power converters where no modulation stage, decoupling network, separate sequence control, complex synchronization unit are employed to achieve the stable, reliable, and efficient system.

1.2 Statement of Problem and Objectives

In spite of the vast progress of MPC for power electronic applications that has occurred over the last decade, there are still some issues that establish an open area for research. Amongst them, steady state performance, power ripple reduction of the MPC technique under different operating conditions, and effective real time implementation (RTI) are some of the important areas that need extra investigation.

Although there are some developing works in terms of compensation for time delay and optimal weighting factor selections, there is not, as of yet, any mathematical way of demonstrating the time-delay of predictive control and selecting optimally the weighting factors. The main objectives of this research project can be described

as follows:

- As the delay for RTI is varied, advanced and flexible control algorithms with a time delayed model are developed. Based on this model, the system performance will be improved with enhanced system stability and reliability.

- To facilitate the RTI of MPC-based algorithms, strategies need to be employed that effectively balance the trade-off between the length of the prediction horizon and the required computation burden.

- To achieve robustness of the MPC technique under different operating conditions, a self-tuning MPC for power flow control and power quality improvement in grid-connected power converters is developed.

- Lastly, an MPC scheme is employed for the power sharing problem of parallel DGs in a microgrid, to attain autonomous power sharing and power quality improvement.

1.3 Chapter Outline

The thesis is organized as follows.

In Chapter 1, the background and motivation of this thesis are introduced followed by defining the main aims and objectives of the thesis.

In Chapter 2, a comprehensive literature review on MPC for power converters and drivers in DGs is provided. DG is a generation unit that generates power at the distribution level of power systems and the main component of a small-scale grid, so-called microgrids. It is essential to have a brief review on the microgrid concepts to form a solid background for this work. Hence, the microgrid structure and its control strategies are discussed, and then the advances and trends of MPC for power converters, which is the main focus of this thesis, are given.

In Chapter 3, a notable drawback of the conventional FCS-MPC is explored. While FCS-MPC carries some benefits [23, 24], the algorithm needs to be reformed for various purposes, mostly due to the variety of the plant characteristics that cause some challenges for the design. In FCS-MPC, the main problem associated with RTI via the digital signal processor (DSP) is the computational burden which leads to a significant delay time [25, 26].

As a result, the system performance will be impaired if the delay time is not reflected in the system model. This issue will be more evident for a longer horizon prediction or multilevel converters where the number of switching possibilities is increased considerably [27–29]. Therefore, FCS-MPC will face a computational challenge and impracticality for RTI and lead to the overrun. An overrun state happens if a task is demanded to start, but its previous execution has not completed yet. A time-delayed FCS-MPC is presented in this chapter where a delay is considered in the input of the system model. Two case studies are considered and the approach shows a better transient and steady state performance while reducing the power ripples significantly in both cases. The proposed method compensates the delay time resulting from DSPs' computation and implementation of the control signal. The delay time in this work is estimated through trial and error [30].

MPC method is effective for power converter control in distributed power generations but requires a large amount of computation, leading to a considerable time delay in the actuation. If the delay is not reflected, the system performance could get worse. Chapter 4 presents a two-step (horizon) prediction algorithm of MPC technique for grid-tied inverters used in distributed generation systems. The control objectives such as active and reactive power tracking, balancing the neutral point and switching loss reduction are reflected in the objective function of the controller. The proposed MPC strategy is verified numerically by using MATLAB/Simulink and implemented in the laboratory experiment [31].

Chapter 5 presents a self-tuning MPC for power flow control and power quality improvement in grid-connected power converters. A multi-objective optimization problem can be formulated to take into account different requirements and constraints with corresponding weighting factors. Therefore, all the control necessities will be observed by the controller simultaneously. Nevertheless, the weighting factor adjustment is generally addressed by heuristic approaches for which there is not a detailed analytical study [32]. FCS-MPC combined with a fuzzy logic control (FLC) approach with several objectives for grid-connected power converters is explored. This method uses an FLC scheme to regulate the fitting value of weighting factors online subject to the specific dynamic conditions, leading to improved power system performance [33].

Chapter 6 focuses on a predictive power flow control in parallel inverters in microgrids, which can improve the transient of the power flow in microgrids [34]. The microgrid under this case study operates in the grid-tied mode with appropriate power sharing capability among parallel DGs and the main grid [35].

In Chapter 7, the conclusions of the thesis are drawn accompanied by the future work proposal.

Bibliography

[1] S. Parhizi, H. Lotfi, A. Khodaei, and S. Bahramirad, "State of the art in research on microgrids: A review," *IEEE Access*, vol. 3, pp. 890–925, 2015.

[2] I. Patrao, E. Figueres, G. Garcerá, and R. González-Medina, "Microgrid architectures for low voltage distributed generation," *Renewable and Sustainable Energy Reviews*, vol. 43, pp. 415–424, 2015.

[3] E. Unamuno and J. A. Barrena, "Hybrid ac/dc microgrids—part i: Review and classification of topologies," *Renewable and Sustainable Energy Reviews*, vol. 52, pp. 1251–1259, 2015.

[4] ——, "Hybrid ac/dc microgrids—part ii: Review and classification of control strategies," *Renewable and Sustainable Energy Reviews*, vol. 52, pp. 1123–1134, 2015.

[5] T. L. Vandoorn, B. Meersman, J. D. De Kooning, and L. Vandevelde, "Analogy between conventional grid control and islanded microgrid control based on a global dc-link voltage droop," *IEEE transactions on power delivery*, vol. 27, no. 3, pp. 1405–1414, 2012.

[6] Y. A.-R. I. Mohamed and A. A. Radwan, "Hierarchical control system for robust microgrid operation and seamless mode transfer in active distribution systems," *IEEE Transactions on Smart Grid*, vol. 2, no. 2, pp. 352–362, 2011.

[7] D. E. Olivares, A. Mehrizi-Sani, A. H. Etemadi, C. A. Cañizares, R. Iravani, M. Kazerani, A. H. Hajimiragha, O. Gomis-Bellmunt, M. Saeedifard, R. Palma-Behnke *et al.*, "Trends in microgrid control," *IEEE Transactions on smart grid*, vol. 5, no. 4, pp. 1905–1919, 2014.

[8] M. Yazdanian and A. Mehrizi-Sani, "Distributed control techniques in microgrids," *IEEE Transactions on Smart Grid*, vol. 5, no. 6, pp. 2901–2909, 2014.

[9] A. M. Bouzid, J. M. Guerrero, A. Cheriti, M. Bouhamida, P. Sicard, and M. Benghanem, "A survey on control of electric power distributed generation systems for microgrid applications," *Renewable and Sustainable Energy Reviews*, vol. 44, pp. 751–766, 2015.

[10] J. M. Guerrero, M. Chandorkar, T.-L. Lee, and P. C. Loh, "Advanced control architectures for intelligent microgrids, part i: decentralized and hierarchical control," *IEEE Transactions on Industrial Electronics*, vol. 60, no. 4, pp. 1254–1262, 2013.

[11] Y. Yoldaş, A. Önen, S. Muyeen, A. V. Vasilakos, and İ. Alan, "Enhancing smart grid with microgrids: Challenges and opportunities," *Renewable and Sustainable Energy Reviews*, vol. 72, pp. 205–214, 2017.

[12] J. Rocabert, A. Luna, F. Blaabjerg, and P. Rodriguez, "Control of power converters in ac microgrids," *Power Electronics, IEEE Transactions on*, vol. 27, no. 11, pp. 4734–4749, 2012.

[13] S. Vazquez, A. Marquez, R. Aguilera, D. Quevedo, J. I. Leon, and L. G. Franquelo, "Predictive optimal switching sequence direct power control for grid-connected power converters," *IEEE Transactions on Industrial Electronics*, vol. 62, no. 4, pp. 2010–2020, 2015.

[14] E. Afshari, G. R. Moradi, R. Rahimi, B. Farhangi, Y. Yang, F. Blaabjerg, and S. Farhangi, "Control strategy for three-phase grid-connected pv inverters enabling current limitation under unbalanced faults," *IEEE Transactions on Industrial Electronics*, vol. 64, no. 11, pp. 8908–8918, 2017.

[15] C. Buccella, C. Cecati, and H. Latafat, "Digital control of power converters—a survey," *IEEE Transactions on Industrial Informatics*, vol. 8, no. 3, pp. 437–447, 2012.

[16] C. Bordons and C. Montero, "Basic principles of mpc for power converters: Bridging the gap between theory and practice," *IEEE Industrial Electronics Magazine*, vol. 9, no. 3, pp. 31–43, 2015.

[17] N. Panten, N. Hoffmann, and F. W. Fuchs, "Finite control set model predictive current control for grid-connected voltage-source converters with lcl filters: A study based on different state feedbacks," *IEEE Transactions on Power Electronics*, vol. 31, no. 7, pp. 5189–5200, 2016.

[18] M. Rivera, J. Rodriguez, and S. Vazquez, "Predictive control in power converters and electrical drives—part ii [guest editorial]," *IEEE Transactions on Industrial Electronics*, vol. 63, no. 7, pp. 4472–4474, 2016.

[19] J. Rodriguez, M. P. Kazmierkowski, J. R. Espinoza, P. Zanchetta, H. Abu-Rub, H. A. Young, and C. A. Rojas, "State of the art of finite control set model predictive control in power electronics," *IEEE Transactions on Industrial Informatics*, vol. 9, no. 2, pp. 1003–1016, 2013.

[20] S. Vazquez, J. I. Leon, L. G. Franquelo, J. Rodriguez, H. A. Young, A. Marquez, and P. Zanchetta, "Model predictive control: A review of its applications in power electronics," *IEEE Industrial Electronics Magazine*, vol. 8, no. 1, pp. 16–31, 2014.

[21] L. Wang, *Model predictive control system design and implementation using MATLAB®*. Springer Science & Business Media, 2009.

[22] G. A. Papafotiou, G. D. Demetriades, and V. G. Agelidis, "Technology readiness assessment of model predictive control in medium-and high-voltage power electronics," *IEEE Transactions on Industrial Electronics*, vol. 63, no. 9, pp. 5807–5815, 2016.

[23] T. Geyer, "A comparison of control and modulation schemes for medium-voltage drives: Emerging predictive control concepts versus pwm-based schemes," *IEEE Transactions on Industry Applications*, vol. 47, no. 3, pp. 1380–1389, 2011.

[24] J. Holtz, "Advanced pwm and predictive control—an overview," *IEEE Transactions on Industrial Electronics*, vol. 63, no. 6, pp. 3837–3844, 2016.

[25] T. Jin, X. Shen, T. Su, and R. C. Flesch, "Model predictive voltage control based on finite control set with computation time delay compensation for pv systems," *IEEE Transactions on Energy Conversion*, 2018.

[26] P. Karamanakos, T. Geyer, and R. Kennel, "A computationally efficient model predictive control strategy for linear systems with integer inputs," *IEEE Transactions on Control Systems Technology*, vol. 24, no. 4, pp. 1463–1471, 2016.

[27] P. Liu, Y. Wang, W. Cong, and W. Lei, "Grouping-sorting-optimized model predictive control for modular multilevel converter with reduced computational load," *IEEE Transactions on Power Electronics*, vol. 31, no. 3, pp. 1896–1907, 2016.

[28] P. Karamanakos, T. Geyer, and R. P. Aguilera, "Computationally efficient long-horizon direct model predictive control for transient operation," in *Energy Conversion Congress and Exposition (ECCE), 2017 IEEE.* IEEE, 2017, pp. 4642–4649.

[29] Z. Zhang, H. Fang, and R. Kennel, "Novel ripple reduced direct model predictive control of three-level npc active front end with reduced computational effort," in *Predictive Control of Electrical Drives and Power Electronics (PRECEDE), 2015 IEEE International Symposium on.* IEEE, 2015, pp. 32–37.

[30] M. M. Aghdam, L. Li, J. Zhu, T. He, and J. Zhang, "Time-delayed model predictive direct power control for vehicle to grid and grid to vehicle applications," in *Industrial Electronics Society, IECON 2017-43rd Annual Conference of the IEEE.* IEEE, 2017, pp. 4662–4667.

[31] M. M. Aghdam, L. Li, and J. Zhu, "A model predictive power control method with longer prediction horizon for distributed power generations," in *Control, Automation, Robotics and Vision (ICARCV), 2016 14th International Conference on.* IEEE, 2016, pp. 1–6.

[32] P. Cortés, S. Kouro, B. L. Rocca, R. Vargas, J. Rodríguez, J. I. León Galván, S. Vázquez Pérez, and L. García Franquelo, "Guidelines for weighting factors design in model predictive control of power converters and drives," in *International Conference On Industrial Technology (ICIT), 1-7. Gippsland, Australia: IEEE.* IEEE, 2009.

[33] M. M. Aghdam, R. P. Aguilera, L. Li, and J. Zhu, "Fuzzy-based self-tuning model predictive direct power control of grid-connected multilevel converters," in *Electrical Machines and Systems (ICEMS), 2017 20th International Conference on.* IEEE, 2017, pp. 1–6.

[34] C. H. Young and A. Bastias, "Finite-control-set predictive voltage control of paralleled inverters in an islanded microgrid," in *2018 IEEE 27th International Symposium on Industrial Electronics (ISIE).* IEEE, 2018, pp. 395–400.

[35] M. M. Aghdam, L. Li, and J. Zhu, "A model predictive control of parallel inverters for distributed generations in microgrids," in *Power System Technology (POWERCON), 2016 IEEE International Conference on.* IEEE, 2016, pp. 1–6.

Chapter 2

THE STATE OF THE ART

2.1 Introduction

In this chapter, a comprehensive literature review of the model predictive control for power converters and drivers in distributed generation (DG) is provided. DG is an approach that generates power at the distribution level of the power system and the main component of a small-scale grid, so-called microgrids. However, it is essential to have a brief review of the microgrid concepts to form a solid background for this work. Hence, the microgrid structure and its control strategies are discussed and then the advances and trends of model predictive control for power converters, which is the main focus of this thesis, are given.

2.2 Microgrid Structure

In recent years, conventional power system infrastructure changed mainly due to the inadequacy of fossil fuel in future, the fast growth of electricity consumption, the environmental impact of conventional power generations, and widespread penetration of distributed energy resources and micro sources. The integration of DGs has initiated a revolutionary concept of microgrid which is defined as a small-scale utility grid. The microgrid consists of DG, energy storage, power conversion, control, communication and load units that collaborate with each other to be served as a controllable load or generator. In a sense, the anticipated macrogrid will be more interactive, intelligent, and scattered [1–4].

In the last decade, microgrids have brought significant advantages for power system operators and consumers. The benefits of microgrid deployments are classified as economic, environmental, and technical points of view [5–8]. The microgrids are able to operate in the island, and grid-connected mode, therefore the implementation of a microgrid in the conventional electric power system will increase the overall resilience, reliability, and sustainability of the power system [9, 10].

Microgrids can be categorized into AC, DC and hybrid AC-DC. The AC microgrids are the most typical form of microgrids where all the components are tied into a common AC bus through power electronic interfaces. However, renewable based DGs mostly generate variable voltage/frequency AC or DC output power. As a result, hybrid AC-DC microgrids, with an AC and DC bus network as shown in Fig. 2.1. A hybrid microgrid reduces the power conversion levels and complexity

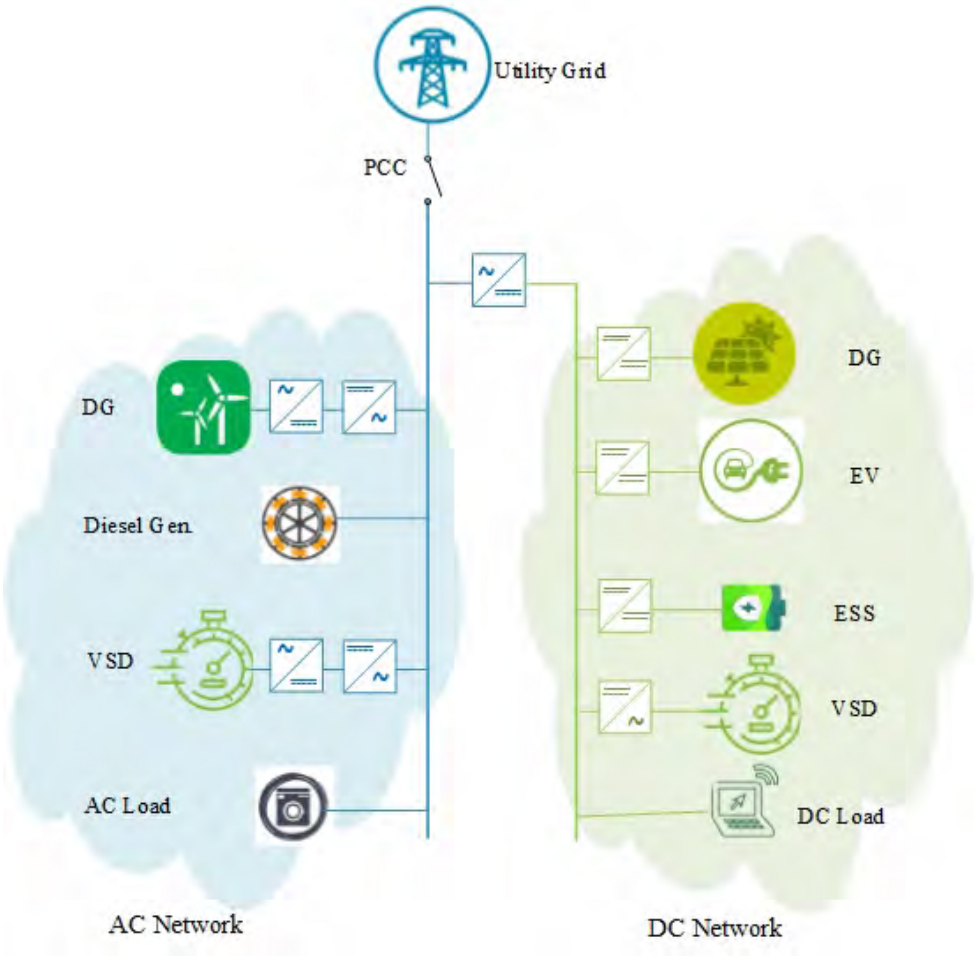

Figure 2.1: Hybrid AC-DC microgrid structure

significantly, as a result, it increases efficiency, flexibility, and controllability. Each type of microgrids has their distinctive features, which brings various benefits and limitations that need to be reflected in [2, 11–14].

Regardless of the type, a microgrid increases the complexity of the power systems, which brings many challenges to generate, store, control, and manage the energy. An operative microgrid is determined by an effective integration of DGs, which can be addressed with a number of issues like power quality, frequency and voltage stability, and black start operation. The power quality issues should be cautiously dealt with to achieve satisfactory values of voltage and frequency in grid-connected and islanded mode of a microgrid in steady state and dynamic state [1, 3]. Therefore, for the effective integration, a hierarchical control structure for microgrids is employed to implement a coordinated interaction with management and controller units of the main grid.

2.3 Hierarchical Control of Microgrids

In any network with an adequately high number of units, a hierarchy of control is one of the approaches to coordinate the system. Therefore, a hierarchical control strategy is essential for the resilient, reliable, and efficient operation of microgrid [15–18]. The requirements for a microgrid control based on variant implications and time

are followed as,

- Frequency/voltage coordination in standalone, transition, and grid-connected mode;
- Power flow control to attain proper load sharing and DG coordination;
- A seamless transition between two modes of operation in microgrid;
- Synchronization between the microgrid and the main grid;
- Optimizing the cost and the reliability.

Hierarchical control of the microgrid includes four levels; the component (zero) level, primary, secondary, and tertiary controls, as shown in Fig. 1.1. The speed of response, operating time frame, and infrastructure requirements of these levels are varied [19, 20].

The primary control provides the required set points for individual DGs based on their operation in microgrid. To improve the power reliability, this level has the fastest response to any variation in generation or demand. A comprehensive study of primary control of power converters in DGs are presented in [21] and [17] respectively.

The responsibility of the secondary control is to regulate the deviations in both voltage and frequency initiated by the performance of the primary controls. In comparison with the primary control, the secondary control has the slower dynamic response to changes [22]. Lastly, the tertiary control is the slowest and handles the power flow as depicted in Fig. 2.2. Indeed, it aims the optimal operation of the MG in terms of technical and economic parts [23].

Improvements in the control of microgrids are enhanced their potential to interact more with the conventional power systems, not only refining their constraints in the network but also featuring grid support functionalities to increase the total performance of the network.

2.4 Control of Power Converters

A power converter in the microgrid is broadly categorized into grid-forming, grid-feeding, and grid supporting converters. The controller in grid-forming power converters is responsible for setting the voltage amplitude and the frequency of the islanded microgrid. Therefore, this converter acts as the reference machine for the rest of the other power converters within the islanded microgrid. Hence, in this mode, the forming power converter acts as an ideal voltage source responsible for achieving stability. The controller in grid-feeding and gird-supporting power converters are aimed to meet the active and reactive power demand and offer ancillary services to the main grid, like regulating the voltage profile, respectively. The basic control structure of these power converters is reviewed in [24]. In grid-connected mode of the microgrid, the main grid sets the voltage magnitude and frequency of DGs. Indeed, most of the power converters in DGs operate as grid-feeding [25].

Control approaches applied in power converters have been the research focus for years [22, 24, 26, 27]. Advances in power switches alongside with digital control platforms conveyed a rapid development in control of power converters. The

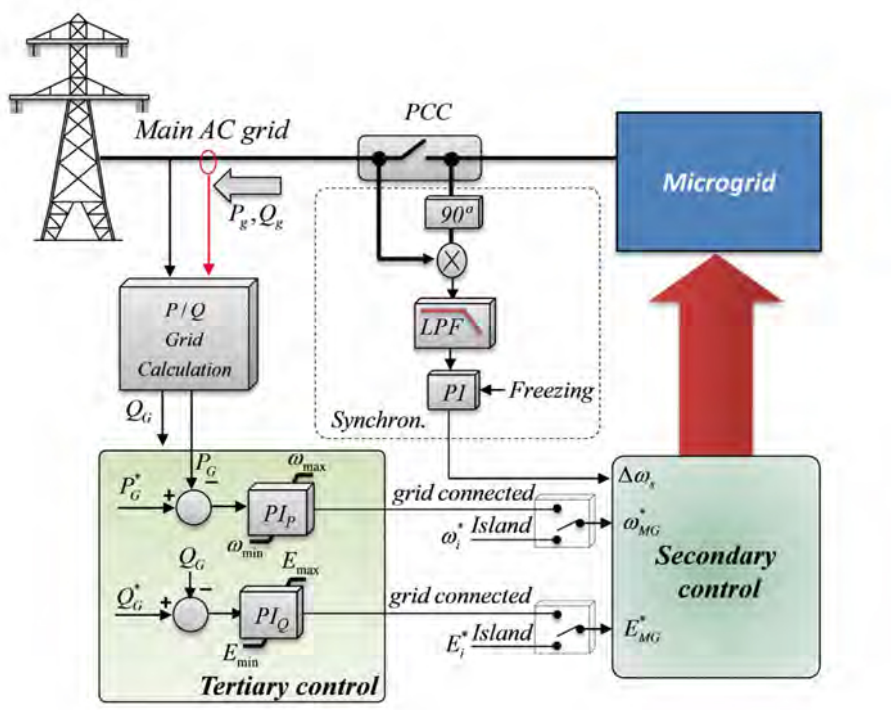

Figure 2.2: Hierarchical control of microgrids [23]

history of power electronics and control concepts applied to power converters is reviewed in [28]. Classical control approaches, including linear and non-linear, are employed and implemented on power converters at different voltage and power levels. Although these schemes bring certain advantages, coordinate transformations and regulation efforts are essential to assure the stability and efficiency [29].

2.4.1 Control strategies of power converters

In power converter control, the strategy defines the control variables. The grid-forming converters can be signified as an AC voltage source with low output impedance, setting the nominal voltage amplitude and reference frequency of the local microgrid by using voltage and current control strategies. Classical control strategies for grid-tied converters adjust both the active and reactive power flow by controlling the current vector orientation with respect to the grid voltage vector. This technique is known as voltage oriented control (VOC).

However, there are more direct strategies to control grid-tied converters. Direct power control (DPC) has become one of the most popular control strategies in power converters not only because of its superb state steady and transient performance, but also its robustness and simplicity. One of the main functions of the DPC is that the control variables are directly the instantaneous active and reactive powers. T. Ohnishi [30] suggested the switching table-based DPC which is based on the principle of direct torque control for electrical machines. Although DPC directly selects the power switch states to follow the desired active and reactive powers, the resulting switching frequency is varied.

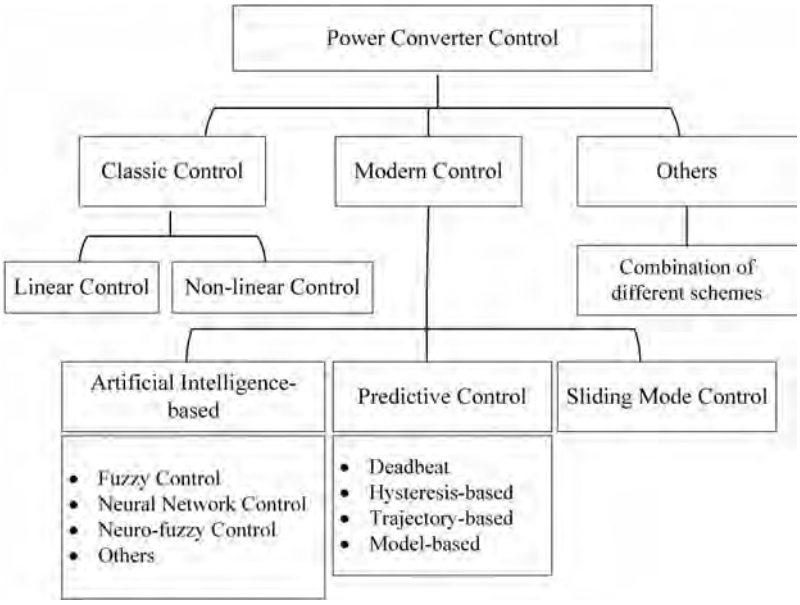

Figure 2.3: Control algorithms for power converters

2.4.2 Control algorithms based on direct power control

In a three-phase system, power converters can be controlled in natural (ABC), stationary ($\alpha\beta$), or synchronous (dq) reference frame. Employment of the control algorithm in dq-frame is widely applied in the different applications of three-phase systems. Although this scheme brings certain advantages like the use of simple PI controller, two-stage coordinate transformations, decoupling network, and regulation efforts are essential to assure the stability and efficiency [29]. Yet, under the unbalanced circumstances, PI controller is incapable to adjust the appeared fluctuations in current [31] .

One solution to this downside is the use of two separate PI controllers for each positive and negative sequence currents [32]. An efficient approach is applied with the help of $\alpha\beta$-frame and proportional resonant controller where neither the decoupling network nor sequence control is required. Nevertheless, both controllers need a complicated synchronization scheme for a seamless transition between two operation modes in microgrids [33, 34].

On the other hand, with the progress of faster, more accurate, and more powerful microprocessors, utilizing digital control platforms has revealed a new horizon for more flexible, consistent and effective approaches [35]. A summary of control algorithms applied to power converters is depicted in Fig. 2.3. A comprehensive study is conducted in [36] on the modulation schemes used for controlling the power converters. Among the modern control algorithm, predictive control and specifically model-based one gained much attention among researchers because of its flexibility and inclusion of nonlinearity and constraints at the same time.

2.4.3 Model predictive control

Model predictive control (MPC) found its industrial applications in the 1970s. It offers a fast control algorithm with high accuracy and stability during complex calculation. Despite complicated calculation, the power electronics industries are

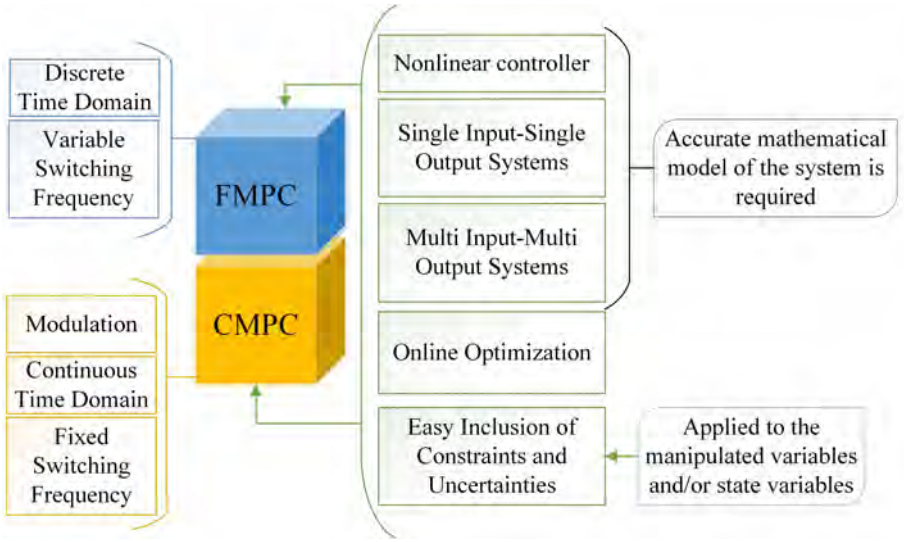

Figure 2.4: Criteria of MPC techniques

able to take the advantages in practice due to development of fast and powerful processors. While classical controllers try to simplify nonlinearities of the system, MPC is able to work with system nonlinearities and constraints instantaneously with the control necessities. Besides, MPC can be applied easily in multiple input-multiple output (MIMO) systems as well as single input-single output (SISO) systems. Yet, a precise system model is essential to have the optimized MPC. A drawback of this control algorithm is its high number of calculations that should be repeated at each sampling time using new state measurements or estimates, which may have a negative effect on the speed of controller. Based on MPC, three choices have been presented in order to decrease calculations: generalized predictive control (GPC) [37], explicit MPC and the finite control set MPC (FCS-MPC) [38].

The MPC has been employed vastly in chemical and process industries [39]. Over the years, MPC has gained much attention among researchers as an alternative modern control for power converters in power system applications [40–44]. In spite of time-consuming calculation, the power electronics industries are able to employ it via digital control platform in practice. MPC is a well-established method and its concepts, operating principles [45], and technology readiness for real-time implementation [46] are well studied. MPC techniques can be categorized into two forms: the FCS-MPC, and the continuous control set based MPC (CCS-MPC). The main criteria for both forms are illustrated in Fig. 2.4. In the FCS-MPC approach, it takes benefit of the limited number of switching states of the power converter to solve the optimization problem.

In particular, FCS-MPC has been verified to be a very effective substitute for traditional control algorithms for power converters which are controlled with pulse width modulation (PWM) techniques [47, 48]. A comparison between FCS-MPC and PWM based algorithms is presented in Table 2.1.

As power electronics applications are commonly controlled by using digital platforms, they fit the system model in the state space form of discrete-time domain [49]. The FCS-MPC has been an intuitive and potent digital approach to control power converters where no modulation stage, decoupling network, separate sequence control, complex synchronization unit are employed to achieve the stable,

Table 2.1: FCS-MPC verses PWM-based Algorithms

Performance Criteria	FCS-MPC	PWM-based
Ripples	High	Low
Switching Frequency	Variable	Fixed
Design of Weighting Factor	Empirical	Not Applicable
Modulation	Not Applicable	Applicable
Adaptation (Non-linearities, Constraints, Uncertainties)	Applicable	Not Applicable
Computation Burden	High	Low
Multi-objectives	Applicable	Not Applicable
Online Optimization	Applicable	Not Applicable

reliable, and efficient system. Generally, FCS-MPC solves an optimization problem over a finite prediction horizon and then forms the best control sequence for the prediction horizon. This searching process is continued with applying the obtained best control of the current sampling instant, the updated estimations and measurements, for the next sampling instant [50].

Although MPC is a robust approach, the algorithm needs to be modified for different purposes due to the difference in the plant characteristics, which poses various challenges for the controller design. To address some of the issues within MPC, a combination of MPC and other control methods has been proposed in different studies [51–55]. The sliding mode control can considerably simplify the resolutions of predictive control difficulties due to parametric uncertainties and disturbances [56, 57]. Fuzzy decision-making has also shown good results when multiple objectives and constraints have to be considered [53, 58]. However, implementation complexity, maintenance, efficiency, and cost are some of the factors that need to be assessed. Nevertheless, industrial approval of MPC in power converters and drives has yet to come. In [46], the authors assessed the technology readiness of MPC with a conclusion that MPC will perform a key role for the next generation of power converters and electrical drives to operate in a more reliable, stable, and efficient way.

2.5 Finite Control Set Model Predictive Control

2.5.1 Finite control set-MPC principles

The basic operating principle of FCS-MPC has been introduced in [28, 40, 41, 49]. In general, FCS-MPC has three fundamental parts: (a) Prediction model which is a mathematical expression of the plant in a discrete state-space form at the step $k + N$,

$$
\begin{aligned}
x_i(k+N) &= f(x_i(k+N-1), u_i(k+N-1)), \\
y_i(k+N) &= g(x_i(k+N))
\end{aligned}
\tag{2.1}
$$

where N is the prediction horizon, $x_i(k), u_i(k)$, and $y_i(k)$ are the state, input, and output vector variables at the time instant kT_s, respectively, T_s is the sampling interval, and $i = 1, ..., n$ the $i-th$ number of possibilities; (b) Objective function structure which can be broad, with the optimization of various objectives for different purposes; and (c) Optimizer. The assessment of the cost function with the n predictions will cause n different costs. Certainly, the control action will be chosen as the one which leads to the minimum cost ($min\, J_i(k+N), for\, i = 1, ..., n$). In the case of tracking the reference, $Y_i^*(k+N)$, the control problem can be optimized via minimizing the following objective function

$$
\begin{aligned}
J_i(k+N) &= \sum_{l=k}^{k+N} ||Y_{i,Err}(l+1)||_2^2 \\
Y_{i,Err}(l+1) &= Y_i^*(l+1) - Y_i(l+1)
\end{aligned}
\tag{2.2}
$$

2.5.2 Power converter topologies controlled by FCS-MPC

FCS-MPC technique has been implemented in various power converter topologies. For an r-level s-phase (rL-sPh) converter, the total number of potential switching positions is $m = r^s$. The estimation of the cost function with the m possibilities will lead to m different costs. Since, in each power converter topology, the number of switching positions is limited, the minimum of the objective function can be determined through an exhaustive search.

2.5.2.1 *Two-level voltage source converter*

This topology is broadly used by industry applications at the low voltage level. The topology of a 2L-3Ph grid-connected voltage source inverter (VSI) is shown in Fig. 2.5. It is formed by a complementary pair of power switches for each phase and linked to the utility grid through a filter [59]. There are a total number of eight possible converter output voltage vectors for this topology ($m = 2^3 = 8$) as follows,

$$
v_m = \begin{cases} \frac{2}{3} e^{j(m-1)\frac{\pi}{3}} V_{DC} & \text{if } m = 1, ..., 6 \\ 0 & \text{if } m = 0, 7 \end{cases}
\tag{2.3}
$$

In [37], FCS-MPC approach is applied to a 2L-3Ph VSI for photovoltaic (PV) systems with flexible power tracking as well as switching loss minimization through DPC. Detailed study of DPC strategies is explored in [38]. A simplified FCS-MPC based on direct current control (DCC) is utilized on a 2L-3Ph voltage source rectifier (VSR) in [60]. Moreover, this configuration is the most common topology chosen for different applications.

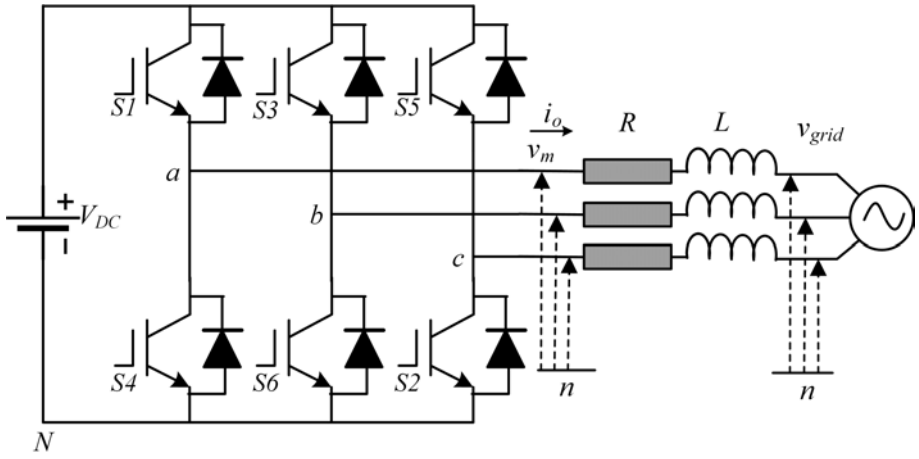

Figure 2.5: Two-level three-phase grid-tied inverter

2.5.2.2 *Multilevel converters*

Multilevel converters, including neutral point diode clamped (NPC), flying-capacitor (FC), and cascaded H-bridge (CHB) [61], are some of the topologies which attained vast industrial success for medium voltage applications. A 3L-3Ph NPC topology is illustrated in Fig. 2.6. There are a total number of twenty-seven possible voltage vectors for this topology ($m = 3^3 = 27$) which, according to their magnitudes, can be divided into four groups as illustrated in Table 2.2. The graphical representation of these voltage vectors in the stationary reference frame is illustrated in Fig. 2.7. For the NPC topology, the neutral point voltage has to be controlled, which is an extra control target besides the main objectives of the application [62]. The output voltage of the inverter in the stationary frame is described by

$$\begin{aligned} v_m^{\alpha\beta} &= \frac{V_{DC}}{2} M S_m \\ S_m &= \begin{bmatrix} S_a^m & S_b^m & S_c^m \end{bmatrix}^T \end{aligned} \tag{2.4}$$

where M is the Clarke transformation matrix, V_DC is the DC-link voltage and $S_m$is the switching signal for $m = 0, ..., 26$. The mathematical model of 3L-3Ph NPC grid-connected inverter with RL filter can be formulated in the stationary frame via matrix M as

$$v_m^{\alpha\beta} = L\frac{di_o^{\alpha\beta}}{dt} + R * i_o^{\alpha\beta} + v_{grid}^{\alpha\beta} \tag{2.5}$$

where i_o is the output current of the inverter and v_{grid} is the main grid voltage [63]. As for FC converters, the topology is mainly similar to the NPC converter topology, but instead of clamping via diodes the FC converters use clamping capacitors [64–66]. For high power applications, adding more voltage levels to the converter can be practical such as four-level NPC [67, 68] and five-level NPC [69] converters. Furthermore, active power filter (APF) through multilevel converter can compensate the current harmonics imposed through non-linear loads along with adjusting the power factor [70].

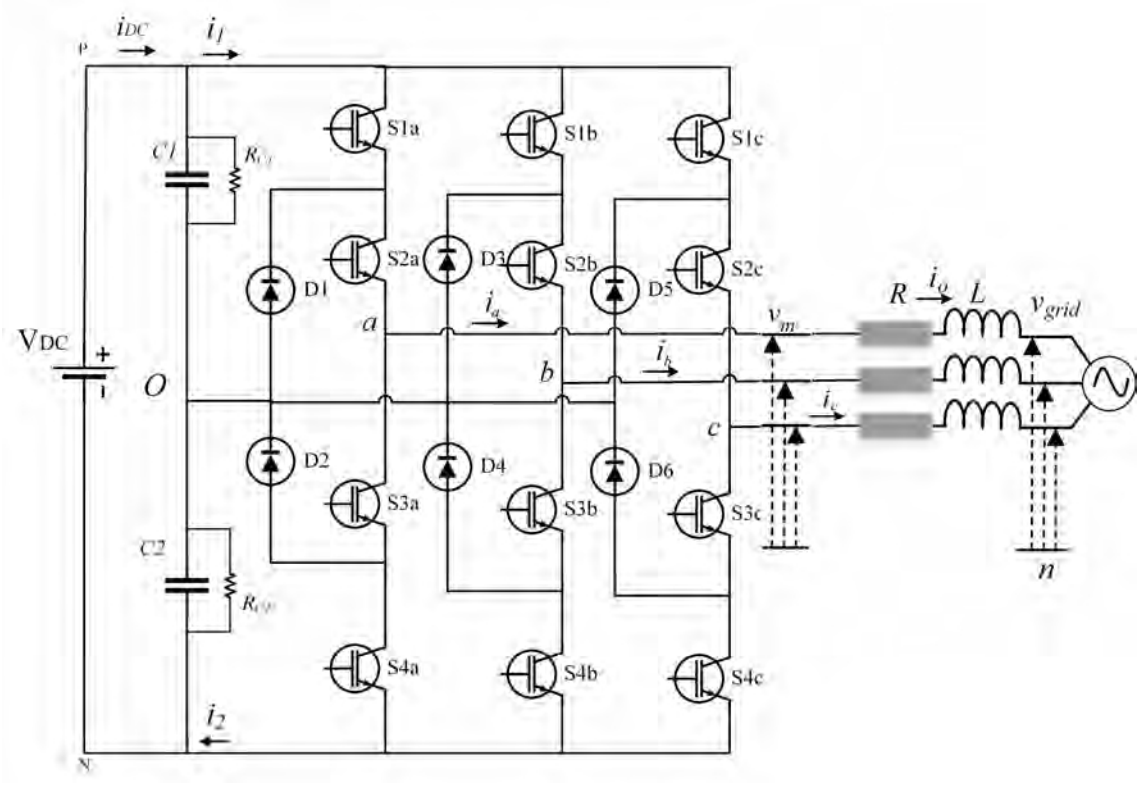

Figure 2.6: 3L-3Ph NPC inverter

Table 2.2: Voltage Vectors of 3L-3Ph NPC Inverter

Voltage Vectors	Number	Comment
Zero Vectors	0,13,26	No current flosws through the neutral point
Small Vectors	1,3,4,9,10,12,14, 16,17,22,23,25	The sign for the neutral current at positive vectors does not alter whereas the negative ones change it
Medium Vectors	5,7,11,15,19,21	Connect a phase current to the neutral
Large Vectors	2,6,8,18,20,24	No current flows through the neutral point

2.5.2.3 *Modular multilevel converters*

The modular multilevel converter (MMC) is the prospective power converter used in applications requiring large capacity and high voltage [71], like high voltage direct current (HVDC) transmission [72] and the static synchronous compensator [73]. For a (r+1)-level s-phase MMC, the number of possible switching states is $m = sC_{2r}^{r}$. For instance, if $r = 5$ and $r = 10$ the possible voltage vectors are 252 and 184756 respectively only for each phase. For controlling MMC, the voltage balancing and circulating current reduction for the sub-module capacitor are two objectives that must be taken into account [74, 75]. Furthermore, lower harmonic distortion and higher efficiency can be reached due to the high modularity [72, 76–78].

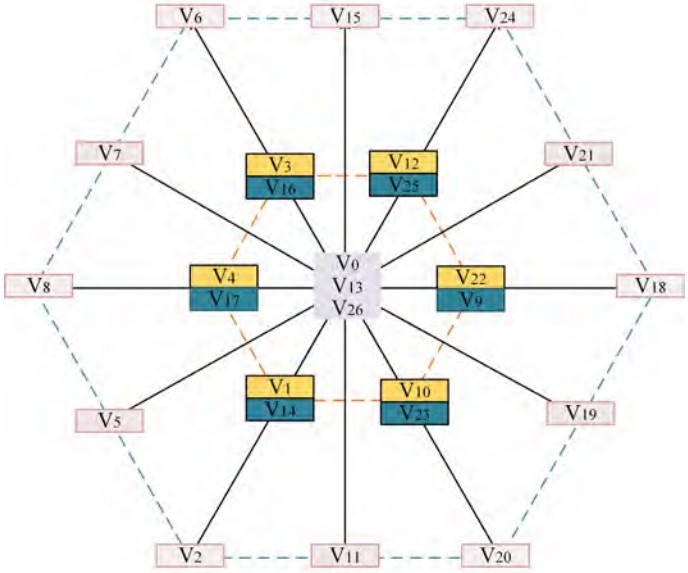

Figure 2.7: Grapgical representation 3L-3Ph NPC inverter voltage vectors

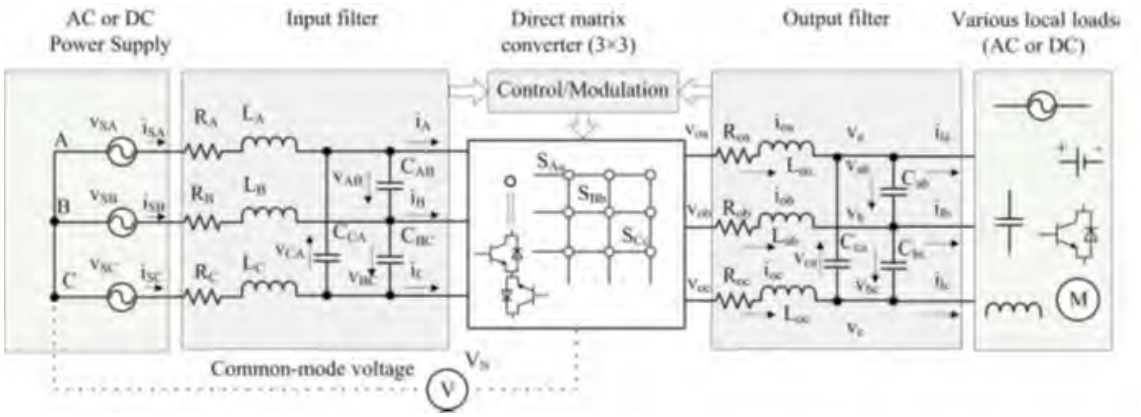

Figure 2.8: Direct matrix converter topology [81]

2.5.2.4 *Direct matrix converter*

The conversion from AC to AC can be determined through direct matrix converter (DMC) directly, as depicted in Fig. 2.8. In this manner, large storage parts and DC-link can be eliminated to increase the system reliability [79]. Another benefit of this topology is that the load frequency can differ from the source frequency [80]. With a matrix converter, different conversions AC-DC, DC-AC, and DC-DC can be utilized if it is needed [81].

2.6 Real-time Implementation of FCS-MPC Algorithm

As digital control is an important element of modern industrial power converters, hardware and software design procedures and implementation barriers must be investigated. With the presence of powerful and high-performance processors, the design procedures are considerably reformed. Generally, the real-time implementa-

tion (RTI) of FCS-MPC in power converters has five stages as shown in Fig. 2.9. Stage I controls the analog to digital conversion (ADC) of electrical and mechanical measures, such as voltage, current, position, and speed, etc. Then, in stage II, the measured values are transformed into the two-phase stationary coordinate. The reference and prediction of the state variables are delivered in stage III. In stage IV, the objective function is minimized through an optimization process, leading to the selection of the best switching states. Finally, stage V contains a register that stores the optimal states [35, 56] .

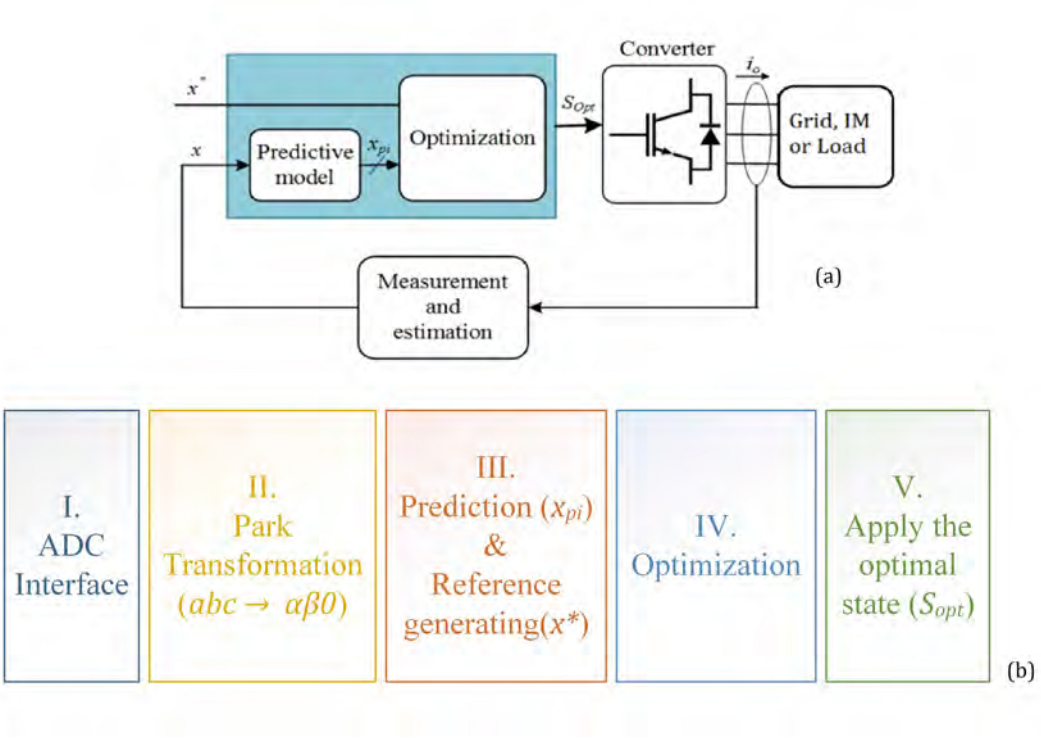

Figure 2.9: FCS-MPC (a) Block diagram (b) Implementation stages

MATLAB Simulink and National Instrument LabVIEW are two commercial tools used to model, simulate, and analyze the real-time systems in different domains. RTI of FCS-MPC algorithm is divided into two groups based on the device which is used for control: (i) Software-based with the aid of digital signal processors (DSPs) such as fixed-point DSPs and floating-point DSPs, and (ii) Hardware-based with the assistance of field programmable gate arrays (FPGAs). A comparison in terms of performance, ease of implementation and device capabilities are summarized in Table 2.3.

Modern DSPs have now much higher computing power than before. Although the fixed-point DSPs have a good performance, embedding a floating-point processing unit to DSPs can enhance mathematical flexibility, computational performance, and accuracy significantly. DSPs are also restricted to lower sampling frequencies (up to 50 kHz) compared to FPGAs (up to hundreds kHz). As FPGAs work with fixed-point numbers, working with them is more complicated compared with floating-point DSPs [49]. Parallel Execution of the control algorithm can reduce the computational delay time notably up to for example 3.52 μs [82] and 2.12 μs [80] for three instantaneous objectives.

The RTI of FCS-MPC based on FPGA using high-level synthesis is proposed

in [83]. It permits to consider trade-offs between energy, speed, and memory requirements in FPGA, and to deliver advice for optimal synthesis for designers. In [84], multiple vector direct power FCS-MPC for grid-tied wind turbine system is implemented with FPGA to enhance the steady-state performance while they kept the sampling frequency similar to DSP. Therefore, it can achieve more advanced objectives and reduce the cost. The dSPACE DS1104 R&D Controller Board together with MATLAB Simulink is another method aimed at RTI which has been widely used by researchers to verify their proposed methods [85, 86]. The dSPACE has attained much attention among researchers due to its user-friendly interface. For example, TMS320F28335 can execute 150 million instructions per second (MIPS) while Xilinx XC3S400 or the modern dSPACE DS1103 platform can execute 2500 MIPS.

Some researchers propose an integrated control platform built via FPGA and floating-point DSP which is designed and implemented in [77, 87]. The time associated with the calculation of FCS-MPC algorithms is much more dependent on the converter topology, objectives, and constraints as shown in Table 2.4.

2.7 Issues and Alternative FCS-MPC Methods

FCS-MPC has proven to be an alternative control approach in power converters and electrical drives. Also, in [91], FCS-MPC is implemented for variable speed drives at the multi-megawatt level. As aforementioned, FCS-MPC is a model based control method, and thus, developing an accurate and tolerable model of the plant is vital. Although many advantages of using FCS-MPC in power system are validated

Table 2.3: DSPs and FPGA Performance Comparison

Criteria	DSP(Fixed)	DSP(Floating)	FPGA
Commonly Used Device	TMS 320F2812	TMS 320F28335	Xilinx XC3S400
Performance Efficiency	Low	High	Medium-High
Computation Capability	Low	High	High
Ease of Implementation	Easy	Easy	Hard
Execution Time	Long	Long	Short
Execution Method	Sequential	Sequential	Parallel
Sampling Frequency	Low	Low	High
Programming Language	C	C	Verilog/VHDL
Cost	Low	Low	Medium
Flexibility	Medium	Medium	High
Reliability	Medium	Medium	Medium
Accuracy	Low	High	Medium

Table 2.4: Time Associated with computational burden in FCS-MPC Algorithm

Converter Topology	Application	number of Objectives	Device	Calculation Time (μs)
2L-3Ph VSI [37, 88]	Grid-tied DGs	Two	TMS 320F28335	68
2L-3Ph VSI [86]	Induction Machine	Two	dSPACE DS1104	20
3L-3Ph NPC-VSI [85]	Induction Machine	Three	dSPACE DS1104	59.15
3L-3Ph NPC-VSI [82]	Grid-tied DGs	Two	FPGA Spartan XC3S500E	Seq.:9.4 Par.:3.52
MMC(N-modules) [89]	HVDC transmission/ STATCOM/ motor drive	Three	TMS 320F28335	124
MMC(2-modules) [76]	Medium voltage applications	Three	FPGA	9.15
B2BC [90]	Grid-tied DGs	Three	FPGA	2
DMC [80]	AC-AC conversion	Three	FPGA	2.12

by lab-based studies, including a more accurate variation of the control variables, constraints, non-linearity, and uncertainties are essential for further analytical and experimental studies. In this section, the issues and their alternative FCS-MPC solution for power converters in different cases in power systems here discussed.

2.7.1 Cost function optimization and design

A Lyapunov-based cost function is suggested for FCS-MPC to guarantee stability and performance (including transient and steady state error (SSE) performances) in [92–94]. The scheme is implemented through a floating-point DSP and FPGA for a 2L-3Ph inverter and through dSPACE for a 2L-3Ph bidirectional converter in [92] and [93], respectively. The simulation and experimental results validate the proposed cost function. However, similar to the linear quadratic program, there is a trade-off between SSE and the losses in power switch. In [95], the SSE is improved by adding an extra term, integrating the error between the reference and predicted variable within a sampling time, in the cost function. An explicit MPC algorithm to enhance the steady-state performance is proposed in [64], where the optimization problem can be resolved offline.

An observer-based optimal voltage control by using Lyapunov theory is proposed in [96] for three-phase UPSs. The controller has feedback and a compensating control term to alleviate the system dynamics and estimate the uncertainties respectively. Under different load scenarios, the proposed control algorithm exposes a better voltage tracking performance, with the total harmonic distortion (THD) value of the output voltage declined by almost 49% in all scenarios.

In [97], a deadbeat control is proposed to solve the FCS-MPC optimization problem more effectively. A generalized FCS-MPC structure for the VSI current controller design is proposed in [98] where Kalman filter is used as an observer. The noise and periodic disturbances for the system output are considered in this model as well. In another approach [99], the control sequence is calculated by CCS-MPC based on the optimal switching sequence model. This method can be used for RTI where the system constraints are considered.

2.7.2 Computational burden and time

A notable flaw of the conventional FCS-MPC is that the state switching cost has to be accounted for, which leads to the enormous computational burden and time [100]. For a longer horizon prediction or multilevel converters where the number of switching possibilities is increased considerably, FCS-MPC will face a computational challenge and impracticality for RTI. This drawback leads to the time delay for DSP-based RTI that needs to be considered in the controller design to sustain the system stability and performance [101, 102]. Excluding the redundant voltage vectors and second-step prediction are common methods to compensate the computation load or time delay [103]. For example, in a 3L-3Ph NPC inverter, there are eight redundant voltage vectors which may be ignored. To achieve this, an extra term is added into the objective function [104]. In [95], by dividing the space into sections and considering the candidate voltage vector for each sector, the calculation effort is reduced to seven possibilities for each enumeration. Furthermore, in the optimal switching sequence based FCS-MPC, by reducing the number of sectors in a 2L-3Ph VSI from twelve to six sectors, the computation time by TMS320F28335 is reduced from 90 μs to 40 μs [29].

With the intention of reducing the computation load for MMC, an FCS-MPC algorithm based on sorting method is proposed in [75], where the sub-module capacitor voltages of every arm are arranged by the current polarity of each arm. Thus, with S modules, the number of possible vectors is reduced to S+1 for each phase. In [105], the optimization problem is formulated as an integer least squares (ILS) problem where the branch and bound technique of sphere decoding is implemented to calculate the best sequence of the manipulated variable. For long horizons (e.g., N=10), the computation load of mentioned strategy is decreased up to 45% compared with the conventional technique used in the FCS-MPC algorithm.

The computational complexity increases with the number of constraints considered. In general, off-line based MPC results in inaccurate predictions as the controller cannot apply the real-time changes. In [106], the proposed optimization method reduces the computation load about five times less than general approaches. In the proposed method, a set of potential active constraints are maintained and updated. A distributed FCS-MPC is proposed in [107] where a cost function is formulated in a distributed way, helping to reduce the computing time for back-to-back power converters. A typical procedure of this method is depicted in Fig. 2.10.

2.7.3 Switching loss

In a hard switched power converter, the higher the switching frequency is, the higher the switching loss will be, which leads to a lower efficiency [108]. A

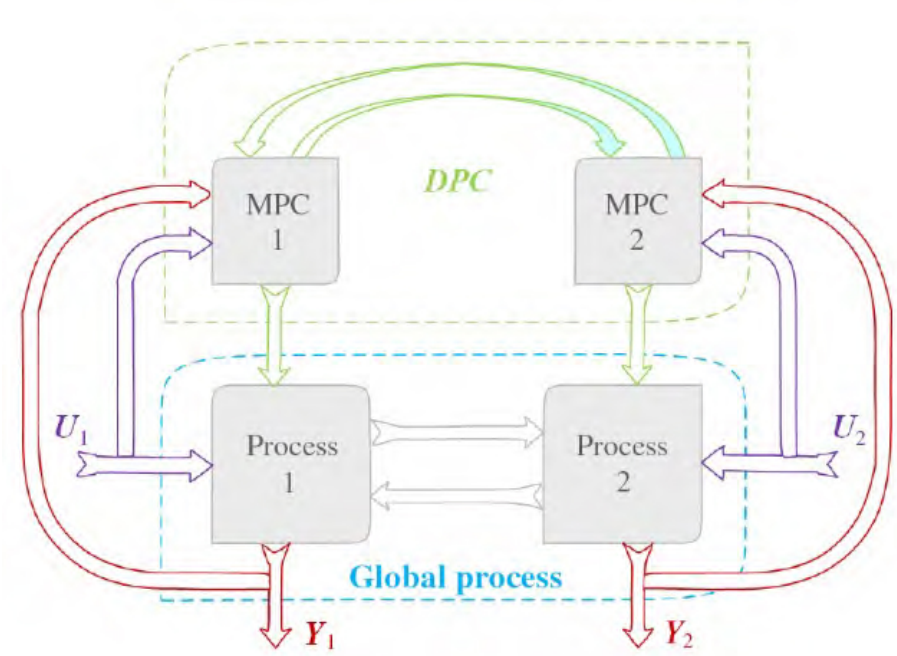

Figure 2.10: A Typical block diagram for distributed MPC [107]

major drawback of FCS-MPC is the variable switching frequency which leads to higher switching losses. To reduce the switching frequency, a two-step prediction algorithm is applied in [37, 109]. In [110], a modulated MPC is proposed to employ a PWM-based modulator to gain a fixed switching frequency. A modified FCS-MPC algorithm is presented in [111] to achieve the lower switching frequency while no additional term is needed in the objective function, just through utilizing the available redundant voltage vectors. Therefore, this algorithm can reduce the total possibilities of switching states at each sampling time and provide outstanding reference tracking abilities. In [112], a duty cycle based on direct power FCS-MPC is proposed to achieve lower average switching frequency, where the modulation stage is by a fuzzy logic modulator.

2.7.4 Ripple reduction

As the traditional FCS-MPC method applies just one switching state through the entire sampling period, the ripples of the tracking variables are more apparent than the indirect controller with the modulator.

An FCS-MPC algorithm based on duty cycle control of the power converter shows lower ripples for tracking purposes based on two-vector [113, 114] and three-vector [29, 100, 113, 115] selection. In [116], an FCS-MPC based direct torque control (DTC) is proposed to minimize the flux and torque ripples at the steady state by adjusting some parameters of voltage vector like magnitude, phase, and time duration. A ripple reduction of 81.43% and 79.65% for flux and torque is obtained respectively using this method in comparison with the conventional FCS-MPC based on DTC. Furthermore, fast dynamic responses can be achieved as well by regulating the parameters of voltage vectors in the transient state.

Although this algorithm shows a much better dynamic performance, it in-

creases the computational burden by about 64%. A different approach is proposed in [117], to reduce the torque ripples in permanent magnet synchronous motors. In this case, the algorithm analyses the relationship between the variables to obtain the angle of the reference vectors.

2.7.5 Harmonic performance

In [118], a dual-stage FCS-MPC for MMC is proposed to improve the harmonic performance as well as reducing the computational burden. For high-power converters working at low switching frequencies, exclusion of low-order harmonics is extremely advantageous [119, 120]. The selective harmonic elimination (SHE) technique is one way to achieve this purpose.

A model predictive switching pattern control with space vector based SHE for a current source converter is proposed in [121, 122] which can eliminate low-order harmonics effectively in the steady state, and enhance the transient responses. Furthermore, this method mitigates the quantization errors in the steady state and evades the use of weighting factors. FCS-MPC can improve the transient performance of the space vector based SHE, and in the steady state, the output PWM waveform can track SHE pattern. In [110], FCS-MPC is modified by introducing a cost function-based modulator which aims to reduce power losses, ripples, and harmonics. As an example, the THD value of load current with this approach is lessened by three times.

2.7.6 Mutual interference

The mutual interference (MI) during control is an issue with the cost function involving of square terms, such as active and reactive power control in DG applications. In [123], the objective function is restructured to resolve the MI problem as

$$\begin{aligned} cf_{recon} &= p_{wf}(p^{ref} - p^{k+2})^2 + q_{wf}(q^{ref} - q^{k+2})^2 \\ p_{wf} &= [\lambda|\tfrac{q^{ref}-q^{k+2}}{q_{rated}}| + 1] \\ q_{wf} &= [\lambda|\tfrac{p^{ref}-p^{k+2}}{p^{rated}}| + 1] \end{aligned} \tag{2.6}$$

where p_{wf} and q_{wf} are the weighting factors for regulating the dynamic performance of active and reactive power, and p^{ref} and q^{ref} the active and reactive reference power, respectively.

2.7.7 Parametric uncertainties

The FCS-MPC technique deals with the mathematical model of the system which is dependent on the system parameters. However, the system parameters may be different from their real values because of measurement errors or vary because of their dependences on the operating conditions. Therefore, parameter uncertainties and model inaccuracy may cause imprecise prediction of the system [124]. In [125], the parameter uncertainties are considered by implementing the feed-forward linearization for discrete-time inputs to enhance the accuracy of prediction for a permanent magnet synchronous motor (PMSM). A systematic methodology to observe

the effect of model parametric uncertainties on the prediction error for FCS-MPC based on current control in a 2L-3Ph inverter with RL load is investigated in [126]. While the inductance mismatch has a significant effect, the pure resistive parametric changes can be neglected. A generalized MPC can reduce the effect of parameter variation by using the transfer function of the system and constraints at the same time [127].

2.7.8 Weighting factor

Adding control objectives and constraints is a significant feature of FCS-MPC. These additional terms can be incorporated simply into the cost function with their specific weighting factors. Consequently, all the control necessities will be observed by the controller simultaneously. However, the weighting factor tuning is a heuristic process for which there is not a precise or analytical approach.

In [128], the calculation of weighting factors is attained via a nontrivial process based on a ranking approach. By using this method, multiple voltage vectors may have the same average ranking. Although priorities can be allocated for each target to overcome this matter, it remains an open discussion in this approach. Furthermore, it also increases the computational burden up to three times more than the heuristic methods. In [129], the ranking-based algorithms are applied to matrix converters.

The main contribution of [130] is the exclusion of weighting factors in the multi-objective function. The algorithm is applied to a 3L-1Ph NPC converter as an APF with three control objectives. A combination of a good current reference generator and choice of redundant switching states can be used to remove the weighting factors and DC capacitor currents. In [114, 131, 132], a two-vector based model predictive torque control is studied where the weighting factors are removed by normalizing all the terms in the objective function. An online fuzzy approach for tuning of weighting factors based on Sugeno technique is discussed in [133].

2.7.9 Longer prediction horizon

In general, implementing FCS-MPC algorithm is computationally challenging, mostly due to the difficulty in direct implementation of switching states. Moreover, the type of optimization problem and the number of manipulated variables may add to the complexity of this method. As a result, a one-step prediction ahead is typically used for reference tracking in power converters, to reduce the computational complexity.

However, a long prediction horizon can lead to better control performance and stability [134–136]. Therefore, the prediction for longer horizons is desired but has to meet the computational demand and handle the system complexity [50, 137]. Three strategies that can attain long prediction horizons within acceptable computation levels are investigated including the extrapolation, move blocking, and event-based horizon strategies [138].

Among these methods, the extrapolation strategy is employed and implemented in practice for power electronic applications frequently [59]. As demonstrated in [134, 137], by adopting the sphere decoding algorithm for optimization, longer predictions can be achieved with a reduction of computational burden.

2.7.10 Filters

Filters play a significant role in the model of the predicted system. The filter is a part of the prediction model and it imposes some hardships for controlling the power converters that have to be taken into account. LCL filters are broadly used in grid-tied power converters [41, 62, 139–142]. This filter is capable of improving the harmonic attenuation presented by series inductors. However, the control problem becomes complex due to the filter capacitor which leads to a delay between the grid and the power converter as well as resonant frequencies. By utilizing the LCL filter, particularly in medium voltage applications, a lower switching frequency can be achieved. In [62], a virtual resistor concept is employed to deal with resonance damping and harmonic attenuation. More accurate decisions and improvements can be gained by longer prediction horizons. Moreover, in [139], an active damping strategy via virtual resistor concept is introduced which can reduce the average switching losses by 17.3% in comparison with carrier-based PWM.

A hysteresis based model predictive control is developed in [141] for high power applications which can possess the average switching frequency within a standard boundary while enhancing the system stability. In some applications, where islanding from the grid is compulsory, LC filters are effective for output voltage control [106, 143].

2.8 Summary

In this chapter, a brief review of the microgrid concept, structure, control, and operation are stated. Developments in the control of microgrids increase their potential to interact more efficiently with the main grid. Therefore, the hierarchical control of microgrid is explored and led us to control of power converters. Among the control approaches applied on power converters in the microgrid, MPC has been employed vastly. Therefore, the FCS-MPC approach which takes benefit of the limited number of switching states of the power converter has been verified to be a very effective substitute for traditional control algorithm. As digital control is an important element of modern industrial power converters, hardware and software design procedures and implementation barriers are investigated. Although FCS-MPC is well established, the algorithm needs to be modified for different purposes due to the difference in the plant characteristics which poses various challenges for the controller design. Nevertheless, the real-time implementation of FCS-MPC for different topologies and applications faces new challenges which give rise to more exploration of MPC approaches. Some of the concerns such as cost function design, computational burden, switching loss, harmonic performance, ripple reduction, weighting factor design, filters, parametric uncertainties are explored in literature, and the possible solutions are discussed. A summary of recent contributions on FCS-MPC for power converters is listed in Table 2.5. As the matter of fact, the employment of the FCS-MPC in power electronics has been increased in power systems with the analytical approach as well as the RTI experiences.

Table 2.5: Summary of Recent Contributions on FCS-MPC for Power Converters

Alternate Solutions	Pros	Cons
Reconfigured Objective Function	The Lyapunov-based function has shown an improved transient and steady state error compared to quadratic-based	Trade-off between steady-state error and switching loss for both functions
Longer Prediction Horizon	Delay compensation, Lower switching losses, Better dynamic performances	Increased computation load and complexity
Multi-objectives	Control several variables simultaneously	Weighting factor design, different units
Duty Cycle Control MPC	Better steady-state performances, Lower switching frequency, Ripple reduction	Increased computation load

Bibliography

[1] E. Planas, J. Andreu, J. I. Gárate, I. M. de Alegría, and E. Ibarra, "Ac and dc technology in microgrids: A review," *Renewable and Sustainable Energy Reviews*, vol. 43, pp. 726–749, 2015.

[2] J. J. Justo, F. Mwasilu, J. Lee, and J.-W. Jung, "Ac-microgrids versus dc-microgrids with distributed energy resources: A review," *Renewable and Sustainable Energy Reviews*, vol. 24, pp. 387–405, 2013.

[3] Y. Yoldaş, A. Önen, S. Muyeen, A. V. Vasilakos, and İ. Alan, "Enhancing smart grid with microgrids: Challenges and opportunities," *Renewable and Sustainable Energy Reviews*, vol. 72, pp. 205–214, 2017.

[4] R. Bayindir, E. Hossain, E. Kabalci, and R. Perez, "A comprehensive study on microgrid technology," *International Journal of Renewable Energy Research*, vol. 4, no. 4, pp. 1094–1107, 2014.

[5] S. Parhizi, H. Lotfi, A. Khodaei, and S. Bahramirad, "State of the art in research on microgrids: A review," *IEEE Access*, vol. 3, pp. 890–925, 2015.

[6] I. Patrao, E. Figueres, G. Garcerá, and R. González-Medina, "Microgrid architectures for low voltage distributed generation," *Renewable and Sustainable Energy Reviews*, vol. 43, pp. 415–424, 2015.

[7] E. Unamuno and J. A. Barrena, "Hybrid ac/dc microgrids—part i: Review and classification of topologies," *Renewable and Sustainable Energy Reviews*, vol. 52, pp. 1251–1259, 2015.

[8] ——, "Hybrid ac/dc microgrids—part ii: Review and classification of control strategies," *Renewable and Sustainable Energy Reviews*, vol. 52, pp. 1123–1134, 2015.

[9] T. L. Vandoorn, B. Meersman, J. D. De Kooning, and L. Vandevelde, "Analogy between conventional grid control and islanded microgrid control based on a global dc-link voltage droop," *IEEE transactions on power delivery*, vol. 27, no. 3, pp. 1405–1414, 2012.

[10] Y. A.-R. I. Mohamed and A. A. Radwan, "Hierarchical control system for robust microgrid operation and seamless mode transfer in active distribution systems," *IEEE Transactions on Smart Grid*, vol. 2, no. 2, pp. 352–362, 2011.

[11] S. K. Sahoo, A. Sinha, and N. Kishore, "Control techniques in ac, dc, and hybrid ac-dc microgrid: A review," *IEEE Journal of Emerging and Selected Topics in Power Electronics*, 2017.

[12] T. Dragičević, X. Lu, J. C. Vasquez, and J. M. Guerrero, "Dc microgrids—part ii: A review of power architectures, applications, and standardization issues," *IEEE transactions on power electronics*, vol. 31, no. 5, pp. 3528–3549, 2016.

[13] H. Lotfi and A. Khodaei, "Ac versus dc microgrid planning," *IEEE Transactions on Smart Grid*, vol. 8, no. 1, pp. 296–304, 2017.

[14] A. Gupta, S. Doolla, and K. Chatterjee, "Hybrid ac-dc microgrid: Systematic evaluation of control strategies," *IEEE Transactions on Smart Grid*, 2017.

[15] A. Bidram and A. Davoudi, "Hierarchical structure of microgrids control system," *IEEE Transactions on Smart Grid*, vol. 3, no. 4, pp. 1963–1976, 2012.

[16] Y. Han, P. Shen, X. Zhao, and J. M. Guerrero, "Control strategies for islanded microgrid using enhanced hierarchical control structure with multiple current-loop damping schemes," *IEEE Transactions on Smart Grid*, vol. 8, no. 3, pp. 1139–1153, 2017.

[17] Y. Han, H. Li, P. Shen, E. A. A. Coelho, and J. M. Guerrero, "Review of active and reactive power sharing strategies in hierarchical controlled microgrids," *IEEE Transactions on Power Electronics*, vol. 32, no. 3, pp. 2427–2451, 2017.

[18] K. Rajesh, S. Dash, R. Rajagopal, and R. Sridhar, "A review on control of ac microgrid," *Renewable and Sustainable Energy Reviews*, 2017.

[19] D. E. Olivares, A. Mehrizi-Sani, A. H. Etemadi, C. A. Cañizares, R. Iravani, M. Kazerani, A. H. Hajimiragha, O. Gomis-Bellmunt, M. Saeedifard, R. Palma-Behnke *et al.*, "Trends in microgrid control," *IEEE Transactions on smart grid*, vol. 5, no. 4, pp. 1905–1919, 2014.

[20] M. Yazdanian and A. Mehrizi-Sani, "Distributed control techniques in microgrids," *IEEE Transactions on Smart Grid*, vol. 5, no. 6, pp. 2901–2909, 2014.

[21] T. Vandoorn, J. De Kooning, B. Meersman, and L. Vandevelde, "Review of primary control strategies for islanded microgrids with power-electronic interfaces," *Renewable and Sustainable Energy Reviews*, vol. 19, pp. 613–628, 2013.

[22] O. Palizban and K. Kauhaniemi, "Hierarchical control structure in microgrids with distributed generation: Island and grid-connected mode," *Renewable and Sustainable Energy Reviews*, vol. 44, pp. 797–813, 2015.

[23] J. M. Guerrero, J. C. Vasquez, J. Matas, L. G. De Vicuña, and M. Castilla, "Hierarchical control of droop-controlled ac and dc microgrids—a general approach toward standardization," *IEEE Transactions on industrial electronics*, vol. 58, no. 1, pp. 158–172, 2011.

[24] J. Rocabert, A. Luna, F. Blaabjerg, and P. Rodriguez, "Control of power converters in ac microgrids," *Power Electronics, IEEE Transactions on*, vol. 27, no. 11, pp. 4734–4749, 2012.

[25] J. Wang, N. C. P. Chang, X. Feng, and A. Monti, "Design of a generalized control algorithm for parallel inverters for smooth microgrid transition operation," *IEEE Transactions on Industrial Electronics*, vol. 62, no. 8, pp. 4900–4914, 2015.

[26] H. Athari, M. Niroomand, and M. Ataei, "Review and classification of control systems in grid-tied inverters," *Renewable and Sustainable Energy Reviews*, vol. 72, pp. 1167–1176, 2017.

[27] R. M. Kamel, "New inverter control for balancing standalone micro-grid phase voltages: A review on mg power quality improvement," *Renewable and Sustainable Energy Reviews*, vol. 63, pp. 520–532, 2016.

[28] S. Kouro, M. A. Perez, J. Rodriguez, A. M. Llor, and H. A. Young, "Model predictive control: Mpc's role in the evolution of power electronics," *IEEE Industrial Electronics Magazine*, vol. 9, no. 4, pp. 8–21, 2015.

[29] S. Vazquez, A. Marquez, R. Aguilera, D. Quevedo, J. I. Leon, and L. G. Franquelo, "Predictive optimal switching sequence direct power control for grid-connected power converters," *IEEE Transactions on Industrial Electronics*, vol. 62, no. 4, pp. 2010–2020, 2015.

[30] T. Ohnishi, "Three phase pwm converter/inverter by means of instantaneous active and reactive power control," in *Industrial Electronics, Control and Instrumentation, 1991. Proceedings. IECON'91., 1991 International Conference on.* IEEE, 1991, pp. 819–824.

[31] N. Bottrell and T. C. Green, "Comparison of current-limiting strategies during fault ride-through of inverters to prevent latch-up and wind-up," *IEEE Transactions on Power Electronics*, vol. 29, no. 7, pp. 3786–3797, 2014.

[32] E. Afshari, G. R. Moradi, R. Rahimi, B. Farhangi, Y. Yang, F. Blaabjerg, and S. Farhangi, "Control strategy for three-phase grid-connected pv inverters enabling current limitation under unbalanced faults," *IEEE Transactions on Industrial Electronics*, vol. 64, no. 11, pp. 8908–8918, 2017.

[33] C. B. Tischer, J. R. Tibola, L. G. Scherer, and R. F. de Camargo, "Proportional-resonant control applied on voltage regulation of standalone seig for micro-hydro power generation," *IET Renewable Power Generation*, vol. 11, no. 5, pp. 593–602, 2017.

[34] M. R. Amin and S. A. Zulkifli, "A framework for selection of grid-inverter synchronisation unit: Harmonics, phase-angle and frequency," *Renewable and Sustainable Energy Reviews*, vol. 78, pp. 210–219, 2017.

[35] C. Buccella, C. Cecati, and H. Latafat, "Digital control of power converters—a survey," *IEEE Transactions on Industrial Informatics*, vol. 8, no. 3, pp. 437–447, 2012.

[36] J. I. Leon, S. Kouro, L. G. Franquelo, J. Rodriguez, and B. Wu, "The essential role and the continuous evolution of modulation techniques for voltage-source inverters in the past, present, and future power electronics," *IEEE Transactions on Industrial Electronics*, vol. 63, no. 5, pp. 2688–2701, 2016.

[37] J. Hu, J. Zhu, and D. G. Dorrell, "Model predictive control of grid-connected inverters for pv systems with flexible power regulation and switching frequency reduction," *IEEE Transactions on Industry Applications*, vol. 51, no. 1, pp. 587–594, 2015.

[38] ——, "In-depth study of direct power control strategies for power converters," *IET Power Electronics*, vol. 7, no. 7, pp. 1810–1820, 2014.

[39] S. Di Cairano, "An industry perspective on mpc in large volumes applications: Potential benefits and open challenges," *IFAC Proceedings Volumes*, vol. 45, no. 17, pp. 52–59, 2012.

[40] C. Bordons and C. Montero, "Basic principles of mpc for power converters: Bridging the gap between theory and practice," *IEEE Industrial Electronics Magazine*, vol. 9, no. 3, pp. 31–43, 2015.

[41] N. Panten, N. Hoffmann, and F. W. Fuchs, "Finite control set model predictive current control for grid-connected voltage-source converters with lcl filters: A study based on different state feedbacks," *IEEE Transactions on Power Electronics*, vol. 31, no. 7, pp. 5189–5200, 2016.

[42] M. Rivera, J. Rodriguez, and S. Vazquez, "Predictive control in power converters and electrical drives—part ii [guest editorial]," *IEEE Transactions on Industrial Electronics*, vol. 63, no. 7, pp. 4472–4474, 2016.

[43] J. Rodriguez, M. P. Kazmierkowski, J. R. Espinoza, P. Zanchetta, H. Abu-Rub, H. A. Young, and C. A. Rojas, "State of the art of finite control set model predictive control in power electronics," *IEEE Transactions on Industrial Informatics*, vol. 9, no. 2, pp. 1003–1016, 2013.

[44] S. Vazquez, J. I. Leon, L. G. Franquelo, J. Rodriguez, H. A. Young, A. Marquez, and P. Zanchetta, "Model predictive control: A review of its applications in power electronics," *IEEE Industrial Electronics Magazine*, vol. 8, no. 1, pp. 16–31, 2014.

[45] L. Wang, *Model predictive control system design and implementation using MATLAB®*. Springer Science & Business Media, 2009.

[46] G. A. Papafotiou, G. D. Demetriades, and V. G. Agelidis, "Technology readiness assessment of model predictive control in medium-and high-voltage power electronics," *IEEE Transactions on Industrial Electronics*, vol. 63, no. 9, pp. 5807–5815, 2016.

[47] T. Geyer, "A comparison of control and modulation schemes for medium-voltage drives: Emerging predictive control concepts versus pwm-based schemes," *IEEE Transactions on Industry Applications*, vol. 47, no. 3, pp. 1380–1389, 2011.

[48] J. Holtz, "Advanced pwm and predictive control—an overview," *IEEE Transactions on Industrial Electronics*, vol. 63, no. 6, pp. 3837–3844, 2016.

[49] M. M. Aghdam, L. Li, J. Zhu, and O. Palizban, "Finite control set model predictive control-a powerful control algorithm for grid-connected power converters," in *Industrial Electronics and Applications (ICIEA), 2016 IEEE 11th Conference on*. IEEE, 2016, pp. 2350–2355.

[50] T. Geyer and D. E. Quevedo, "Performance of multistep finite control set model predictive control for power electronics," *IEEE Transactions on power electronics*, vol. 30, no. 3, pp. 1633–1644, 2015.

[51] A. C. Z. de Souza, M. Santos, M. Castilla, J. Miret, L. G. de Vicuña, and D. Marujo, "Voltage security in ac microgrids: a power flow-based approach considering droop-controlled inverters," *IET Renewable Power Generation*, vol. 9, no. 8, pp. 954–960, 2015.

[52] J. Liu, S. Vazquez, H. Gao, and L. G. Franquelo, "Robust control for three-phase grid connected power converters via second order sliding mode," in *Industrial Technology (ICIT), 2015 IEEE International Conference on.* IEEE, 2015, pp. 1149–1154.

[53] C. A. Rojas, S. Kouro, M. Perez, and F. Villarroel, "Multiobjective fuzzy predictive torque control of an induction machine fed by a 3l-npc inverter," in *Predictive Control of Electrical Drives and Power Electronics (PRECEDE), 2015 IEEE International Symposium on.* IEEE, 2015, pp. 21–26.

[54] R. Errouissi, A. Al-Durra, and S. Muyeen, "Design and implementation of a nonlinear pi predictive controller for a grid-tied photovoltaic inverter," *IEEE Transactions on Industrial Electronics*, vol. 64, no. 2, pp. 1241–1250, 2017.

[55] F. Wang, S. A. Davari, Z. Chen, Z. Zhang, D. A. Khaburi, J. Rodríguez, and R. Kennel, "Finite control set model predictive torque control of induction machine with a robust adaptive observer," *IEEE Transactions on Industrial Electronics*, vol. 64, no. 4, pp. 2631–2641, 2017.

[56] M. Curkovic, K. Jezernik, and R. Horvat, "Fpga-based predictive sliding mode controller of a three-phase inverter," *IEEE Transactions on Industrial Electronics*, vol. 60, no. 2, pp. 637–644, 2013.

[57] I. M.-B. Hassine, M. W. Naouar, and N. Mrabet-Bellaaj, "Extended model predictive-sliding mode control for three-phase grid connected converters," *variations*, vol. 23, p. 24, 2016.

[58] F. Villarroel, J. R. Espinoza, C. A. Rojas, J. Rodriguez, M. Rivera, and D. Sbarbaro, "Multiobjective switching state selector for finite-states model predictive control based on fuzzy decision making in a matrix converter," *IEEE Transactions on Industrial Electronics*, vol. 60, no. 2, pp. 589–599, 2013.

[59] M. M. Aghdam, L. Li, and J. Zhu, "A model predictive power control method with longer prediction horizon for distributed power generations," in *Control, Automation, Robotics and Vision (ICARCV), 2016 14th International Conference on.* IEEE, 2016, pp. 1–6.

[60] C. Xia, T. Liu, T. Shi, and Z. Song, "A simplified finite-control-set model-predictive control for power converters," *IEEE Transactions on Industrial Informatics*, vol. 10, no. 2, pp. 991–1002, 2014.

[61] C. D. Fuentes, C. A. Rojas, H. Renaudineau, S. Kouro, M. A. Perez, and T. Meynard, "Experimental validation of a single dc bus cascaded h-bridge multilevel inverter for multistring photovoltaic systems," *IEEE Transactions on Industrial Electronics*, vol. 64, no. 2, pp. 930–934, 2017.

[62] J. Scoltock, T. Geyer, and U. K. Madawala, "Model predictive direct power control for grid-connected npc converters," *IEEE Transactions on industrial Electronics*, vol. 62, no. 9, pp. 5319–5328, 2015.

[63] M. M. Aghdam, R. P. Aguilera, L. Li, and J. Zhu, "Fuzzy-based self-tuning model predictive direct power control of grid-connected multilevel converters," in *Electrical Machines and Systems (ICEMS), 2017 20th International Conference on*. IEEE, 2017, pp. 1–6.

[64] R. P. Aguilera, P. Lezana, and D. E. Quevedo, "Switched model predictive control for improved transient and steady-state performance," *IEEE Transactions on Industrial Informatics*, vol. 11, no. 4, pp. 968–977, 2015.

[65] T. J. Vyncke, S. Thielemans, and J. A. Melkebeek, "Finite-set model-based predictive control for flying-capacitor converters: Cost function design and efficient fpga implementation," *IEEE Transactions on Industrial Informatics*, vol. 9, no. 2, pp. 1113–1121, 2013.

[66] F. Salinas, M. A. González, and M. F. Escalante, "Finite control set-model predictive control of a flying capacitor multilevel chopper using petri nets," *IEEE Transactions on Industrial Electronics*, vol. 63, no. 9, pp. 5891–5899, 2016.

[67] V. Yaramasu, B. Wu, and J. Chen, "Model-predictive control of grid-tied four-level diode-clamped inverters for high-power wind energy conversion systems," *IEEE transactions on power electronics*, vol. 29, no. 6, pp. 2861–2873, 2014.

[68] V. Yaramasu and B. Wu, "Model predictive decoupled active and reactive power control for high-power grid-connected four-level diode-clamped inverters," *IEEE Transactions on Industrial Electronics*, vol. 61, no. 7, pp. 3407–3416, 2014.

[69] F. Kieferndorf, P. Karamanakos, P. Bader, N. Oikonomou, and T. Geyer, "Model predictive control of the internal voltages of a five-level active neutral point clamped converter," in *Energy Conversion Congress and Exposition (ECCE), 2012 IEEE*. IEEE, 2012, pp. 1676–1683.

[70] J. D. Barros and J. F. Silva, "Optimal predictive control of three-phase npc multilevel converter for power quality applications," *IEEE Transactions on Industrial Electronics*, vol. 55, no. 10, pp. 3670–3681, 2008.

[71] S. Debnath, J. Qin, B. Bahrani, M. Saeedifard, and P. Barbosa, "Operation, control, and applications of the modular multilevel converter: A review," *IEEE transactions on power electronics*, vol. 30, no. 1, pp. 37–53, 2015.

[72] J.-W. Moon, J.-S. Gwon, J.-W. Park, D.-W. Kang, and J.-M. Kim, "Model predictive control with a reduced number of considered states in a modular multilevel converter for hvdc system," *IEEE Transactions on Power Delivery*, vol. 30, no. 2, pp. 608–617, 2015.

[73] M. R. Nasiri, S. Farhangi, and J. Rodriguez, "Model predictive control of multilevel chb statcom in wind farm application using diophantine equations," *IEEE Transactions on Industrial Electronics*, 2018.

[74] L. Ben-Brahim, A. Gastli, M. Trabelsi, K. A. Ghazi, M. Houchati, and H. Abu-Rub, "Modular multilevel converter circulating current reduction using model predictive control," *IEEE Transactions on Industrial Electronics*, vol. 63, no. 6, pp. 3857–3866, 2016.

[75] P. Liu, Y. Wang, W. Cong, and W. Lei, "Grouping-sorting-optimized model predictive control for modular multilevel converter with reduced computational load," *IEEE Transactions on Power Electronics*, vol. 31, no. 3, pp. 1896–1907, 2016.

[76] J. Böcker, B. Freudenberg, A. The, and S. Dieckerhoff, "Experimental comparison of model predictive control and cascaded control of the modular multilevel converter," *IEEE Transactions on Power Electronics*, vol. 30, no. 1, pp. 422–430, 2015.

[77] Z. Gong, P. Dai, X. Yuan, X. Wu, and G. Guo, "Design and experimental evaluation of fast model predictive control for modular multilevel converters," *IEEE Transactions on Industrial Electronics*, vol. 63, no. 6, pp. 3845–3856, 2016.

[78] M. Vatani, B. Bahrani, M. Saeedifard, and M. Hovd, "Indirect finite control set model predictive control of modular multilevel converters," *IEEE Transactions on Smart Grid*, vol. 6, no. 3, pp. 1520–1529, 2015.

[79] H. Dan, Q. Zhu, T. Peng, S. Yao, and P. Wheeler, "Preselection algorithm based on predictive control for direct matrix converter," *IET Electric Power Applications*, vol. 11, no. 5, pp. 768–775, 2017.

[80] O. Gulbudak and E. Santi, "Fpga-based model predictive controller for direct matrix converter," *IEEE Transactions on Industrial Electronics*, vol. 63, no. 7, pp. 4560–4570, 2016.

[81] J. Zhang, L. Li, T. He, M. M. Aghdam, and D. G. Dorrell, "Investigation of direct matrix converter working as a versatile converter (ac/ac, ac/dc, dc/ac, dc/dc conversion) with predictive control," in *43rd Annual Conference Industrial Electronics Society*, 2017.

[82] P. M. Sanchez, O. Machado, E. J. B. Peña, F. J. Rodríguez, and F. J. Meca, "Fpga-based implementation of a predictive current controller for power converters," *IEEE Transactions on Industrial Informatics*, vol. 9, no. 3, pp. 1312–1321, 2013.

[83] S. Lucia, D. Navarro, O. Lucia, P. Zometa, and R. Findeisen, "Optimized fpga implementation of model predictive control for embedded systems using high level synthesis tool," *IEEE Transactions on Industrial Informatics*, 2017.

[84] Z. Zhang, H. Fang, F. Gao, J. Rodriguez, and R. Kennel, "Multiple-vector model predictive power control for grid-tied wind turbine system with enhanced steady-state control performance," *IEEE Transactions on Industrial Electronics*, vol. 64, no. 8, pp. 6287–6298, 2017.

[85] M. Habibullah, D. D.-C. Lu, D. Xiao, and M. F. Rahman, "Finite-state predictive torque control of induction motor supplied from a three-level npc voltage source inverter," *IEEE Transactions on Power Electronics*, vol. 32, no. 1, pp. 479–489, 2017.

[86] M. Uddin, S. Mekhilef, and M. Rivera, "Experimental validation of minimum cost function-based model predictive converter control with efficient reference tracking," *IET Power Electronics*, vol. 8, no. 2, pp. 278–287, 2014.

[87] E. J. Bueno, A. Hernandez, F. J. Rodriguez, C. Girón, R. Mateos, and S. Cobreces, "A dsp-and fpga-based industrial control with high-speed communication interfaces for grid converters applied to distributed power generation systems," *IEEE transactions on industrial electronics*, vol. 56, no. 3, pp. 654–669, 2009.

[88] J. Hu, J. Zhu, and D. G. Dorrell, "Model predictive control of inverters for both islanded and grid-connected operations in renewable power generations," *IET Renewable Power Generation*, vol. 8, no. 3, pp. 240–248, 2013.

[89] B. S. Riar, T. Geyer, and U. K. Madawala, "Model predictive direct current control of modular multilevel converters: Modeling, analysis, and experimental evaluation," *IEEE Transactions on Power Electronics*, vol. 30, no. 1, pp. 431–439, 2015.

[90] Z. Zhang, F. Wang, T. Sun, J. Rodríguez, and R. Kennel, "Fpga-based experimental investigation of a quasi-centralized model predictive control for back-to-back converters," *IEEE Transactions on Power Electronics*, vol. 31, no. 1, pp. 662–674, 2016.

[91] T. J. Besselmann, S. Almér, P. Jörg, H. J. Ferreau *et al.*, "Model predictive control in the multi-megawatt range," *IEEE Transactions on Industrial Electronics*, vol. 63, no. 7, pp. 4641–4648, 2016.

[92] R. P. Aguilera and D. E. Quevedo, "Predictive control of power converters: Designs with guaranteed performance," *IEEE Transactions on Industrial Informatics*, vol. 11, no. 1, pp. 53–63, 2015.

[93] M. P. Akter, S. Mekhilef, N. M. L. Tan, and H. Akagi, "Modified model predictive control of a bidirectional ac–dc converter based on lyapunov function for energy storage systems," *IEEE Transactions on Industrial Electronics*, vol. 63, no. 2, pp. 704–715, 2016.

[94] T. Barisa, S. Iles, D. Sumina, and J. Matusko, "Model predictive direct current control of permanent magnet synchronous generator based on flexible lyapunov function considering converter dead time," *IEEE Transactions on Industry Applications*, 2018.

[95] R. P. Aguilera, P. Lezana, and D. E. Quevedo, "Finite-control-set model predictive control with improved steady-state performance," *IEEE Transactions on Industrial Informatics*, vol. 9, no. 2, pp. 658–667, 2013.

[96] E.-K. Kim, F. Mwasilu, H. H. Choi, and J.-W. Jung, "An observer-based optimal voltage control scheme for three-phase ups systems," *IEEE Transactions on Industrial Electronics*, vol. 62, no. 4, pp. 2073–2081, 2015.

[97] W. Xie, X. Wang, F. Wang, W. Xu, R. M. Kennel, D. Gerling, and R. D. Lorenz, "Finite-control-set model predictive torque control with a deadbeat solution for pmsm drives," *IEEE Transactions on Industrial Electronics*, vol. 62, no. 9, pp. 5402–5410, 2015.

[98] G. Mirzaeva, G. C. Goodwin, B. P. McGrath, C. Teixeira, and M. E. Rivera, "A generalized mpc framework for the design and comparison of vsi current controllers," *IEEE Transactions on Industrial Electronics*, vol. 63, no. 9, pp. 5816–5826, 2016.

[99] S. Vazquez, R. P. Aguilera, P. Acuna, J. Pou, J. I. Leon, L. G. Franquelo, and V. G. Agelidis, "Model predictive control for single-phase npc converters based on optimal switching sequences," *IEEE Transactions on Industrial Electronics*, vol. 63, no. 12, pp. 7533–7541, 2016.

[100] Z. Zhang, H. Fang, and R. Kennel, "Novel ripple reduced direct model predictive control of three-level npc active front end with reduced computational effort," in *Predictive Control of Electrical Drives and Power Electronics (PRECEDE), 2015 IEEE International Symposium on.* IEEE, 2015, pp. 32–37.

[101] B. Gutierrez and S. Kwak, "Model predictive control with preselection technique for reduced calculation burden in modular multilevel converters," *IEEE Transactions on Power Electronics*, 2018.

[102] B. Stellato, T. Geyer, and P. J. Goulart, "High-speed finite control set model predictive control for power electronics," *IEEE Transactions on power electronics*, vol. 32, no. 5, pp. 4007–4020, 2017.

[103] P. Cortes, J. Rodriguez, C. Silva, and A. Flores, "Delay compensation in model predictive current control of a three-phase inverter," *IEEE Transactions on Industrial Electronics*, vol. 59, no. 2, pp. 1323–1325, 2012.

[104] J. D. Barros, J. F. A. Silva, and É. G. Jesus, "Fast-predictive optimal control of npc multilevel converters," *IEEE Transactions on Industrial Electronics*, vol. 60, no. 2, pp. 619–627, 2013.

[105] P. Karamanakos, T. Geyer, and R. Kennel, "A computationally efficient model predictive control strategy for linear systems with integer inputs," *IEEE Transactions on Control Systems Technology*, vol. 24, no. 4, pp. 1463–1471, 2016.

[106] M. Nauman and A. Hasan, "Efficient implicit model-predictive control of a three-phase inverter with an output lc filter," *IEEE Transactions on Power Electronics*, vol. 31, no. 9, pp. 6075–6078, 2016.

[107] L. Tarisciotti, G. L. Calzo, A. Gaeta, P. Zanchetta, F. Valencia, and D. Sáez, "A distributed model predictive control strategy for back-to-back converters," *IEEE Transactions on Industrial Electronics*, vol. 63, no. 9, pp. 5867–5878, 2016.

[108] A. Dekka, B. Wu, V. Yaramasu, and N. R. Zargari, "Integrated model predictive control with reduced switching frequency for modular multilevel converters," *IET Electric Power Applications*, vol. 11, no. 5, pp. 857–863, 2017.

[109] V. Yaramasu, B. Wu, M. Rivera, and J. Rodriguez, "A new power conversion system for megawatt pmsg wind turbines using four-level converters and a simple control scheme based on two-step model predictive strategy—part ii: Simulation and experimental analysis," *IEEE Journal of Emerging and Selected Topics in Power Electronics*, vol. 2, no. 1, pp. 14–25, 2014.

[110] L. Tarisciotti, A. Formentini, A. Gaeta, M. Degano, P. Zanchetta, R. Rabbeni, and M. Pucci, "Model predictive control for shunt active filters with fixed switching frequency," *IEEE Transactions on Industry Applications*, vol. 53, no. 1, pp. 296–304, 2017.

[111] D. Mathew, A. Shukla, and S. Bandyopadhyay, "Modified predictive current control of neutral-point clamped converter with reduced switching frequency," in *Applied Power Electronics Conference and Exposition (APEC), 2016 IEEE*. IEEE, 2016, pp. 3286–3290.

[112] A. M. Bozorgi, H. Gholami-Khesht, M. Farasat, S. Mehraeen, and M. Monfared, "Model predictive direct power control of three-phase grid-connected converters with fuzzy-based duty cycle modulation," *IEEE Transactions on Industry Applications*, 2018.

[113] H. Fang, Z. Zhang, X. Feng, and R. Kennel, "Ripple-reduced model predictive direct power control for active front-end power converters with extended switching vectors and time-optimised control," *IET Power Electronics*, vol. 9, no. 9, pp. 1914–1923, 2016.

[114] Y. Zhang and H. Yang, "Two-vector-based model predictive torque control without weighting factors for induction motor drives," *IEEE Transactions on Power Electronics*, vol. 31, no. 2, pp. 1381–1390, 2016.

[115] Z. Song, W. Chen, and C. Xia, "Predictive direct power control for three-phase grid-connected converters without sector information and voltage vector selection," *IEEE Transactions on Power Electronics*, vol. 29, no. 10, pp. 5518–5531, 2014.

[116] M. H. Vafaie, B. M. Dehkordi, P. Moallem, and A. Kiyoumarsi, "Minimizing torque and flux ripples and improving dynamic response of pmsm using a voltage vector with optimal parameters," *IEEE Transactions on Industrial Electronics*, vol. 63, no. 6, pp. 3876–3888, 2016.

[117] Y. Cho, K.-B. Lee, J.-H. Song, and Y. I. Lee, "Torque-ripple minimization and fast dynamic scheme for torque predictive control of permanent-magnet synchronous motors," *IEEE Transactions on Power Electronics*, vol. 30, no. 4, pp. 2182–2190, 2015.

[118] A. Dekka, B. Wu, V. Yaramasu, and N. R. Zargari, "Dual-stage model predictive control with improved harmonic performance for modular multilevel

converter," *IEEE Transactions on Industrial Electronics*, vol. 63, no. 10, pp. 6010–6019, 2016.

[119] M. Sharifzadeh, A. Sheikholeslami, H. Vahedi, H. Ghoreishy, P.-A. Labbé, and K. Al-Haddad, "Optimised harmonic elimination modulation extended to four-leg neutral-point-clamped inverter," *IET Power Electronics*, vol. 9, no. 3, pp. 441–448, 2016.

[120] M. S. Dahidah, G. Konstantinou, and V. G. Agelidis, "A review of multilevel selective harmonic elimination pwm: formulations, solving algorithms, implementation and applications," *IEEE Transactions on Power Electronics*, vol. 30, no. 8, pp. 4091–4106, 2015.

[121] H. Gao, B. Wu, D. Xu, R. P. Aguilera, and P. Acuna, "Model predictive switching pattern control for current-source converters with space-vector-based selective harmonic elimination," *IEEE Transactions on Power Electronics*, vol. 32, no. 8, pp. 6558–6569, 2017.

[122] R. P. Aguilera, P. Acuña, P. Lezana, G. Konstantinou, B. Wu, S. Bernet, and V. G. Agelidis, "Selective harmonic elimination model predictive control for multilevel power converters," *IEEE Transactions on Power Electronics*, vol. 32, no. 3, pp. 2416–2426, 2017.

[123] D.-K. Choi and K.-B. Lee, "Dynamic performance improvement of ac/dc converter using model predictive direct power control with finite control set," *IEEE Transactions on Industrial Electronics*, vol. 62, no. 2, pp. 757–767, 2015.

[124] M. Siami, D. A. Khaburi, and J. Rodríguez, "Torque ripple reduction of predictive torque control for pmsm drives with parameter mismatch," *IEEE Transactions on Power Electronics*, vol. 32, no. 9, pp. 7160–7168, 2017.

[125] M. Siami, D. A. Khaburi, A. Abbaszadeh, and J. Rodríguez, "Robustness improvement of predictive current control using prediction error correction for permanent-magnet synchronous machines," *IEEE Transactions on Industrial Electronics*, vol. 63, no. 6, pp. 3458–3466, 2016.

[126] H. A. Young, M. A. Perez, and J. Rodriguez, "Analysis of finite-control-set model predictive current control with model parameter mismatch in a three-phase inverter," *IEEE Transactions on Industrial Electronics*, vol. 63, no. 5, pp. 3100–3107, 2016.

[127] M. G. Judewicz, S. A. Gonzalez, N. I. Echeverria, J. R. Fischer, and D. O. Carrica, "Generalized predictive current control (gpcc) for grid-tie three-phase inverters," *IEEE Transactions on Industrial Electronics*, vol. 63, no. 7, pp. 4475–4484, 2016.

[128] C. A. Rojas, J. Rodriguez, F. Villarroel, J. R. Espinoza, C. A. Silva, and M. Trincado, "Predictive torque and flux control without weighting factors," *IEEE Transactions on Industrial Electronics*, vol. 60, no. 2, pp. 681–690, 2013.

[129] M. Siami, H. K. Savadkoohi, A. Abbaszadeh, D. Khaburi, J. Rodriguez, and M. Rivera, "Predictive torque control of a permanent magnet synchronous motor fed by a matrix converter without weighting factor," in *Power Electronics and Drive Systems Technologies Conference (PEDSTC), 2016 7th.* IEEE, 2016, pp. 614–619.

[130] P. Acuna, L. Morán, M. Rivera, R. Aguilera, R. Burgos, and V. G. Agelidis, "A single-objective predictive control method for a multivariable single-phase three-level npc converter-based active power filter," *IEEE Transactions on Industrial Electronics*, vol. 62, no. 7, pp. 4598–4607, 2015.

[131] Y. Zhang, Y. Peng, and H. Yang, "Performance improvement of two-vectors-based model predictive control of pwm rectifier," *IEEE Transactions on Power Electronics*, vol. 31, no. 8, pp. 6016–6030, 2016.

[132] L. Guo, X. Zhang, S. Yang, Z. Xie, L. Wang, and R. Cao, "Simplified model predictive direct torque control method without weighting factors for permanent magnet synchronous generator-based wind power system," *IET Electric Power Applications*, vol. 11, no. 5, pp. 793–804, 2017.

[133] D. Zhou, J. Zhao, and Y. Liu, "Online tuning of weighting factors based on sugeno fuzzy method in predictive torque control of four-switch three-phase inverter-fed im," in *Power Electronics, Electrical Drives, Automation and Motion (SPEEDAM), 2016 International Symposium on.* IEEE, 2016, pp. 734–739.

[134] T. Geyer and D. E. Quevedo, "Multistep finite control set model predictive control for power electronics," *IEEE Transactions on power electronics*, vol. 29, no. 12, pp. 6836–6846, 2014.

[135] T. Dragičević, "Model predictive control of power converters for robust and fast operation of ac microgrids," *IEEE Transactions on Power Electronics*, vol. 33, no. 7, pp. 6304–6317, 2018.

[136] R. Baidya, R. P. Aguilera, P. Acuna, S. Vazquez, and H. du Toit Mouton, "Multistep model predictive control for cascaded h-bridge inverters: Formulation and analysis," *IEEE Transactions on Power Electronics*, vol. 33, no. 1, pp. 876–886, 2018.

[137] P. Karamanakos, T. Geyer, and R. Kennel, "Reformulation of the long-horizon direct model predictive control problem to reduce the computational effort," in *Energy Conversion Congress and Exposition (ECCE), 2014 IEEE.* IEEE, 2014, pp. 3512–3519.

[138] P. KaraMaNaKOS, T. Geyer, N. Oikonomou, F. D. KIEFErNDOrF, and S. MaNIaS, "Direct model predictive control: A review of strategies that achieve long prediction intervals for power electronics," *IEEE Industrial Electronics Magazine*, vol. 8, no. 1, pp. 32–43, 2014.

[139] J. Scoltock, T. Geyer, and U. Madawala, "Model predictive direct power control for a grid-connected converter with an lcl-filter," in *Industrial Technology (ICIT), 2013 IEEE International Conference on.* IEEE, 2013, pp. 588–593.

[140] J. Wang, J. D. Yan, L. Jiang, and J. Zou, "Delay-dependent stability of single-loop controlled grid-connected inverters with lcl filters," *IEEE Transactions on Power Electronics*, vol. 31, no. 1, pp. 743–757, 2016.

[141] X. Zhang, Y. Wang, C. Yu, L. Guo, and R. Cao, "Hysteresis model predictive control for high-power grid-connected inverters with output lcl filter," *IEEE Transactions on Industrial Electronics*, vol. 63, no. 1, pp. 246–256, 2016.

[142] P. Falkowski and A. Sikorski, "Finite control set model predictive control for grid-connected ac–dc converters with lcl filter," *IEEE Transactions on Industrial Electronics*, vol. 65, no. 4, pp. 2844–2852, 2018.

[143] V. Yaramasu, M. Rivera, M. Narimani, B. Wu, and J. Rodriguez, "Model predictive approach for a simple and effective load voltage control of four-leg inverter with an output *lc* filter," *IEEE Transactions on Industrial Electronics*, vol. 61, no. 10, pp. 5259–5270, 2014.

Chapter 3

FINITE CONTROL SET-MODEL PREDICTIVE CONTROL OF POWER CONVERTERS: DELAY-TIME COMPENSATION

3.1 Introduction

In this chapter, a notable drawback of the conventional finite control set model predictive control (FCS-MPC) is explored. While FCS-MPC carries some benefits [1, 2], the algorithm needs to be reformed for various purposes, mostly due to the variety of the plant characteristics that cause some challenges for the design. In FCS-MPC, the main problem associated with real-time implementation (RTI) via the digital signal processor (DSP) is the computational load which leads to a significant delay time [3, 4]. As a result, the system performance will be impaired if the delay time is not reflected in the system model. This issue will be more evident for a longer horizon prediction or multilevel converters where the number of switching possibilities is increased considerably [5–7]. Therefore, FCS-MPC will face a computational challenge and impracticality for RTI and lead to the overrun. An overrun state happens if a task is demanded to start, but its previous execution has not completed yet. In Fig. 3.1 the action of an RTI is compared to a simulation program where the computational time is not reflected. $\mathbf{x}(k)$ and $\mathbf{u}(k)$ are the state, and input vector at the current instant. Excluding the redundant voltage vectors and second-step prediction are common methods to compensate the computation load or time delay [8]. Moreover, the computational complexity increases with the number of considered constraints and objectives.

3.2 Theory of FCS-MPC

3.2.1 Conventional FCS-MPC principles

Aforementioned, in FCS-MPC, developing a precise dynamic model is essential [9]. The dynamic model of the power converter in the discrete-time domain for conventional FCS-MPC can be written in the state space form as

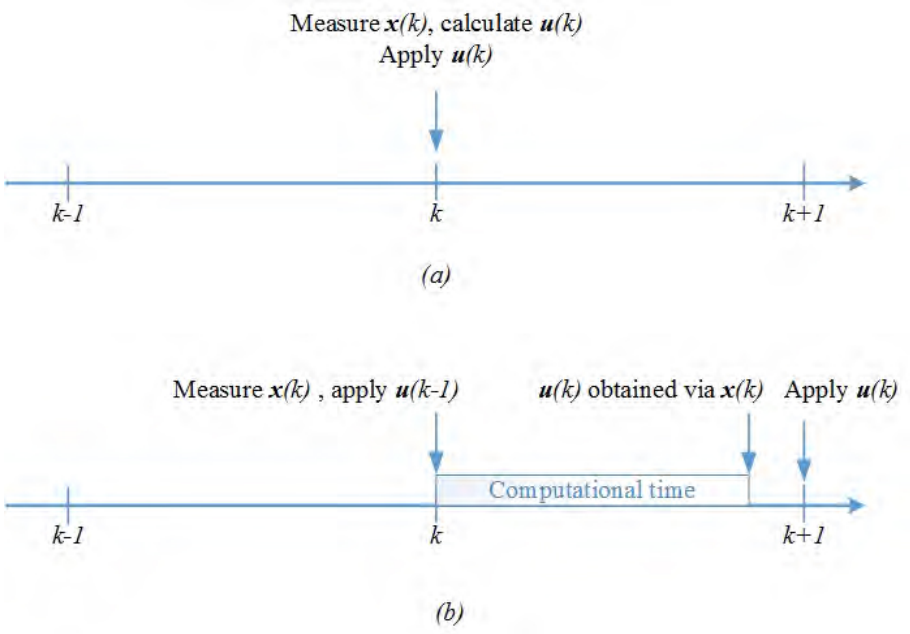

Figure 3.1: Behavior of simulation program versus RTI

$$\begin{aligned} \mathbf{x}_i(k+1) &= A\mathbf{x}(k) + B\mathbf{u}_i(k) \\ \mathbf{y}_i(k+1) &= C\mathbf{x}_i(k+1) \end{aligned} \tag{3.1}$$

$\mathbf{x}(k), \mathbf{u}(k)$, and $\mathbf{y}(k)$ are the state, input, and output vector at the time instant kT_s, respectively, T_s is the sampling interval, $i = 1, ..., n$ is the index of possible control actions, and n is the total number of possibilities. A, B and C are discrete matrices which are derived from discretization of the continuous-time model. The state variable $x(k)$, is accessible via measurement. The future state variables at the step $k + N$, where N is the prediction horizon, can be represented as

$$\mathbf{Y}_i(k) = \begin{bmatrix} CA \\ CA^2 \\ . \\ . \\ . \\ CA^N \end{bmatrix} \mathbf{x}(k) + \begin{bmatrix} CB & 0 & ... & 0 \\ CAB & CB & ... & 0 \\ . & . & . & . \\ . & . & . & . \\ . & . & . & . \\ CA^{N-1}B & ... & ... & CB \end{bmatrix} \mathbf{U}_i(k) \tag{3.2}$$

$$\begin{aligned} \mathbf{Y}_i(k) &= \begin{bmatrix} \mathbf{y}_i(k+1) & \mathbf{y}_i(k+2) & ... & \mathbf{y}_i(k+N) \end{bmatrix}^T \\ \mathbf{U}_i(k) &= \begin{bmatrix} \mathbf{u}_i(k) & \mathbf{u}_i(k+1) & ... & \mathbf{u}_i(k+N-1) \end{bmatrix}^T \end{aligned} \tag{3.3}$$

where $\mathbf{Y}_i$ and $\mathbf{U}_i$ are the output and input sequences for N prediction horizon. The control objective, in the case of tracking the reference, $\mathbf{Y}^*$, can be defined as

$$J_i(k) = ||\mathbf{Y}^*(k) - \mathbf{Y}_i(k)||_2^2 \tag{3.4}$$

The optimization problem can be solved via minimization of the objective function

$$U_{opt}(k) = \arg\min_{U_i(k)} J_i(k) \tag{3.5}$$

Succeeding to the receding horizon control (RHC) concept [10], in Fig. 3.2, the first element of the optimizing sequence $U_{opt}(k)$ is applied to the insulated-gate bipolar transistor (IGBT) switches. In RTI [11, 12], a major part of sampling time may be used to determine the control sequence, causing a considerable delay. This delay time has to be reflected in the controller as illustrated in Fig. 3.3. In contrast to Fig. 3.1, the system state at the next instant is predicted and used to obtain the values of the input variables. As the number of possible switching states increases, the delay time will increases as well. The effect of such a delay will be reflected in the prediction, particularly when a one-step horizon algorithm is in place.

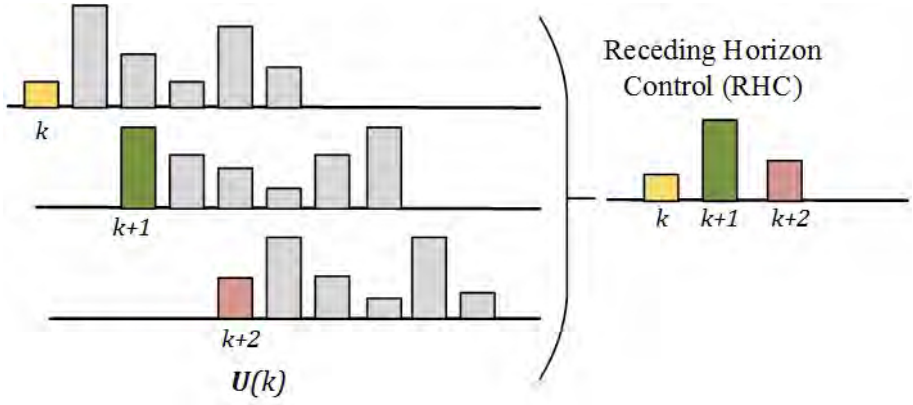

Figure 3.2: Receding horizon control principle

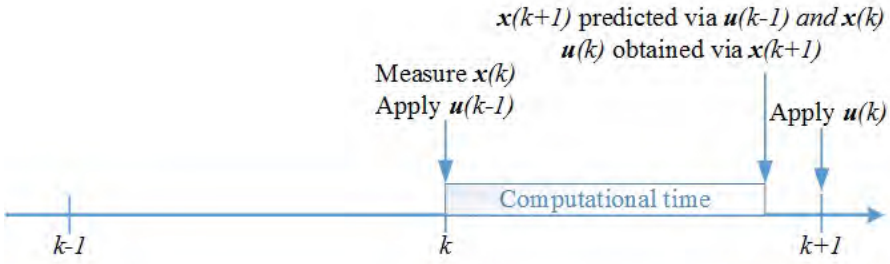

Figure 3.3: FCS-MPC principle

3.2.2 Proposed time-delayed FCS-MPC

A general method to deal with the delay is two-step prediction ahead rather than one-step [8]. As the delay is not constant for RTI, a time-delayed model is proposed. Based on this model, the system performance will be improved with enhanced system stability and reliability. If we consider a delay time τ in the system input, the state space system model in the continuous-time domain will be as follows,

$$\begin{aligned} \frac{d\mathbf{x}}{dt} &= D\mathbf{x}(t) + F\mathbf{u}(t-\tau) \\ \mathbf{y}(t) &= G\mathbf{x}(t) \end{aligned} \tag{3.6}$$

where D, F and G are matrices derived from the system model. Through discretization as can be seen in Fig. 3.4, by applying the delay time, τ, between kT_S and $(k+1)T_S$, the state space model of the system can be obtained as

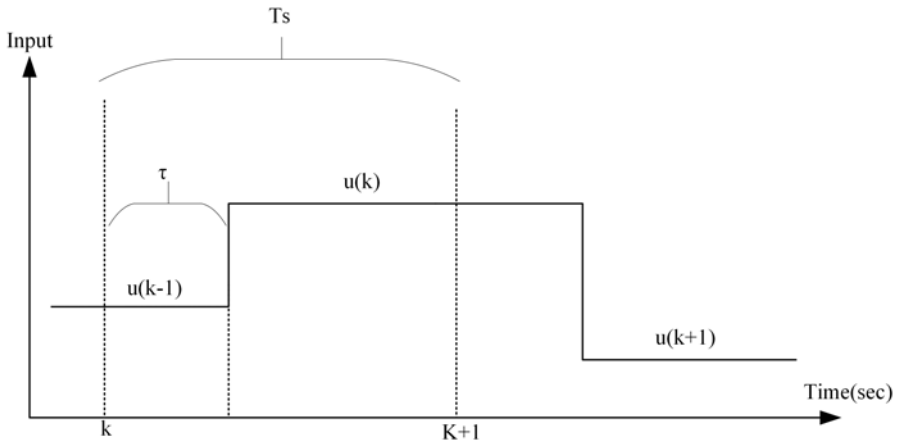

Figure 3.4: Graphical representation of time-delayed MPC

$$\begin{aligned} \mathbf{x}_i(k+1) &= A\mathbf{x}(k) + B_1\mathbf{u}_i(k-1) + B_2\mathbf{u}_i(k) \\ \mathbf{y}_i(k+1) &= C\mathbf{x}_i(k+1) \end{aligned} \tag{3.7}$$

where A, B_1, and B_2 can be calculated as follows,

$$\begin{aligned} A &= e^{DT_s} \\ B_1 &= e^{D(T_s-\tau)} \int_0^{\tau} e^{D\delta} F d\delta \\ B_2 &= \int_0^{T_s-\tau} e^{D\delta} F d\delta \end{aligned} \tag{3.8}$$

Following the RHC principle and the assumption of $u(k) = ... = u(k+N-1)$, the future output variables can be represented as

$$\mathbf{Y}_i(k) = \begin{bmatrix} CA \\ CA^2 \\ \cdot \\ \cdot \\ \cdot \\ CA^N \end{bmatrix} \mathbf{x}(k) + \begin{bmatrix} CB_1 \\ CAB_1 \\ \cdot \\ \cdot \\ \cdot \\ CA^{N-1}B_1 \end{bmatrix} \mathbf{u}(k-1) + \begin{bmatrix} CB_2 \\ C(AB_2 + B_1 + B_2) \\ \cdot \\ \cdot \\ \cdot \\ \sum_{l=0}^{N-2} C(A^{N-l-1} + A^{N-l-2}B_1) + CB_2 \end{bmatrix} \mathbf{U}_i(k) \tag{3.9}$$

$$\mathbf{Y}_i(k) = \begin{bmatrix} \mathbf{y}_i(k+1) & \mathbf{y}_i(k+2) & ... & \mathbf{y}_i(k+N) \end{bmatrix}^T \tag{3.10}$$

3.3 Case Study I: Two-level Three-phase Grid-connected Voltage Source Inverter (VSI)

3.3.1 Mathematical model of grid-connected VSI

This topology is broadly used by industry applications and dominates the market at low voltage (LV). The structure of the two-level three-phase (2L-3Ph) grid-connected inverter is represented in Fig. 3.5. It is formed by a complementary pair of power switches for each phase and linked to the utility grid through an RL filter.

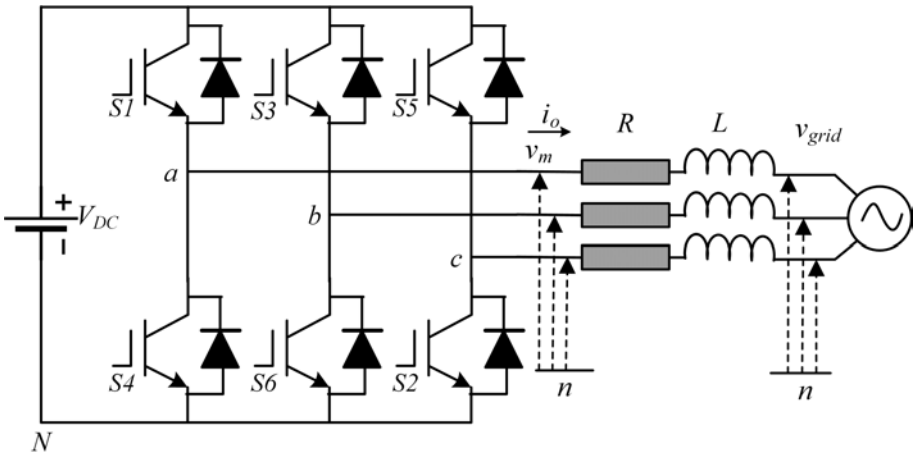

Figure 3.5: Two-level three-phase grid-tied inverter

There are a total number of eight possible output voltage vectors for this topology ($m = 2^3 = 8$) as follows,

$$v_m = \begin{cases} \frac{2}{3} e^{j(m-1)\frac{\pi}{3}} V_{DC}, & \text{if } m = 1, ..., 6 \\ 0 & \text{if } m = 0, 7 \end{cases} \tag{3.11}$$

The graphical representation of the eight voltage vectors in stationary reference frame is illustrated in Fig. 3.6, which consists of six active $v_1, ..., v_6$ and two zero v_0, v_7 voltage vectors.

The mathematical model of this system can be formulated in the stationary frame via matrix M (Clarke's transformation) which is a mathematical transformation for simplification in the analysis of the three-phase system [13, 14].

$$M = \frac{2}{3} \begin{bmatrix} 1 & -\frac{1}{2} & -\frac{1}{2} \\ 0 & \frac{\sqrt{3}}{2} & -\frac{\sqrt{3}}{2} \end{bmatrix} \tag{3.12}$$

$$v_m^{\alpha\beta} = L \frac{di_o^{\alpha\beta}}{dt} + R i_o^{\alpha\beta} + v_{grid}^{\alpha\beta} \tag{3.13}$$

Furthermore, for a balanced and positive sequence system, the active power P and the reactive power Q can be obtained in $\alpha\beta$-stationary frame as

$$\begin{aligned} P &= \frac{3}{2}(v_{grid}^{\alpha} i_o^{\alpha} + v_{grid}^{\beta} i_o^{\beta}) \\ Q &= \frac{3}{2}(v_{grid}^{\beta} i_o^{\alpha} - v_{grid}^{\alpha} i_o^{\beta}) \end{aligned} \tag{3.14}$$

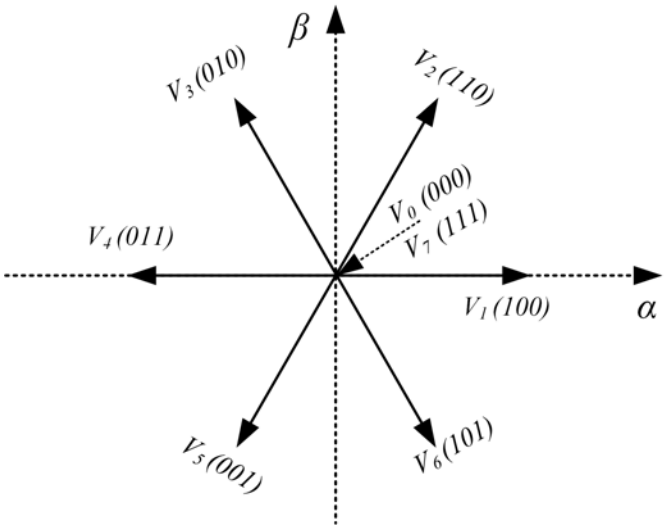

Figure 3.6: The graphical representation of the voltage vectors

For the power flow control based on direct power control (DPC) strategy [15], we can take the first derivative from Eq. (3.14) to obtain the mathematical model of the grid-connected VSI as follows,

$$\begin{bmatrix} \frac{dP}{dt} \\ \frac{dQ}{dt} \\ \frac{dv^{\alpha}_{grid}}{dt} \\ \frac{dv^{\beta}_{grid}}{dt} \end{bmatrix} = \begin{bmatrix} -\frac{R}{L} & -\omega & -\frac{3v^{\alpha}_{grid}}{2L} & -\frac{3v^{\beta}_{grid}}{2L} \\ \omega & -\frac{R}{L} & 0 & 0 \\ 0 & 0 & 0 & -\omega \\ 0 & 0 & \omega & 0 \end{bmatrix} \begin{bmatrix} P \\ Q \\ v^{\alpha}_{grid} \\ v^{\beta}_{grid} \end{bmatrix} + \frac{3}{2L} \begin{bmatrix} v^{\alpha}_{grid} & v^{\beta}_{grid} \\ v^{\beta}_{grid} & -v^{\alpha}_{grid} \end{bmatrix} \begin{bmatrix} v^{\alpha}_{m} \\ v^{\beta}_{m} \end{bmatrix} \quad (3.15)$$

As can be seen, the system model is in the non-linear form, and therefore, to predict the future system behavior, linearization approach is applied. Define the following state and control variables,

$$\mathbf{x} = \begin{bmatrix} P & Q & v^{\alpha}_{grid} & v^{\beta}_{grid} \end{bmatrix}^T, \mathbf{u} = \begin{bmatrix} v^{\alpha}_{m} & v^{\beta}_{m} \end{bmatrix}^T \quad (3.16)$$

Define $\Delta x = x - \bar{x}$, $\Delta u = u - \bar{u}$, where $\bar{x}$ and $\bar{u}$ are the steady state, and x is the state variables including the active power P, reactive power Q, grid voltages in $\alpha\beta$-frame. Then the linearized system model is as follows,

$$\frac{d\Delta\mathbf{x}}{dt} = D\Delta\mathbf{x}(t) + F\Delta\mathbf{u}(t) \quad (3.17)$$

$$D = \begin{bmatrix} -\frac{R}{L} & -\omega & -\frac{6}{2L}\bar{v}^{\alpha}_{grid} + \frac{3}{2L}\bar{v}^{\alpha}_{m} & -\frac{6}{2L}\bar{v}^{\beta}_{grid} + \frac{3}{2L}\bar{v}^{\beta}_{m} \\ \omega & -\frac{R}{L} & -\frac{3}{2L}\bar{v}^{\beta}_{m} & \frac{3}{2L}\bar{v}^{\alpha}_{m} \\ 0 & 0 & 0 & -\omega \\ 0 & 0 & \omega & 0 \end{bmatrix}, F = \frac{3}{2L} \begin{bmatrix} \bar{v}^{\alpha}_{grid} & \bar{v}^{\beta}_{grid} \\ \bar{v}^{\beta}_{grid} & -\bar{v}^{\alpha}_{grid} \\ 0 & 0 \\ 0 & 0 \end{bmatrix} \quad (3.18)$$

By discretizing the state space model, the future value of output variables can be estimated. Backward Euler method has been used for discretizing the plant. In this way, the future value of the system inputs is used to predict the future value of the controlled variables. If the system dynamics is described by,

$$\frac{dx}{dt} = f(x, u) \tag{3.19}$$

where x and u represent the controlled variable and input, a backward Euler can be applied as

$$x(k+1) = x(k) + T_s f(x(k+1), u(k+1)) \tag{3.20}$$

3.3.2 Conventional FCS-MPC

To improve the system stability and power quality, flexible active and reactive power regulation based on demand have to be gained. Hence, the goal of MPC is to control the active and reactive powers [16, 17]. The MPC chooses the optimal switching sequence in order to control the power flow of the grid-tied VSI. This strategy requires a predictive model of the instantaneous power evolution. In the stationary reference frame and for a balanced three-phase system, the predicted active and the reactive powers injected into the grid can be defined as

$$y = \begin{bmatrix} P(k+1) \\ Q(k+1) \end{bmatrix} = \frac{3}{2} \begin{bmatrix} v_{grid}^{\alpha} & v_{grid}^{\beta} \\ -v_{grid}^{\beta} & v_{grid}^{\alpha} \end{bmatrix} \begin{bmatrix} i_o^{\alpha}(k+1) \\ i_o^{\beta}(k+1) \end{bmatrix} \tag{3.21}$$

The block diagram of the direct power MPC in a 2L-3Ph VSI is depicted in Fig. 3.7. The current and grid voltage are measured at present and used as the input for the predictive model that computes the optimal values of P and Q at the next sampling time.

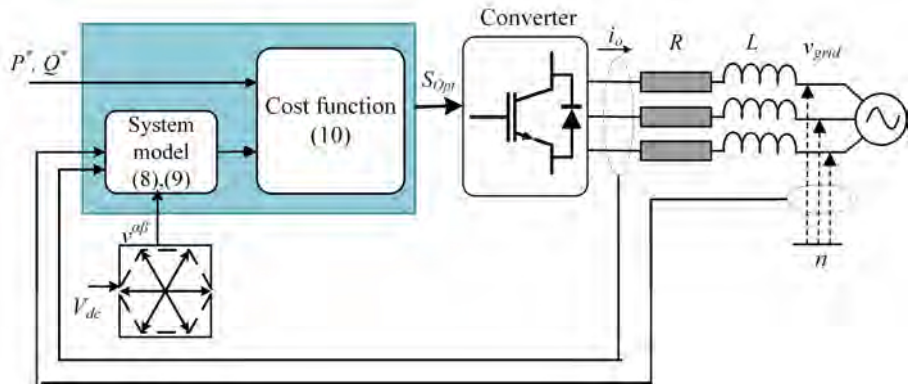

Figure 3.7: Block diagram of grid-tied VSI controlled by FCS-MPC

The predictions are then evaluated so that the switching state, which minimizes the cost function, is applied to the converter. The cost function is defined as

$$J_m = [P^*(k+1) - P_i(k+1)]^2 + [Q^*(k+1) - Q_i(k+1)]^2 \quad \text{for} \quad m = 0, ..., 7 \tag{3.22}$$

In order to compare the proposed methods, the simulation and experimental validation of conventional FCS-MPC are presented. The state-space model of the plant is discretized by selecting backward Euler method. The flowchart of the control algorithm of conventional FCS-MPC is illustrated in Fig. 3.8. The system parameters are listed in Table 3.1.

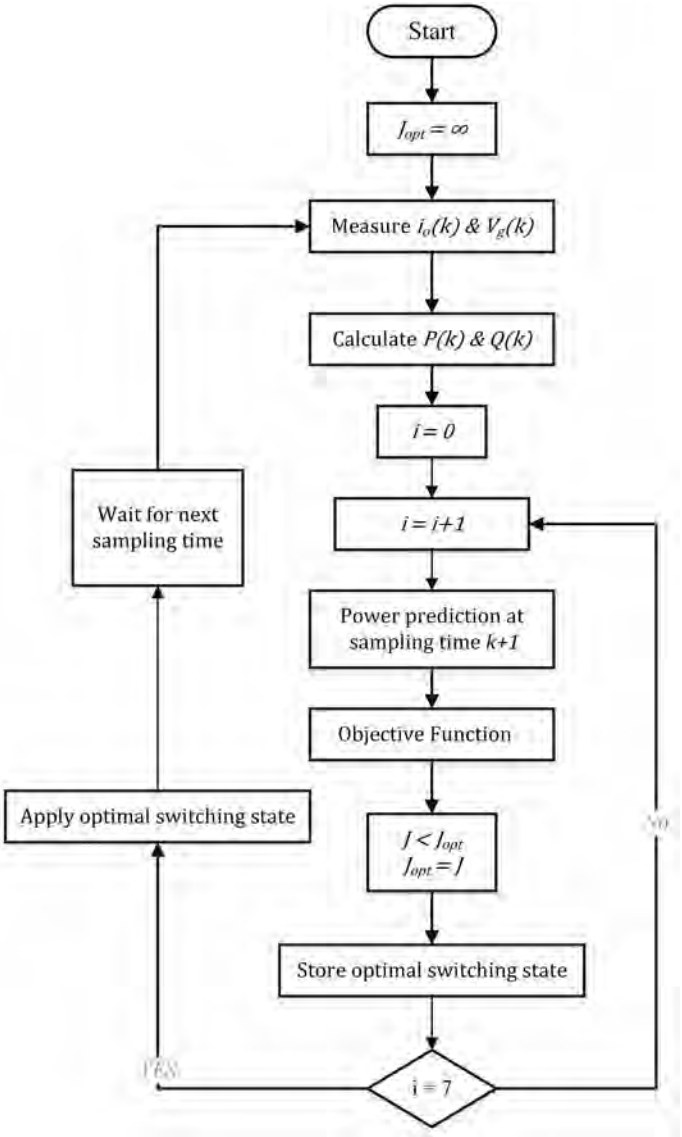

Figure 3.8: Conventional FCS-MPC flowchart

Table 3.1: Parameters of the system

Filter resistance	R	0.4 Ω
Filter inductance	L	4.6 mH
DC-link capacitor	C	680 μF
Grid voltage(L-n)	v_{grid}	65 V_{rms}
DC-link voltage	V_{DC}	180 V
Grid frequency	f	50 Hz

3.3.2.1 Simulation results

Simulation of a 2L-3Ph VSI with L filter is carried out using MATLAB/Simulink. The initial active and reactive power references are both set to zero. The active

power reference is increased to $-400\ W$ at $0.1s$ and decreased from -400 to $100\ W$ at $0.2s$. After that, the active power reference is kept to zero. The reactive power reference is altered to -100 and $200\ Var$ at $0.3s$ and $0.4s$, respectively. Fig. 3.9 demonstrates the controller performances of a 2L-3Ph VSI with conventional FCS-MPC in terms of the power flow control with different filter values. Although using the larger filter improves the system performance in terms of power ripples and total harmonic distortion (THD), it has disadvantages as well, such as higher cost and bigger space for implementation. Furthermore, the output currents in ABC-frame, and grid voltages in $\alpha\beta$-frame are illustrated in Fig. 3.10.

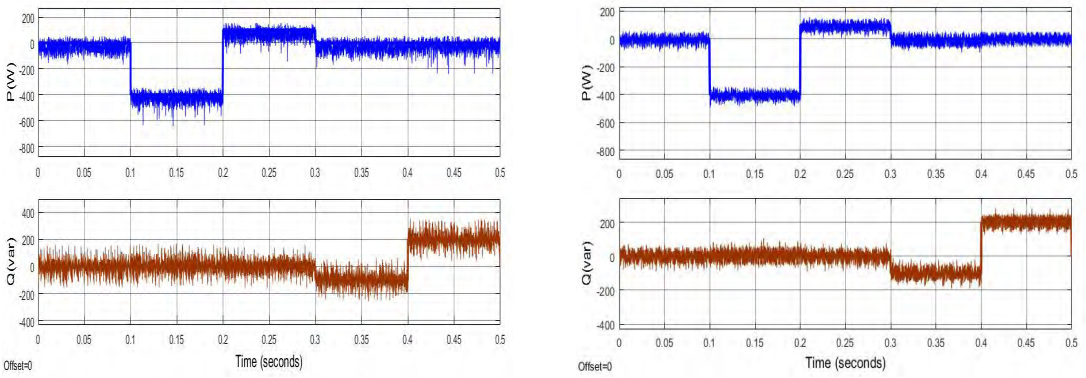

(a) (b)

Figure 3.9: Power flow control (a) $L = 4.6\,mH$ (b) $L = 8.84\,mH$

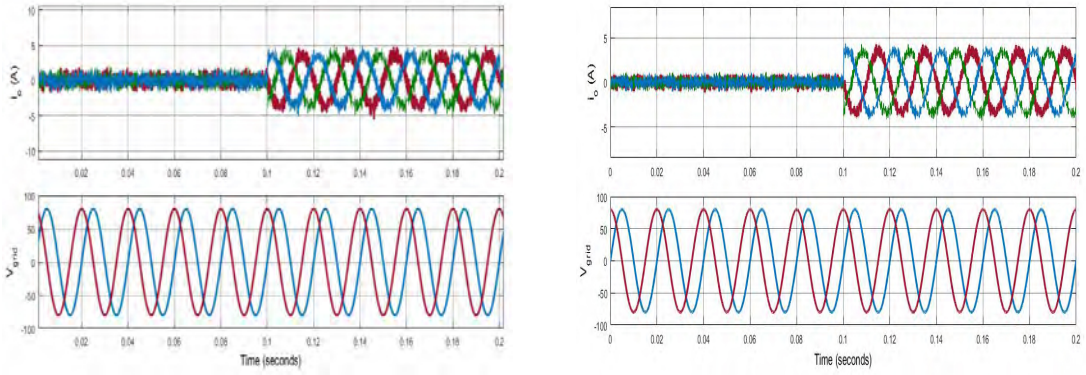

(a) (b)

Figure 3.10: Output currents in ABC-frame and grid voltages in $\alpha\beta$-frame (a) $L = 4.6mH$ (b) $L = 8.84\,mH$

3.3.2.2 Experimental results

To validate the simulation results, a series of experiments have been conducted. The set-up is depicted in Fig. 3.11 which consists of three Semikron IGBT power modules as the inverter, an TDK-Lambda DC source, a three-phase L filter, and a variac for main grid connection. To implement the control algorithm, a digital signal processor (DSP) through a dSPACE R&DS1104 control board is used. The voltages and currents are sampled through sensors and ADC of the CLP1104 using ControlDesk. The system parameters are kept the same as simulation.

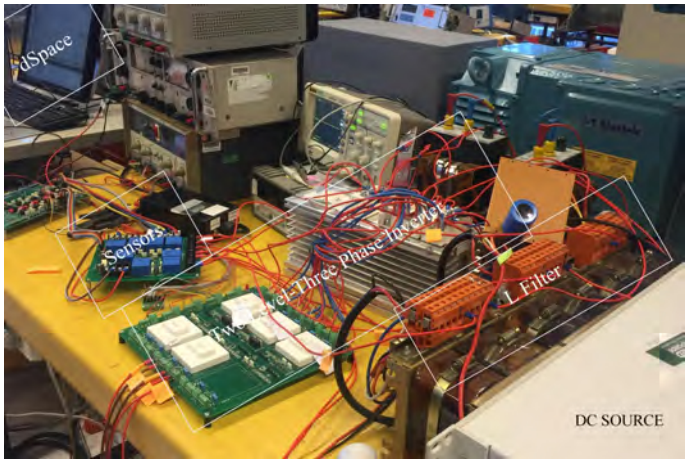

Figure 3.11: Experimental set-up

Fig. 3.12 demonstrates the RTI of the conventional FCS-MPC with different values for filter. The experimental output currents in ABC-frame, and grid voltages in $\alpha\beta$-frame are illustrated in Fig. 3.13.

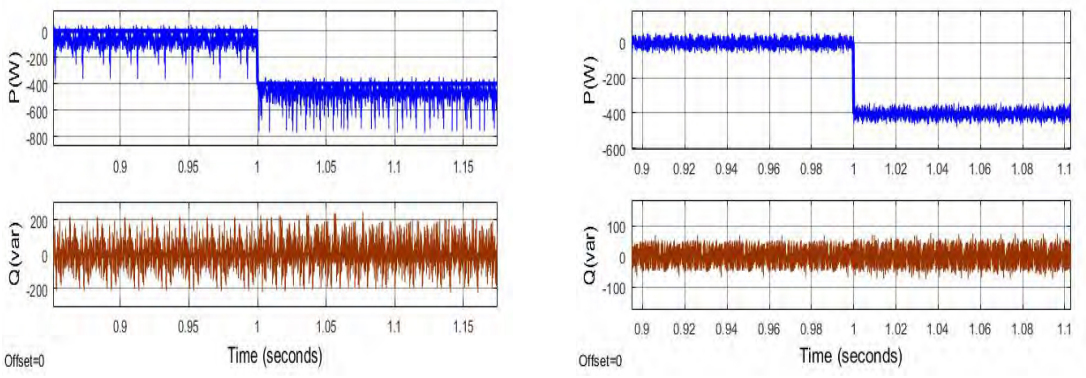

(a) (b)

Figure 3.12: Experimental power flow control (a) $L = 4.6\,mH$ (b) $L = 8.84\,mH$

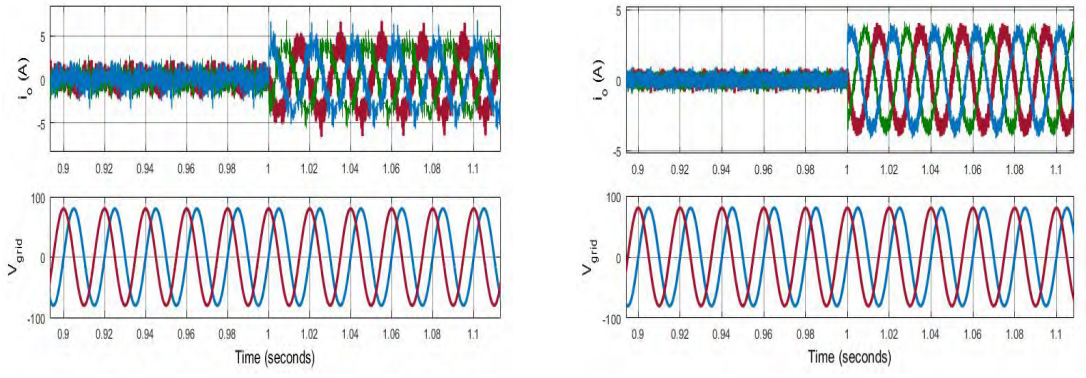

(a) (b)

Figure 3.13: Experimental output currents in ABC-frame and grid voltages in $\alpha\beta$-frame (a) $L = 4.6\,mH$ (b) $L = 8.84\,mH$

3.3.3 FCS-MPC based on space vector modulation

Space vector modulation (SVM) is an algorithm for the control of pulse width modulation (PWM). In the SVM technique, a reference voltage space vector V^* is provided, from which the switching patterns can be generated. The six non-zero voltage vectors $(v_1, ..., v_6)$ can have the positions as shown in Fig. 3.14, forming a regular hexagon. With the six active vectors, the area between any two adjacent vectors is defined as a sector. The remaining two zero space vectors create no output voltage, and therefore they remain at the origin in the $\alpha\beta$-plane defining no sector. At any time, V^* is estimated by two active space vectors and a zero pace vector [18].

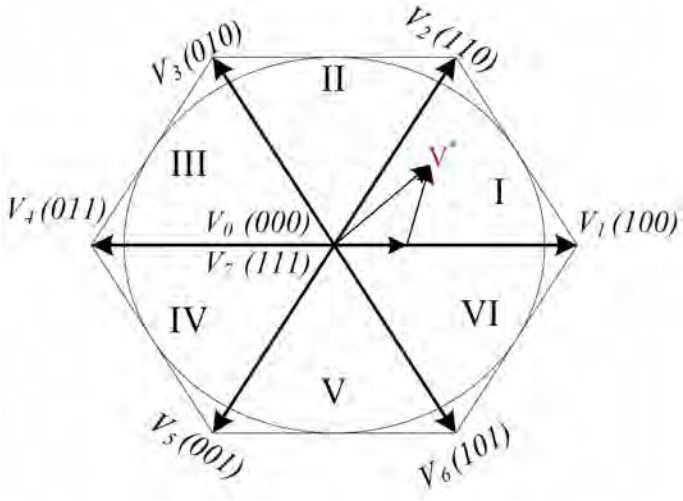

Figure 3.14: Voltage vectors and sectors of 2L-3Ph VSI

For example, as can be seen in Fig. 3.14, if V^* is in Sector I, the voltage vector can be expressed as

$$\begin{aligned} T_s V^* &= T_1 V_1 + T_2 V_2 \\ V^* &= \sqrt{V_\alpha^2 + V_\beta^2} \\ tan\theta &= \frac{V_\beta}{V_\alpha} \end{aligned} \tag{3.23}$$

where $(z-1)\frac{\pi}{6} < \theta < z\frac{\pi}{6}$ for $z = 1, ..., n$ (number of sectors). Switching time durations T_0, T_1 and T_2 at any instant can be attained for $z = 1, ..., n$ as follows,

$$\begin{aligned} T_1 &= \frac{\sqrt{3}}{V_{DC}} V^* T_s sin(\frac{z\pi}{3} - \theta) \\ T_2 &= \frac{\sqrt{3}}{V_{DC}} V^* T_s sin(\theta - \frac{(z-1)\pi}{3}) \\ T_0 &= T_s - T_1 - T_2 \end{aligned} \tag{3.24}$$

The order of on and off of the top three switches should satisfy the following principle: only one of the top three switches can change the switching status, for a

change of one basic voltage vector to another vector. The VSI will switch six times in one cycle. For example, given the voltage vector V^* in Sector I, V^* is made up of vectors $V_0, V_1, V_2, V_7, V_2, V_1$ and V_0. Corresponding switch S_a, S_b, S_c values and switching function waveforms for Sector I are shown in Table 3.2 and Fig. 3.15.

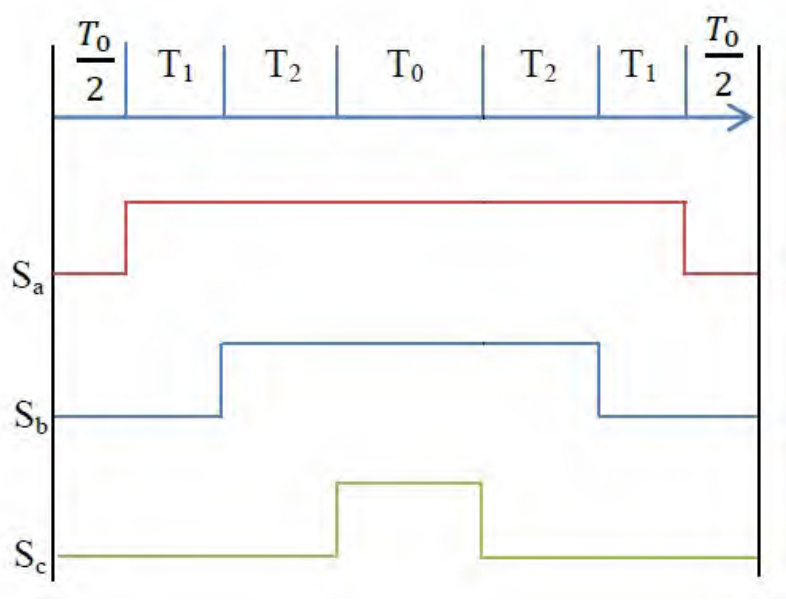

Figure 3.15: Conventional FCS-MPC flowchart

Table 3.2: Switching pattern for Sector I

Switch	V_0	V_1	V_2	V_7	V_2	V_1	V_0
S_a	0	1	1	1	1	1	0
S_b	0	0	1	1	1	0	0
S_c	0	0	0	1	0	0	0

A direct power control scheme of the three-phase inverter based on a combination of MPC and SVM (MPC-SVM) approaches is presented. The MPC technique operates with constant switching frequency SVM. For this purpose, an MPC principle is developed to calculate the required voltage vector. The computed inverter voltage vector, in the stationary reference frame, is converted into a sequence of switching states by SVM technique [19].

The MPC-SVM based power control block is shown in Fig. 3.16. At the beginning of each sampling time T_s, the inverter voltage vector is computed. After that, the SVM method is used to generate a sequence of inverter switching states, to attain the control objective with constant switching frequency. The cost function (3.22) is used for minimizing the error between the predicted output and reference. The optimal value of cost function is determined and the corresponding control action $V^{\alpha\beta}$, is computed. Hence, a sequence of switching states is applied to the VSI in the next sampling instant through the SVM.

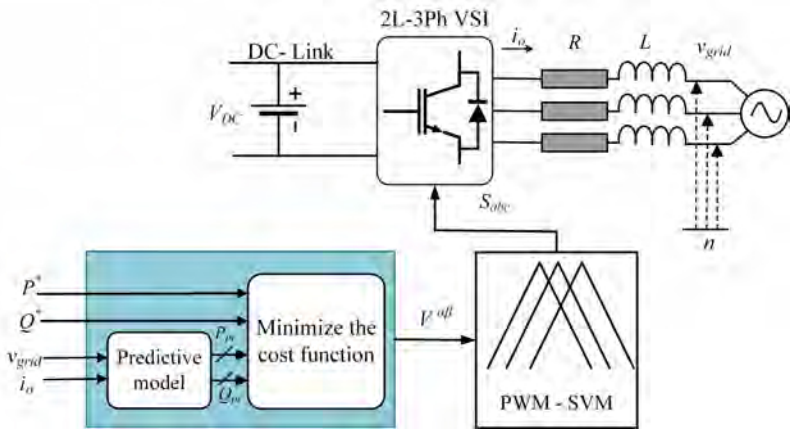

Figure 3.16: Block diagram of MPC-SVM

3.3.3.1 Simulation results

Simulation of a 2L-3Ph VSI with L filter is carried out using MATLAB/Simulink. The initial active and reactive power references are both set to zero. The active power reference is increased to $-400\ W$ at $0.1s$ and decreased from -400 to $100\ W$ at $0.2s$. After that, the active power reference is kept to zero. The reactive power reference is altered to -100 and $200\ Var$ at $0.3s$ and $0.4s$, respectively. Fig. 3.17 and Fig. 3.18 demonstrate the power flow control, the output currents in ABC-frame, and grid voltages in $\alpha\beta$-frame.

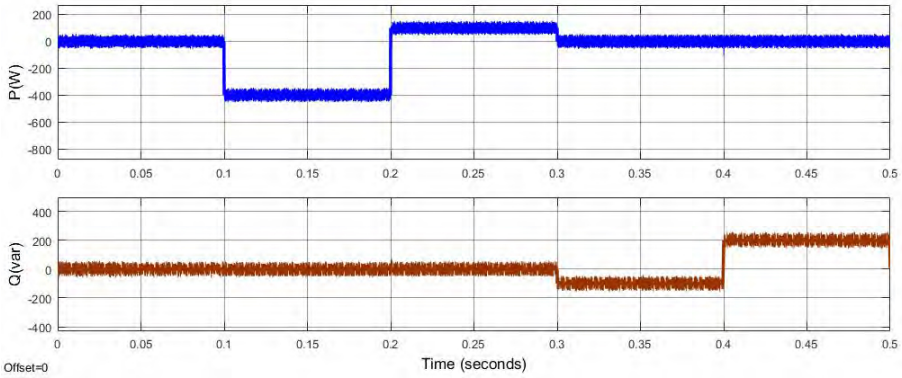

Figure 3.17: Power flow control

3.3.3.2 Experimental results

An RTI of the system is tested through the mentioned experimental set-up. The power flow control, the output currents in ABC-frame, and grid voltages in $\alpha\beta$-frame are illustrated in Fig. 3.19 and Fig. 3.20.

3.3.4 Time-delayed FCS-MPC

Aforementioned, a common approach to consider delay for RTI by DSP-based devices is the two-step or more prediction. However, the delay time differs in RTI for different applications [3, 20, 21]. Moreover, it is essential to consider variable sampling time, especially in systems with variable main frequencies. In [22], an

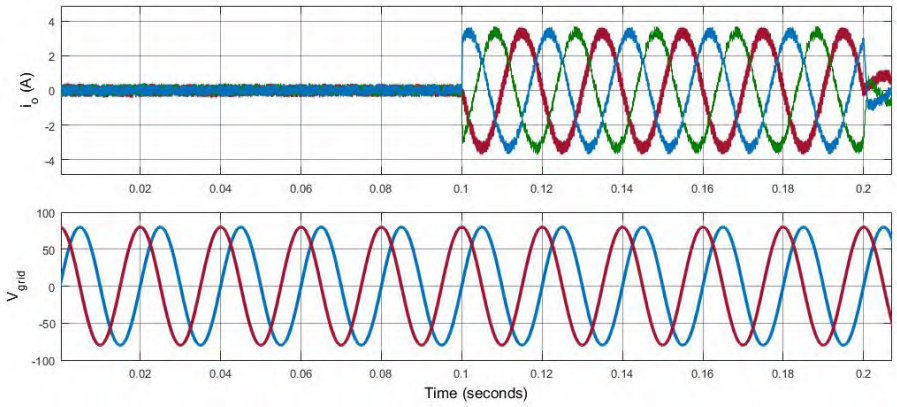

Figure 3.18: Output current and grid voltage

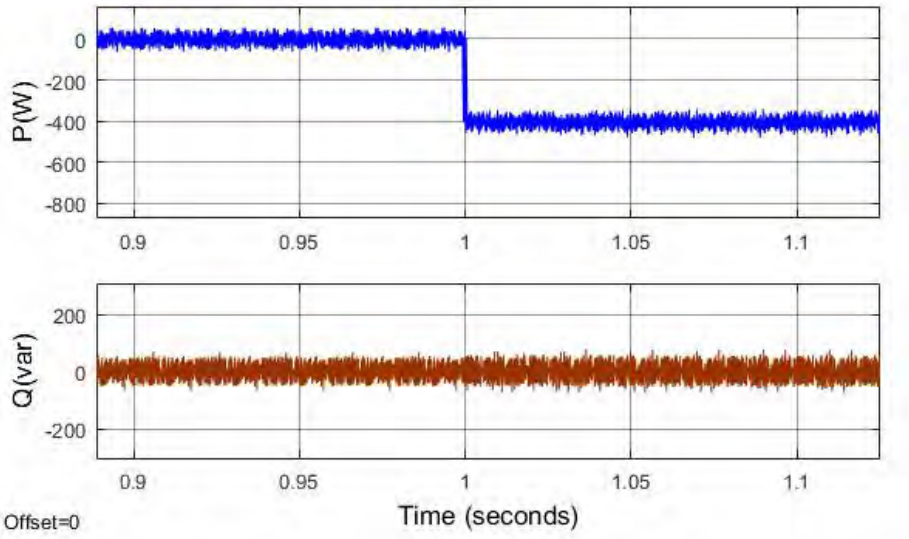

Figure 3.19: Experimental power flow control

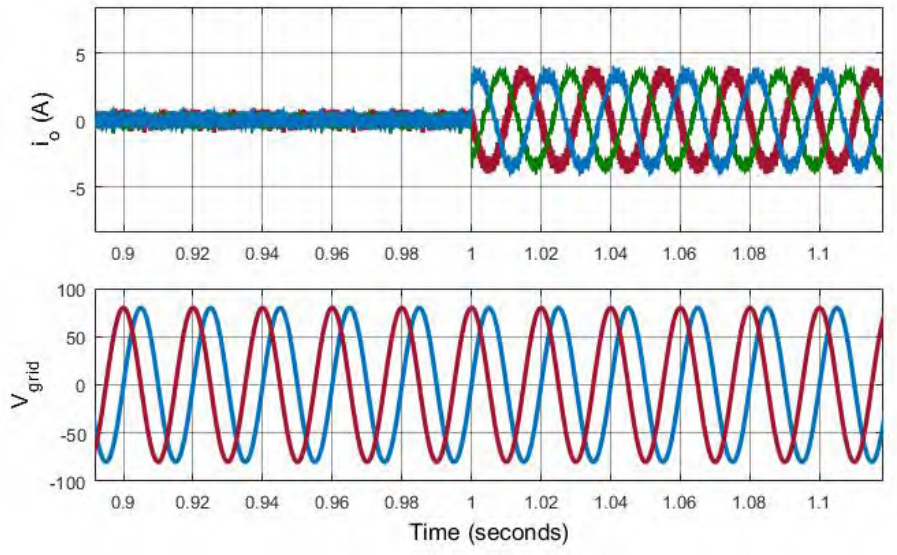

Figure 3.20: Experimental output current and grid voltage

improved FCS-MPC for a variable grid frequency environment is proposed in order to get a proper response. In this algorithm, a parameter estimator is employed to obtain the variable sampling time. Therefore, considering variable sampling time in FCS-MPC can enhance the system performance, particularly in networks with variable frequency deviation range. Consequently, a delayed model, in which the control and input voltage vector sequences are delayed, is proposed as follows,

$$\begin{aligned} \frac{d\mathbf{x}}{dt} &= D\mathbf{x}(t) + F\mathbf{u}(t-\tau) \\ \mathbf{y}(t) &= G\mathbf{x}(t) \end{aligned} \tag{3.25}$$

where D, F and G are matrices derived from the system model and τ is the input delay time.

In DSP-based RTI, τ consists of delay from measurements and signal conversion, calculation and application of the control sequence. The calculation time varies based on the length and complexity of the algorithm. To avoid that, the delay has to be considered as part of the sampling time. For each system, the time associated with the measurements, analog to digital conversion (ADC), and application of the controlled sequence can be assumed constant and reliant on the DSP hardware.

$$\begin{aligned} \tau &= \tau_{constant} + \tau_{comp} \\ \tau_{constant} &= \tau_{mes} + \tau_{conv} + \tau_{app} \end{aligned} \tag{3.26}$$

where τ_{mes}, τ_{conv}, τ_{comp}, and τ_{app} are the time needed for measurements, ADC, calculation and application of the control sequence, respectively. $\tau_{constant}$ is sum of τ_{mes}, τ_{conv}, and τ_{app} which is almost constant for each system.

By discretizing the state space model, the future value of output variables can be estimated by (3.7). Following the RHC principle and the assumption of $u(k) = ... = u(k+N-1)$, the future state variables at the step $k+N$ can be obtained by (3.9).

The flowchart of time-delayed FCS-MPC is depicted in Fig. 3.21. After grid voltage and line current measurements and power calculation, the resulting computational time τ_{comp} is added to the constant delay time $\tau_{constant}$, which gives the total delay time for RTI based on individual application. By comparing T_s and τ, the required number of prediction horizon is obtained. Next, the discrete-time domain A, B_1, and B_2 matrices are calculated. Then the optimization problem is solved based on an exhaustive search for eight possibilities to attain the optimal control sequence.

3.3.4.1 Simulation results

Simulation of a 2L-3Ph VSI with L filter is carried out using MATLAB/Simulink. The initial active and reactive power references are both set to zero. The active power reference is increased to $-400\ W$ at $0.1s$ and decreased from -400 to $100\ W$ at $0.2s$. After that, the active power reference is kept to zero. The reactive power reference is altered to -100 and $200\ Var$ at $0.3s$ and $0.4s$, respectively. Fig. 3.22 and Fig. 3.23 demonstrate the power flow control, the output currents in ABC-frame, and grid voltages in $\alpha\beta$-frame.

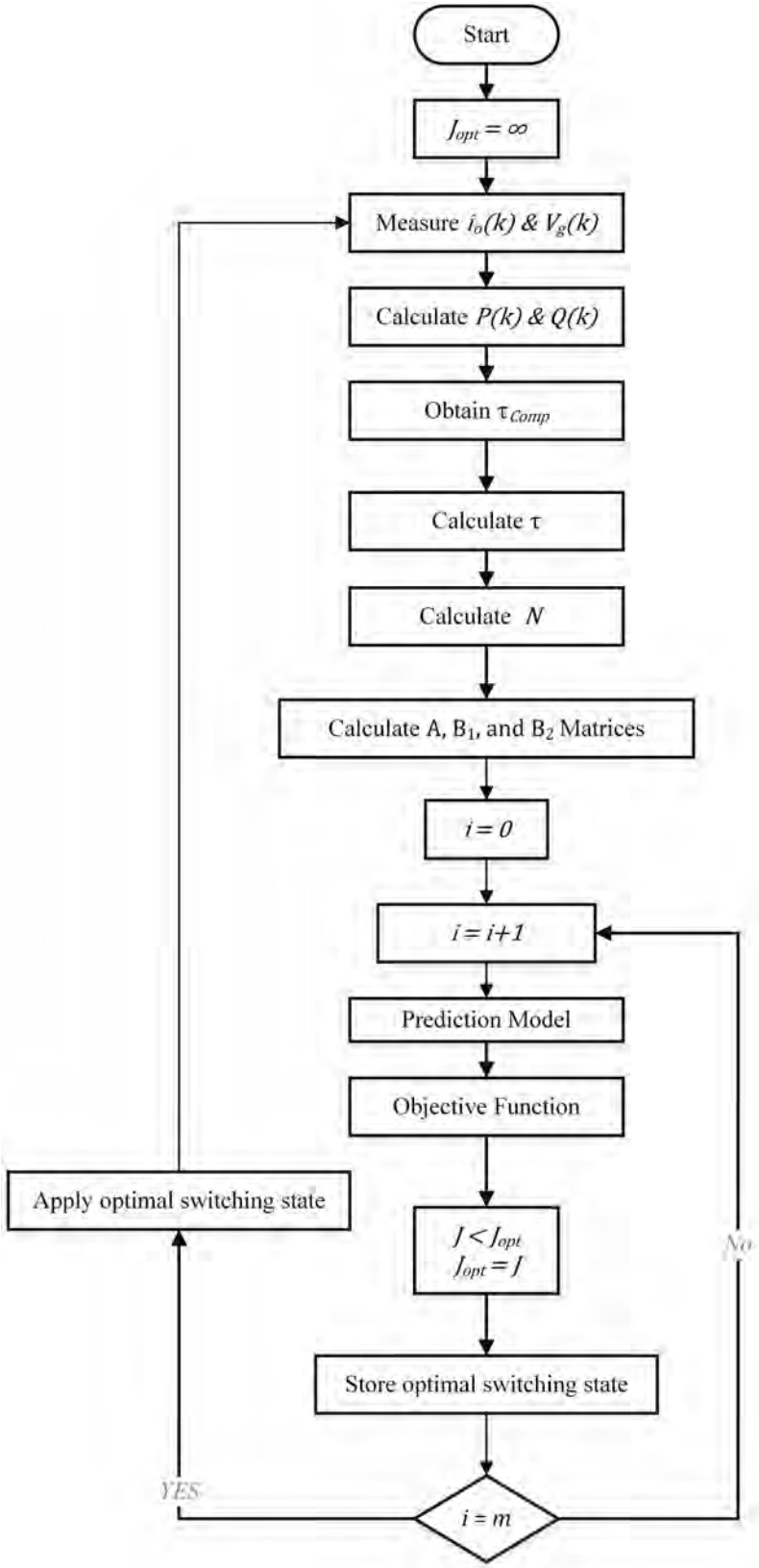

Figure 3.21: Flowchart of time-delayed FCS-MPC

3.3.4.2 Experimental results

An RTI of the system is tested through the mentioned experimental set-up. The power flow control, the output currents in ABC-frame, and grid voltages in

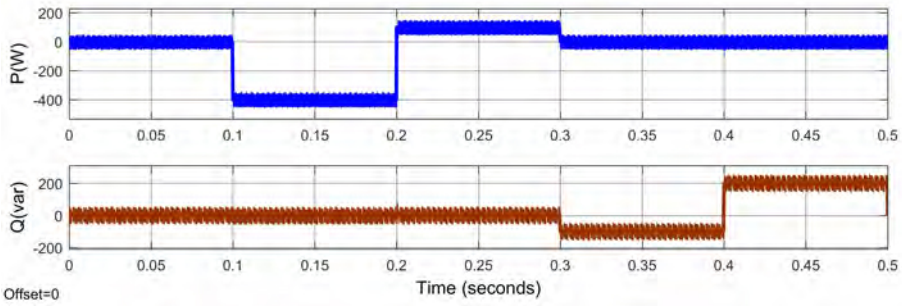

Figure 3.22: Power flow control

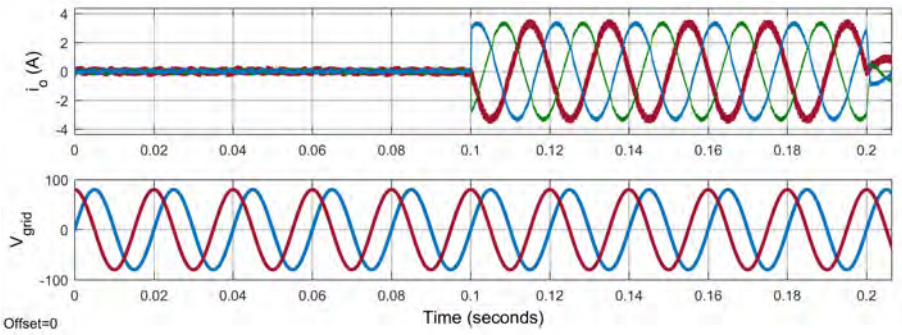

Figure 3.23: Output current and grid voltage

$\alpha\beta$-frame are illustrated in Fig. 3.24 and Fig. 3.25.

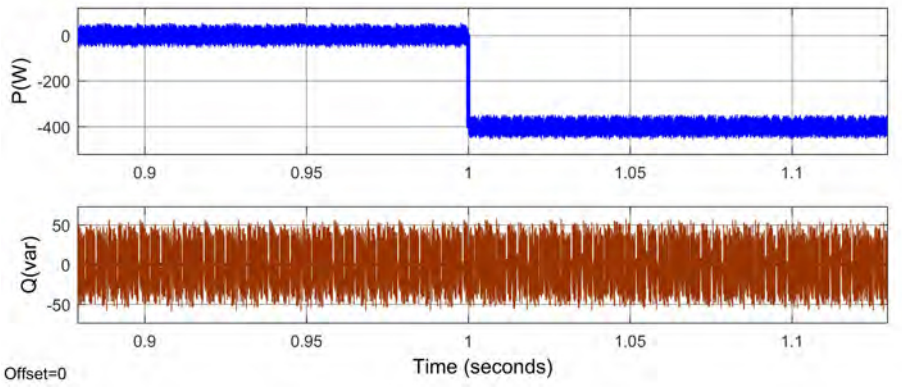

Figure 3.24: Experimental power flow control

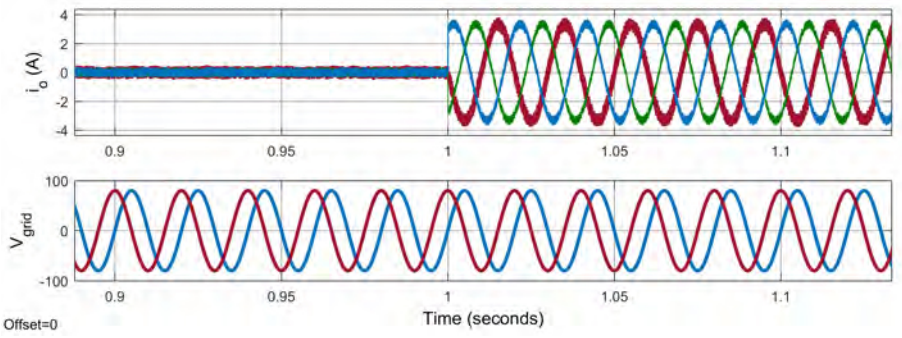

Figure 3.25: Experimental output current and grid voltage

Additionally, the proposed model has shown a good performance to a different value of time which is considered for the delay. The results are listed in Table 3.3 for the operating point of $P = -400\,W$, $Q = 0\,Var$.

Table 3.3: Time-delayed FCS-MPC with different τ

Indices	$\tau = 35\,\mu s$	$\tau = 85\,\mu s$	$\tau = 105\,\mu s$
$f_{sw}(Hz)$	1.56	1.71	1.88
$P_{rip}(W)$	0.31	0.34	0.41
$Q_{rip}(var)$	0.36	0.41	0.504
THD(%)	4.3	4.72	5.6
$f_s(kHz)$	20	20	20

3.3.5 Quantitative comparison and discussion

A quantitative comparison of the indices like the average switching frequency, power ripples, THD, overshoot, settling and rise time are tabulated in Tables 3.4 and 3.5 for all the mentioned control approaches. The power ripple at the specific operating points can be obtained using the standard deviation approach in [23] as follows,

$$\begin{aligned} P_{rip} &= \sqrt{\frac{1}{N_r}\sum_{\varsigma=1}^{N_r}(P_\varsigma - \frac{1}{N_r}\sum_{\varsigma=1}^{N_r}P_\varsigma)^2} \\ Q_{rip} &= \sqrt{\frac{1}{N_r}\sum_{\varsigma=1}^{N_r}(Q_\varsigma - \frac{1}{N_r}\sum_{\varsigma=1}^{N_r}Q_\varsigma)^2} \end{aligned} \tag{3.27}$$

where N_r is the sampling number in a period of $0.1s$. For more explicit quantitative comparison, the indices such as settling time, rise time, P_{rip} and Q_{rip} are normalized by sampling time and the nominal values for active and reactive power, respectively. With the intention of conducting a better comparison, two operating points of $P = -400\,W$, $Q = 0\,Var$ and $P = 0\,W$, $Q = 200\,Var$ are chosen. The quantities are extracted from the experimental results.

It can be realized that by applying the time-delayed compensation method, the active and reactive power ripples are reduced by 70.05 % and 80.8% in comparison with the conventional FCS-MPC and MPC-SVM respectively. The FCS-MPC with the time-delayed approach also gains lower THD percentage among all the three approaches as depicted in Figs. 3.26, 3.27, and 3.28 . However, MPC-SVM attains the lowest switching frequency where it is increased slightly in the time-delayed FCS-MPC method, by only 14.3%. Although the MPC-SVM shows an improved steady-state performance, the time-delayed FCS-MPC illustrates better steady-state and transient performances.

Table 3.4: Quantitative comparison of experimental results at the operating point of P = -400 W and $Q = 0\,Var$

Operating points	P = -400 W and $Q = 0\,Var$		
Indices	FCS-MPC ($L = 4.6\,mH$)	MPC-SVM	Time-delayed FCS-MPC
$f_s(kHz)$	20	20	20
$\overline{f_{sw}}(kHz)$	2.1	1.2	1.56
P_{rip}	0.71	0.27	0.31
Q_{rip}	0.83	0.29	0.36
$\text{THD}_{i_{oa}}(\%)$	16.18	8.1	4.3
Settling time	0.135	0.126	0.111
Rise time	0.189	0.158	0.119
Overshoot(%)	31.05	24.94	18.1

Table 3.5: Quantitative comparison of experimental results at the operating point of $P = 0\,W$, $Q = 200\,Var$

Operating points	$P = 0\,W$, $Q = 200\,Var$		
Indices	FCS-MPC ($L = 4.6\,mH$)	MPC-SVM	Time-delayed FCS-MPC
$f_s(kHz)$	20	20	20
$\overline{f_{sw}}(kHz)$	1.9	1.2	1.5
P_{rip}	0.75	0.35	0.44
Q_{rip}	0.69	0.31	0.35
$\text{THD}_{i_{oa}}(\%)$	24.83	18.04	8.19
Settling time	0.129	0.121	0.09
Rise time	0.176	0.152	0.1
Overshoot (%)	28.95	21.01	17.59

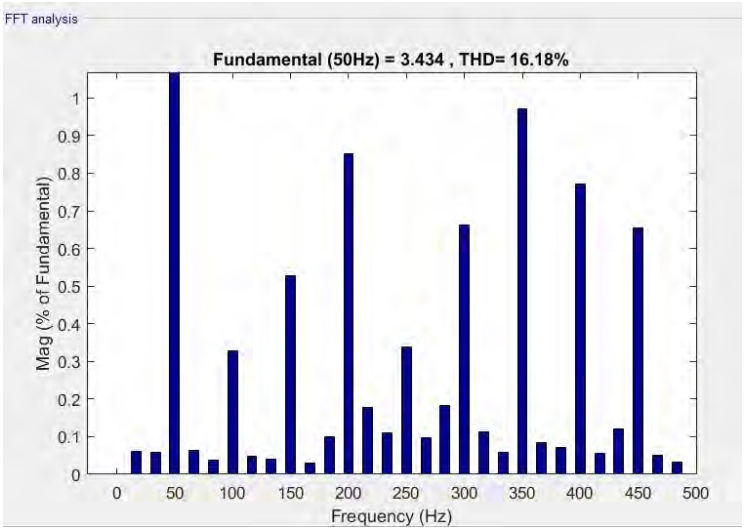

Figure 3.26: FFT analysis of conventional FCS-MPC

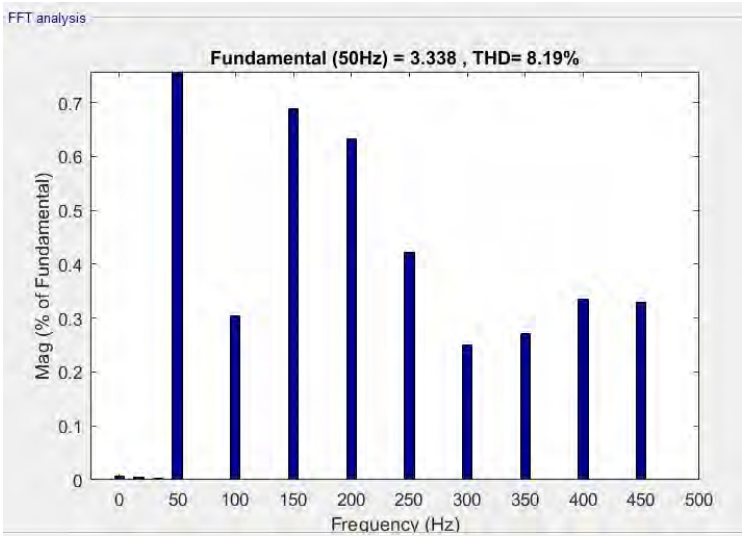

Figure 3.27: FFT analysis of MPC-SVM

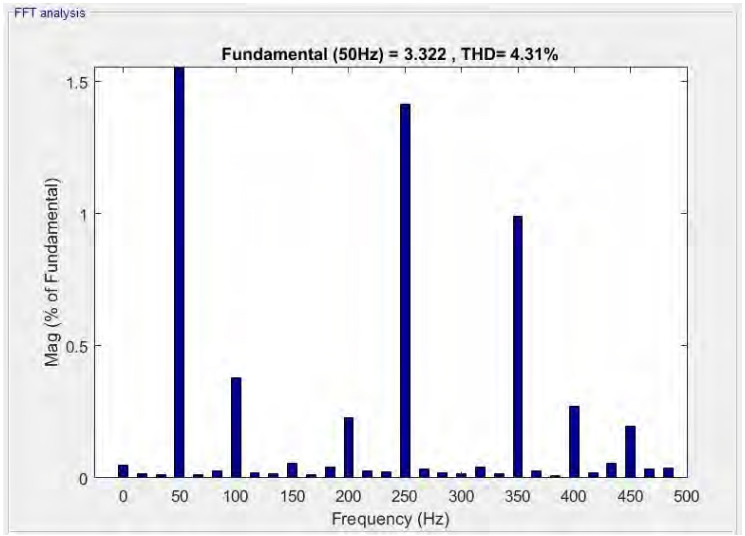

Figure 3.28: FFT analysis of time-delayed FCS-MPC

3.4 Case Study II: Three-level Three-phase Grid-connected Neutral Point Clamped Voltage Source Inverter

3.4.1 Three-level three-phase grid-connected neutral point clamped voltage source inverter

At medium voltage (MV) level, there is a wide range of topologies which share the market. In fact, for high-power applications, like industrial MV drives, it is possible to employ direct converters (without DC-link) as well as indirect converters (with DC-link). Among the all, neutral point clamped (NPC)-VSI is used widely for high-power industrial applications. The topology of 3L-3Ph NPC-VSI is represented in Fig. 3.29. The inverter consists of six complementary pairs of IGBTs. On the DC side, the inverter has two series-connected capacitors C_1 and C_2 which divide the DC-link voltage into three levels of $\frac{V_{DC}}{2}$, 0, and $-\frac{V_{DC}}{2}$. The mid-point of the capacitors, O, is the neutral point. The clamping diode connects the neutral point O to the midpoint of the IGBTs.

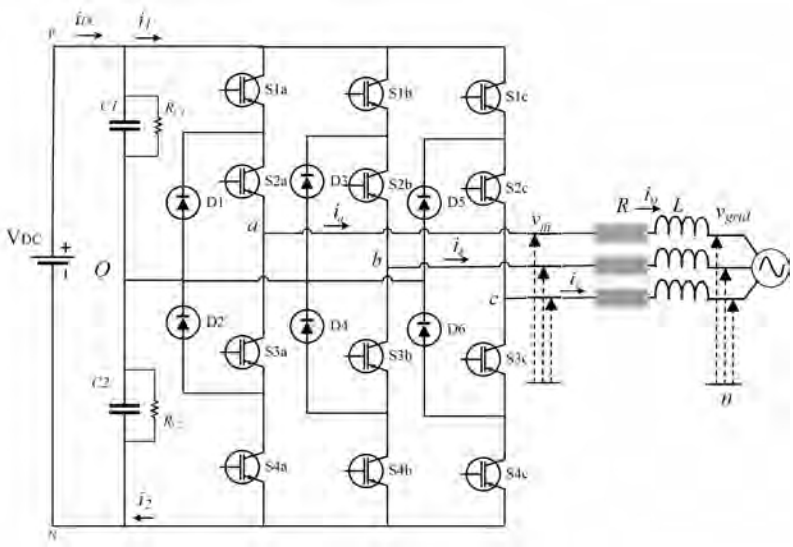

Figure 3.29: Topology of 3L-3Ph NPC-VSI

In this topology [17], to avoid forbidden states, there is a limiting condition that two adjacent switches must be ON at any time. Each switch is in a complementary mode $S_1 = \overline{S_3}$ and $S_2 = \overline{S_4}$, the respective diode pair provides access to the mid-point. The conduction states are tabulated in Table 3.6.

The output voltage of 3L-3Ph NPC inverter can be obtained as follows,

$$V_m = \frac{2}{3}(V_{an} + aV_{bn} + a^2V_{cn}) \tag{3.28}$$

To control the switches, only one transition at the same time is allowed. Therefore, there are $m = r^s = 27$ possible voltage vectors, including three zero, twelve small, six medium and six large voltage vectors as illustrated in Fig. 3.30 and tabulated in Table 3.7.

Table 3.6: Three-level switching state ($\xi \in a, b, c$)

$\mathbf{u}_\xi$	$S1_\xi$	$S2_\xi$	$S3_\xi$	$S4_\xi$	v_ξ
1	1	1	0	0	$\frac{V_{DC}}{2}$
0	0	1	1	0	0
-1	0	0	1	1	$-\frac{V_{DC}}{2}$

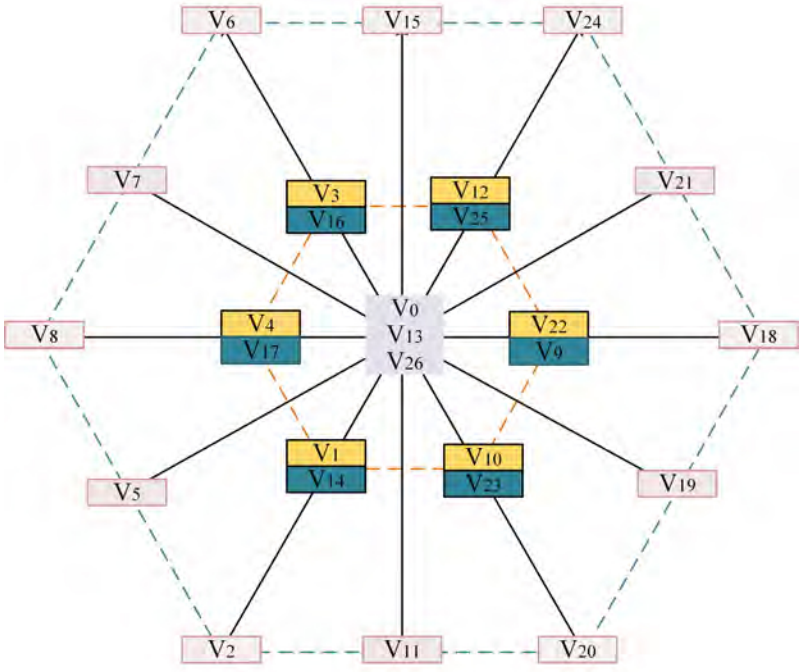

Figure 3.30: Voltage vectors of 3L-3Ph NPC-VSI

Table 3.7: Voltage vectors of 3L-3Ph NPC inverter based on the magnitude

Voltage Vectors	Number	Comment
Zero Vectors	0,13,26	No current flows through the neutral point
Small Vectors	1,3,4,9,10,12,14, 16,17,22,23,25	The sign for the neutral current at positive vectors does not alter whereas the negative ones change it
Medium Vectors	5,7,11,15,19,21	Connect the phase current to the neutral
Large Vectors	2,6,8,18,20,24	No current flows through the neutral point

3.4.2 Mathematical model of grid-connected NPC-VSI

The mathematical model of the system under consideration contains the 3L-3Ph NPC-VSI connected to the grid through an L filter, which can be formulated in the stationary frame via matrix M as follows,

$$M = \frac{2}{3}\begin{bmatrix} 1 & -\frac{1}{2} & -\frac{1}{2} \\ 0 & \frac{\sqrt{3}}{2} & -\frac{\sqrt{3}}{2} \end{bmatrix} \tag{3.29}$$

$$v_m^{\alpha\beta} = L\frac{di_o^{\alpha\beta}}{dt} + Ri_o^{\alpha\beta} + v_{grid}^{\alpha\beta} \tag{3.30}$$

In NPC-VSI, the balance of voltage across the capacitors is one the most important objectives to achieve high power quality. Therefore, the mathematical model for capacitor voltages and their prediction is an essential. In our modeling, we assume that the direction of power flow is from the inverter towards the grid. The total DC-link voltage is the sum of voltages across the capacitors $V_{DC} = V_{C1} + V_{C2}$. Under the balanced situations, the neutral point voltage V_n is zero and can be obtained as

$$V_n = \frac{V_{C2} - V_{C1}}{2} \tag{3.31}$$

The output voltage vectors, v_m, in the natural frame (ABC) can be represented as

$$v_{m\xi} = \begin{cases} \frac{u_\xi V_{DC}}{2}, & \text{if } u_\xi \in \{-1, 1\} \\ V_n & \text{if } u_\xi = 0 \end{cases} \tag{3.32}$$

where $\xi \in \{a, b, c\}$ and $u_\xi \in \{-1, 0, 1\}$ defined in Table 3.6. $v_{m\xi}$ is defined relative to the mid point of DC-link. The output voltage vectors of the NPC-VSI can be converted into stationary-frame, $v_m^{\alpha\beta}$, via the matrix M.

As the neutral point voltage has a different nature, it is suitable to use two mathematical models [17, 24, 25]. The first, which describes the continuous-time dynamics of the state vectors and the last, which is the continuous-time dynamics of the neutral point.

$$\frac{d\mathbf{x}}{dt} = D\mathbf{x}(t) + F\mathbf{u}(t) \tag{3.33}$$

The state variables $\mathbf{x}$, input variables $\mathbf{u}$, D and F matrices are given by, for m = 0, ..., 27,

$$\mathbf{x} = \begin{bmatrix} i_o^\alpha & i_o^\beta & v_{grid}^\alpha & v_{grid}^\beta \end{bmatrix}^T, \mathbf{u} = \begin{bmatrix} v_m^\alpha & v_m^\beta \end{bmatrix}^T = M\frac{V_{DC}}{2}\begin{bmatrix} u_{am} & u_{bm} & u_{cm} \end{bmatrix}^T \tag{3.34}$$

$$D = \begin{bmatrix} -\frac{R}{L} & 0 & -\frac{1}{L} & 0 \\ 0 & -\frac{R}{L} & 0 & -\frac{1}{L} \\ 0 & 0 & 0 & -\omega \\ 0 & 0 & \omega & 0 \end{bmatrix}, \; F = \begin{bmatrix} \frac{1}{L} & 0 \\ 0 & \frac{1}{L} \\ 0 & 0 \\ 0 & 0 \end{bmatrix} \tag{3.35}$$

where L and R are the filter inductance and resistance, respectively. $\omega = 2\pi f$, where f is the frequency of the grid. For a balanced and positive sequence system, the active power P and the reactive power Q can be obtained in $\alpha\beta$-stationary frame as

$$\begin{aligned} P &= \frac{3}{2}(v_{grid}^\alpha i_o^\alpha + v_{grid}^\beta i_o^\beta) \\ Q &= \frac{3}{2}(v_{grid}^\beta i_o^\alpha - v_{grid}^\alpha i_o^\beta) \end{aligned} \tag{3.36}$$

The neutral point voltage is a virtual voltage across the neutral point and mid-point of the DC-link and its dynamics can be expressed as

$$\frac{dV_n}{dt} = \frac{1}{2C}[u_{abc}]^T i_{abc} \tag{3.37}$$

where $C_1 = C_2 = C$, $i_{abc} = [\ i_a\ \ i_b\ \ i_c]^T$, and $u_{abc} = [\ u_{am}\ u_{bm}\ u_{cm}]^T, u_{\xi_m} \in \{-1, 0, 1\}, \xi = a, b, c$, for $m = 0, ..., 27$.

3.4.3 Conventional FCS-MPC

For the FCS-MPC, a discrete time state space model is employed with $t = kT_s$, where $t \in R$, $k \in N$, and T_s denotes the continuous time, the current time-step, and the sampling interval. The input vector $\mathbf{u}(k)$ is a function of switching states, DC-link voltage and neutral point voltage. To obtain the discrete time state space model, the dynamics of state vectors and neutral point voltage are discretized through forward Euler approach.

$$\mathbf{x}_{(k+1)} = A\mathbf{x}(k) + B\mathbf{u}(k) \tag{3.38}$$

where A, and B are the discrete time matrices and can be calculated as

$$\begin{aligned} A &= e^{DT_s} \\ B &= \int_0^{T_s} e^{D\delta} F d\delta \end{aligned} \tag{3.39}$$

Finally the output vector contains the variables which are seeking the objectives of the controller. The output vector is given by

$$\begin{aligned} Y &= \begin{bmatrix} P(k+1) & Q(k+1) & V_n(k+1) \end{bmatrix}^T \\ \begin{bmatrix} P(k+1) \\ Q(k+1) \end{bmatrix} &= \frac{3}{2} \begin{bmatrix} v_{grid}^{\alpha} & v_{grid}^{\beta} \\ -v_{grid}^{\beta} & v_{grid}^{\alpha} \end{bmatrix} \begin{bmatrix} i_o^{\alpha}(k+1) \\ i_o^{\beta}(k+1) \end{bmatrix} \\ V_n(k+1) &= \frac{T_s}{2C}[u_m(k)]^T i_o^{\alpha\beta}(k) + V_n(k) \end{aligned} \tag{3.40}$$

At each time-step k, the upper and lower DC-link capacitor voltages and the currents and grid voltages at each phase are measured. The upper and lower capacitor voltages determines the $V_{DC}(k)$ and $V_n(k)$. Then, the measured currents and grid voltages are transformed from the natural frame to the stationary frame. These measured values are used to calculate the active and reactive powers at the current time for the controller. The calculated value along with the references are given to the controller. The switching sequence $u_m(k)$ is in $\alpha\beta$-frame using the Clarke transformation. The predictions are then evaluated in a way that the switching states, which minimize the cost function, will be applied to the 3L-3Ph NPC-VSI. The cost function is defined as

$$J_m = Err_{pwr}(k+1) + \lambda_1 Err_{V_n}(k+1) + \lambda_2 Err_{SW}(k+1) \qquad \text{for} \quad m = 1, ..., 27 \tag{3.41}$$

where λ_1 and λ_2 are the weighting factors, Err_{pwr}, Err_{V_n}, and Err_{SW} are given as

$$\begin{aligned} Err_{pwr}(k+1) &= [P^*(k+1) - P_m(k+1)]^2 + [Q^*(k+1) - Q_m(k+1)]^2 \\ Err_{V_n}(k+1) &= [V_n^*(k+1) - V_{nm}(k+1)]^2 \\ Err_{SW}(k+1) &= \sum_{\xi=a,b,c} [u_{\xi_m(k+1)} - u_{\xi_m(k)}]^2 \qquad \text{for} \quad m = 1, ..., 27 \end{aligned} \tag{3.42}$$

In order to compare the proposed methods, the simulation and experimental validation of conventional FCS-MPC are presented. Simulation of a 3L-3Ph NPC-VSC with L filter is carried out using MATLAB/Simulink. The state-space model of the plant is discretized by selecting backward Euler method. The system parameters are listed in Table 3.8.

Table 3.8: Parameters of the system

Filter resistance	R	0.3 Ω
Filter inductance	L	10 mH
DC-link capacitor	C	1800 μF
Grid voltage(L-n)	v_{grid}	110 V_{rms}
DC-link voltage	V_{DC}	340 V
Grid frequency	f	50 Hz

3.4.3.1 Simulation and experimental results

Simulation of a 3L-3Ph NPC-VSI with L filter is carried out using MATLAB/Simulink. The initial active and reactive power references are both set to zero. The active power reference is set to 700 W at 1s and increased from 700 to 1800 W at 2s . After that, the active power reference is kept to zero. The reactive power reference is altered to 350 and 800 Var at 3s and 4s , respectively.

To validate the simulation results, a series of experiments have been conducted. The set-up is depicted in Fig. 3.31 and consists of three three-level Semikron IGBT power modules as the converter, a DC power supply, a three-phase L filter, and a variac for main grid connection. To implement the control algorithm, a digital signal processor (DSP) through a dSPACE R&DS1104 control board and FPGA Digilent Cmod A7 is used. The voltages and currents are sampled through sensors and ADC of the CLP1104 using ControlDesk. The system parameters are kept the same as the simulation. The block diagram in Fig. 3.32 shows the RTI procedures.

Fig. 3.33 demonstrates the simulation and RTI performances of a 3L-3Ph NPC-VSI with conventional FCS-MPC in terms of the power flow control. Furthermore, the output currents in ABC-frame are illustrated in Fig. 3.34. Fig. 3.35 depicts the capacitor voltages and neutral point voltage.

Figure 3.31: Experimental set-up

3.4.4 Time-delayed FCS-MPC

A delayed model, in which the control and input voltage vector sequences are delayed, is employed for 3L-3Ph NPC-VSI.

$$\begin{aligned} \frac{d\mathbf{x}}{dt} &= D\mathbf{x}(t) + F\mathbf{u}(t-\tau) \\ \mathbf{y}(t) &= G\mathbf{x}(t) \end{aligned} \tag{3.43}$$

where D, F and G are matrices derived from the system model and τ is the input delay time.

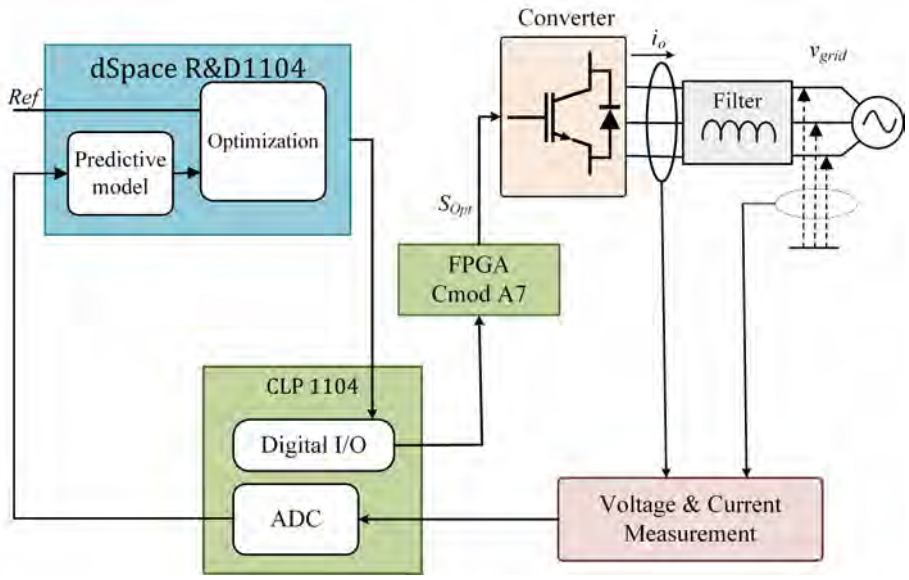

Figure 3.32: Block diagram of the experimental set-up

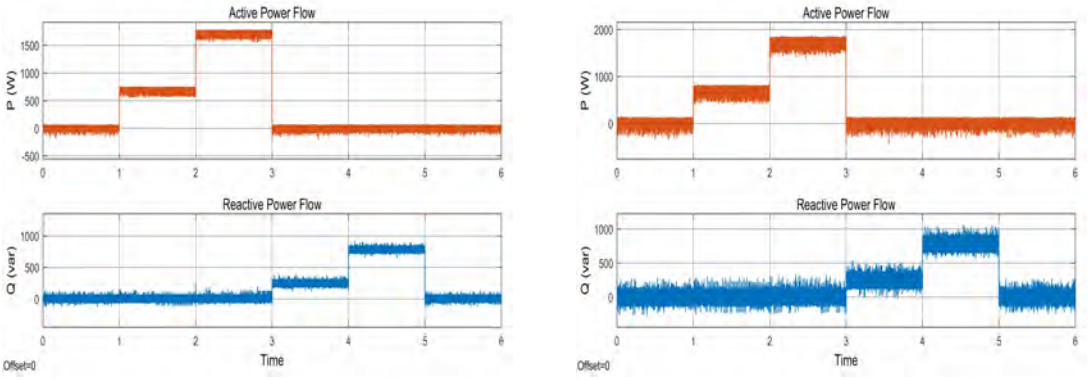

(a) (b)

Figure 3.33: Power flow control (a) Simulation (b) RTI

The flowchart of time-delayed FCS-MPC is illustrated in Fig. 3.21. After grid voltage and line current measurements and power calculation, the resulting computational time τ_{comp} is added to the constant delay time $\tau_{constant}$, which gives the total delay time for RTI based on individual application. By comparing T_s and τ, the required number of prediction horizon is obtained. Next, based on the calculated τ, the discrete-time domain A, B_1, and B_2 matrices are calculated. Then the optimization problem is solved based on an exhaustive search for 27 possibilities to attain the optimal control sequence.

3.4.4.1 Simulation and experimental results

A series of experiments have been conducted to verify the simulation results using MATLAB/Simulink. The active and reactive power references are kept the same as the previous section. Fig. 3.36 demonstrates the simulation and RTI performances of a 3L-3Ph NPC-VSI with conventional FCS-MPC in terms of the power flow control. Furthermore, the output currents, capacitor and neutral point voltage in ABC-frame are illustrated in Figs. 3.37 and 3.38 .

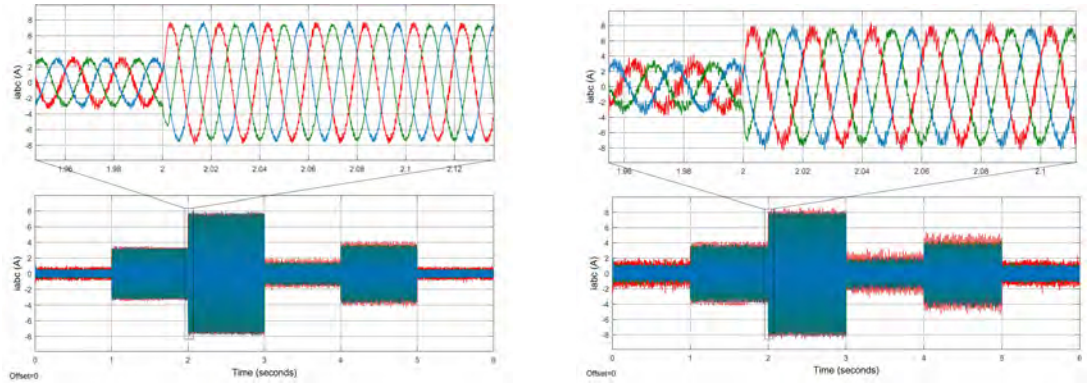

(a) (b)

Figure 3.34: Output current (a) Simulation (b) RTI

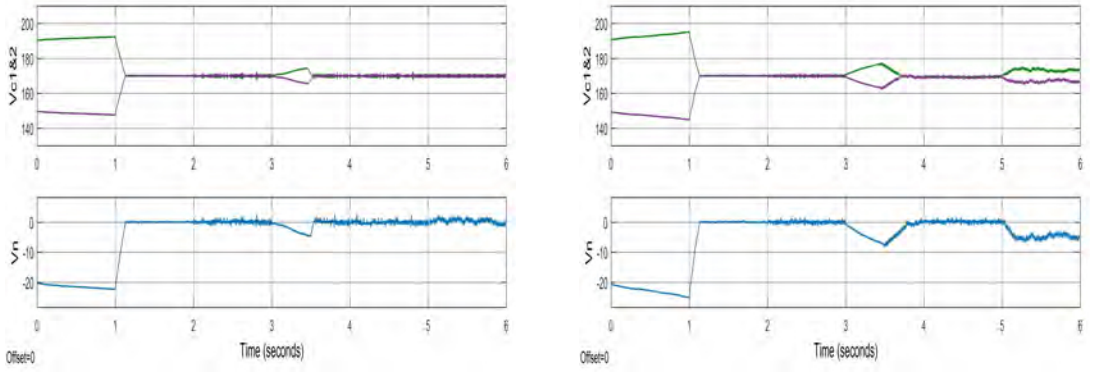

(a) (b)

Figure 3.35: Capacitor voltages and neutral point voltage (a) Simulation (b) RTI

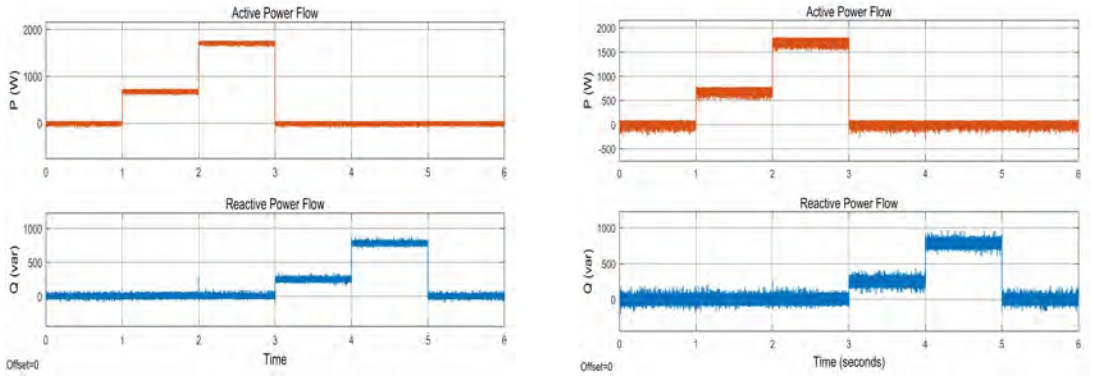

(a) (b)

Figure 3.36: Power flow control (a) Simulation (b) RTI

Additionally, the proposed model has shown a good performance to a different value of time which is considered for the delay. The results are listed in Table 3.9 for the operating point of $P = 1680\,W$, $Q = 0\,Var$.

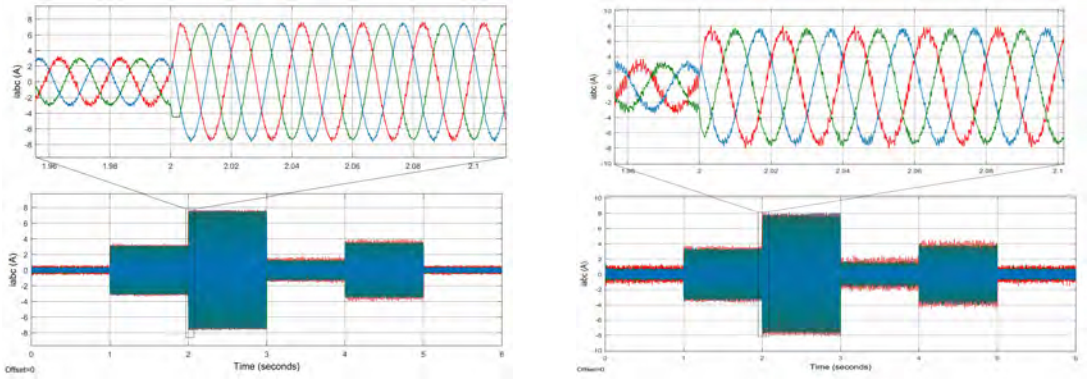

(a) (b)

Figure 3.37: Output current (a) Simulation (b) RTI

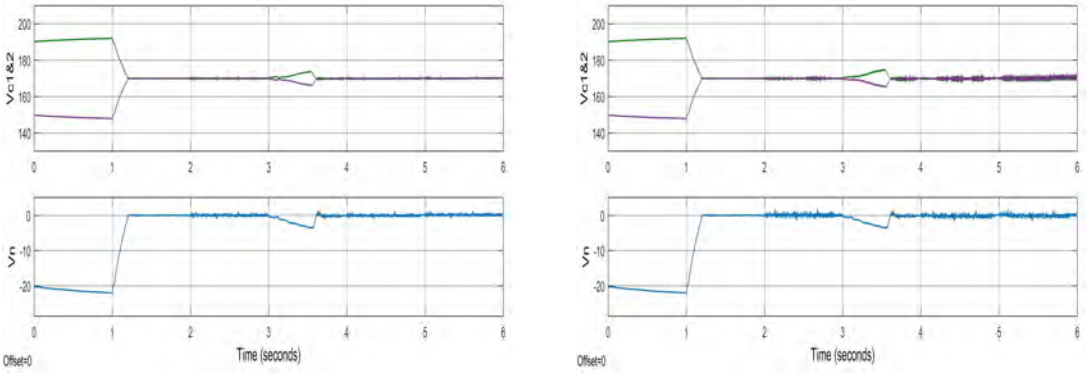

(a) (b)

Figure 3.38: Capacitor and neutral point voltage (a) Simulation (b) RTI

Table 3.9: Time-delayed FCS-MPC with different τ, at the operating point of $P = 1680W$, $Q = 0Var$

Indices	$\tau = 85\ \mu s$	$\tau = 125\ \mu s$
$f_{sw}(Hz)$	1.79	1.93
P_{rip}	0.44	0.38
Q_{rip}	0.51	0.43
THD(%)	4.77	4.64
$f_s(kHz)$	10	10

3.4.5 Quantitative comparison and discussion

A quantitative comparison of the indices like the average switching frequency, power ripples, THD, overshoot, the settling and rise time are tabulated in Table 3.10 for both control approaches. The quantities are extracted from the experimental results. The power ripple at the specific operating points can be obtained using the standard deviation as mentioned.

It can be realized that by applying the time-delayed compensation method,

Table 3.10: Quantitative comparison of experimental results at the operating point of $P = 1680W$, $Q = 0Var$

Operating points	$P = 1680\,W$, $Q = 0\,Var$	
Indices	FCS-MPC	Time-delayed FCS-MPC
$f_s(kHz)$	10	10
$\overline{f_{sw}}(kHz)$	2.1	1.79
P_{rip}	0.69	0.48
Q_{rip}	0.78	0.51
$\text{THD}_{i_{oa}}(\%)$	6.98	4.77
Settling time	0.25	0.22
Rise time	0.17	0.13
Overshoot(%)	26.67	17.32

the active and reactive power ripples are reduced by 30 % and 35% in comparison with the conventional FCS-MPC, respectively. The FCS-MPC with the time-delayed approach also gains lower THD as depicted in Fig 3.39. In term of transient response, the time-delayed FCS-MPC obtains about 10% less settling time and overshoot.

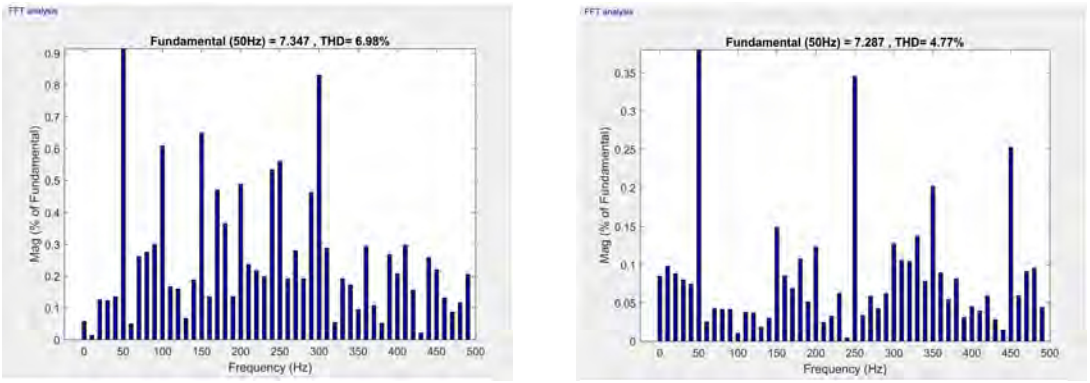

(a) (b)

Figure 3.39: FFT analysis (experimental) (a) Conventional FCS-MPC (b) Time-delayed FCS-MPC

3.5 Summary

For a longer horizon prediction of multilevel converters where the number of switching possibilities is increased considerably, FCS-MPC will face a computational challenge and impracticality for RTI. This drawback leads to the time delay for DSP-based RTI that needs to be considered in the controller design to sustain the

system stability and performance. A time-delayed FCS-MPC is presented in this chapter where a delay is considered in the input of the system model. Two case studies are investigated and compared with conventional and space vector MPC. As a result, the proposed time-delayed approach shows a better transient and steady state performance while reducing the power ripples significantly in both cases. The proposed method compensates the delay time resulting from DSPs' computation and implementation of the control signal. The delay time in this work is estimated through trial and error.

Bibliography

[1] T. Geyer, "A comparison of control and modulation schemes for medium-voltage drives: Emerging predictive control concepts versus pwm-based schemes," *IEEE Transactions on Industry Applications*, vol. 47, no. 3, pp. 1380–1389, 2011.

[2] J. Holtz, "Advanced pwm and predictive control—an overview," *IEEE Transactions on Industrial Electronics*, vol. 63, no. 6, pp. 3837–3844, 2016.

[3] T. Jin, X. Shen, T. Su, and R. C. Flesch, "Model predictive voltage control based on finite control set with computation time delay compensation for pv systems," *IEEE Transactions on Energy Conversion*, 2018.

[4] P. Karamanakos, T. Geyer, and R. Kennel, "A computationally efficient model predictive control strategy for linear systems with integer inputs," *IEEE Transactions on Control Systems Technology*, vol. 24, no. 4, pp. 1463–1471, 2016.

[5] P. Liu, Y. Wang, W. Cong, and W. Lei, "Grouping-sorting-optimized model predictive control for modular multilevel converter with reduced computational load," *IEEE Transactions on Power Electronics*, vol. 31, no. 3, pp. 1896–1907, 2016.

[6] P. Karamanakos, T. Geyer, and R. P. Aguilera, "Computationally efficient long-horizon direct model predictive control for transient operation," in *Energy Conversion Congress and Exposition (ECCE), 2017 IEEE*. IEEE, 2017, pp. 4642–4649.

[7] Z. Zhang, H. Fang, and R. Kennel, "Novel ripple reduced direct model predictive control of three-level npc active front end with reduced computational effort," in *Predictive Control of Electrical Drives and Power Electronics (PRECEDE), 2015 IEEE International Symposium on*. IEEE, 2015, pp. 32–37.

[8] P. Cortes, J. Rodriguez, C. Silva, and A. Flores, "Delay compensation in model predictive current control of a three-phase inverter," *IEEE Transactions on Industrial Electronics*, vol. 59, no. 2, pp. 1323–1325, 2012.

[9] C. Bordons and C. Montero, "Basic principles of mpc for power converters: Bridging the gap between theory and practice," *IEEE Industrial Electronics Magazine*, vol. 9, no. 3, pp. 31–43, 2015.

[10] W. H. Kwon and S. H. Han, *Receding horizon control: model predictive control for state models*. Springer Science & Business Media, 2006.

[11] C. D. Fuentes, C. A. Rojas, H. Renaudineau, S. Kouro, M. A. Perez, and T. Meynard, "Experimental validation of a single dc bus cascaded h-bridge multilevel inverter for multistring photovoltaic systems," *IEEE Transactions on Industrial Electronics*, vol. 64, no. 2, pp. 930–934, 2017.

[12] E. J. Bueno, A. Hernandez, F. J. Rodriguez, C. Girón, R. Mateos, and S. Cobreces, "A dsp-and fpga-based industrial control with high-speed communication interfaces for grid converters applied to distributed power generation systems," *IEEE transactions on industrial electronics*, vol. 56, no. 3, pp. 654–669, 2009.

[13] J. Hu, J. Zhu, and D. G. Dorrell, "Model predictive control of inverters for both islanded and grid-connected operations in renewable power generations," *IET Renewable Power Generation*, vol. 8, no. 3, pp. 240–248, 2013.

[14] ——, "Model predictive control of grid-connected inverters for pv systems with flexible power regulation and switching frequency reduction," *IEEE Transactions on Industry Applications*, vol. 51, no. 1, pp. 587–594, 2015.

[15] ——, "In-depth study of direct power control strategies for power converters," *IET Power Electronics*, vol. 7, no. 7, pp. 1810–1820, 2014.

[16] P. KaraMaNaKOS, T. Geyer, N. Oikonomou, F. D. KIEFErNDOrF, and S. MaNIaS, "Direct model predictive control: A review of strategies that achieve long prediction intervals for power electronics," *IEEE Industrial Electronics Magazine*, vol. 8, no. 1, pp. 32–43, 2014.

[17] J. Scoltock, T. Geyer, and U. K. Madawala, "Model predictive direct power control for grid-connected npc converters," *IEEE Transactions on industrial Electronics*, vol. 62, no. 9, pp. 5319–5328, 2015.

[18] H. Gao, B. Wu, D. Xu, R. P. Aguilera, and P. Acuna, "Model predictive switching pattern control for current-source converters with space-vector-based selective harmonic elimination," *IEEE Transactions on Power Electronics*, vol. 32, no. 8, pp. 6558–6569, 2017.

[19] A. Bouafia, J.-P. Gaubert, and F. Krim, "Predictive direct power control of three-phase pulsewidth modulation (pwm) rectifier using space-vector modulation (svm)," *IEEE Transactions on Power Electronics*, vol. 25, no. 1, pp. 228–236, 2010.

[20] T. Barisa, S. Iles, D. Sumina, and J. Matusko, "Model predictive direct current control of permanent magnet synchronous generator based on flexible lyapunov function considering converter dead time," *IEEE Transactions on Industry Applications*, 2018.

[21] C. D. Townsend, G. Mirzaeva, and G. C. Goodwin, "Deadtime compensation for model predictive control of power inverters," *IEEE Transactions on Power Electronics*, vol. 32, no. 9, pp. 7325–7337, 2017.

[22] J. A. Rohten, J. R. Espinoza, J. A. Muñoz, D. G. Sbarbaro, M. A. Perez, P. E. Melín, J. J. Silva, and E. E. Espinosa, "Enhanced predictive control for a wide time-variant frequency environment," *IEEE Transactions on Industrial Electronics*, vol. 63, no. 9, pp. 5827–5837, 2016.

[23] Y. Zhang, Y. Peng, and C. Qu, "Model predictive control and direct power control for pwm rectifiers with active power ripple minimization," *IEEE Transactions on Industry Applications*, vol. 52, no. 6, pp. 4909–4918, 2016.

[24] M. Habibullah, D. D.-C. Lu, D. Xiao, and M. F. Rahman, "Finite-state predictive torque control of induction motor supplied from a three-level npc voltage source inverter," *IEEE Transactions on Power Electronics*, vol. 32, no. 1, pp. 479–489, 2017.

[25] J. D. Barros and J. F. Silva, "Optimal predictive control of three-phase npc multilevel converter for power quality applications," *IEEE Transactions on Industrial Electronics*, vol. 55, no. 10, pp. 3670–3681, 2008.

Chapter 4

FCS-MPC OF POWER CONVERTERS: LONGER PREDICTION HORIZON

4.1 Introduction

In many model predictive controller, a long prediction horizon is an essential to ensure an improved performance and to avoid stability issues [1]. However, to implement model predictive control (MPC) a large amount of computations are required, leading to a considerable time delay, and making the implementation of such approaches in real time a difficult and challenging task. If the delay is not reflected in the controller design, the system performance could get worse. The computational concerns become predominantly significant for longer prediction horizons, since the number of possible switching sequences rises exponentially as the horizon length is increased. This chapter presents a longer prediction algorithm of MPC technique for grid-connected inverters.

4.2 State of the Art

Since the optimization problem must be solved at each time step, the time required to solve demanding MPC problems is often much longer than the usual sampling interval used in power converters. In general, implementing FCS-MPC algorithm is computationally challenging, mostly due to the difficulty in direct implementation of switching states. Moreover, the type of optimization problem and the number of manipulated variables may add to the complexity of this method [2]. As a result, a two-step prediction is typically used for reference tracking in power converters, to reduce the computational complexity.

However, a longer prediction horizon can lead to better control performance and stability [3–5]. Therefore, the prediction with longer horizons is desired but has to meet the computational demand and handle the system complexity [6, 7]. To facilitate the real time implementation (RTI) of MPC-based algorithms, strategies need to be employed that effectively balance the trade-off between the length of the prediction horizon and the computation burden. In [8], computationally efficient approaches to achieve long prediction horizon applicable to FCS-MPC algorithms

for power converters are discussed, including the extrapolation, move blocking, and event-based horizon strategies.

Among these methods, the extrapolation strategy is employed and implemented in practice for power electronic applications frequently [9]. In the extrapolation strategy [10, 11], the method utilizes the concept of switching horizon as the number of steps within which the power converter switches can change. As demonstrated in [3, 7], by adopting the sphere decoding algorithm for optimization, longer predictions can be achieved with a reduction of computational burden and have been successfully implemented in practice [12]. The extrapolation strategy evaluates the prediction model over the switching horizon for all possible control input sequences. Then, it determines a set of valid sequences and calculates the evolution of the variables of interest for this set by extrapolating their trajectories from the previous step. The extrapolation strategy presents a variable prediction horizon.

4.3 A Brief Theory

As mentioned before, MPC is a model based control technique; thus, developing an acceptable model of the plant is a key. As power electronics applications are commonly controlled by using digital platforms, it fits to model the system in discrete-time domain state space form. Therefore, the mathematical analysis of the system is narrowed to the discrete-time domain. For an r-level s-phase (rL-sPh) converter, the total number of possible switching states is $m = r^s$. The dynamics of the grid-connected power converter system in the discrete time domain can be written as

$$\begin{aligned} \mathbf{x}_i(k+1) &= f(\mathbf{x}(k), \mathbf{u}_i(k)) \\ \mathbf{y}_i(k+1) &= g(\mathbf{x}_i(k+1)) \end{aligned} \tag{4.1}$$

where $\mathbf{x}(k), \mathbf{u}(k)$, and $\mathbf{y}(k)$ are the state, input, and output vector at the time instant kT_s, respectively, T_s is the sampling interval, $i = 1, ..., m$ is the index of possible control actions, and m is the total number of possible sequences for IGBTs. The state variables are available through measurement and estimation, which provides the current plant information, at the sampling instant k ($k > 0$). In one sampling time ahead, the predicted state $x_i(k+1)$ can be obtained based on a prediction function $f(.,.)$. The future state variables at the step $k + N$, where N is the prediction horizon, can be represented as

$$\begin{aligned} \mathbf{x}_i(k+N) &= f(\mathbf{x}(k+N-1), \mathbf{u}_i(k+N-1)) \\ \mathbf{y}_i(k+N) &= g(\mathbf{x}_i(k+N)) \end{aligned} \tag{4.2}$$

Apart from predicting the future state within the finite horizon, incorporating constraints in the controller can improve the system performance effectively [13]. In this way the plant is able to operate at its physical limits without violating them. Thus, the most appropriate operation can be gained, while the operational constrains of the plant are enforced. Constraints can be imposed to the state variables and/or to the input variables. For the control objectives of tracking the reference, $y^*(k+N)$,

and switching loss reduction, Err_{SW}, over a finite prediction horizon N, the control problem solves the minimization of the objective function, J, as follows,

$$\begin{aligned} J_i &= \sum_{l=k}^{k+N-1} [||Y_{(i,Err)}(l+1)||_2^2 + \lambda_1 ||Err_{SW_i}(l+1)||_2^2] \\ Y_{(i,Err)}(l+1) &= ||\mathbf{y}^*(l+1) - \mathbf{y}_i(l+1)||_2^2 \\ Err_{SW_i}(l+1) &= [\mathbf{u}_i(l+1) - \mathbf{u}_i(l)]^2 \end{aligned} \tag{4.3}$$

where λ_1 is the weighting factors. MPC is a flexible control scheme that permits the easy presence of system objectives; this has raised much interest in recent years [12]. For example, in MPC, switching losses can be controlled by adding another term to the cost function. Err_{SW} is the second objective of the controller and it helps to minimize the switching loss.

The valuation of the cost function with the m predictions ($i = 1, ..., m$) will lead to m different costs. Certainly, the control action will be chosen as the one which leads to the minimum cost. The switching sequence can be defined as

$$\mathbf{U}_i(k) = \begin{bmatrix} \mathbf{u}_i(k) & \mathbf{u}_i(k+1) & ... & \mathbf{u}_i(k+N-1) \end{bmatrix}^T \tag{4.4}$$

which characterizes the sequence of power converter switch positions. The optimization problem can then be stated as

$$U_{opt}(k) = \arg\min_{U_i(k)} J_i(k) \tag{4.5}$$

The cost function J depends on the state vector $x(k)$, the last chosen switch position $\mathbf{u}(k-1)$ and the switching sequence $\mathbf{U}(k)$. Subsequent to the receding horizon optimization principle, the first element of the optimizing sequence $U_{opt}(k)$ is applied to the semiconductor switches at each time step.

In terms of the length of prediction horizon, there is no theoretical boundary to the number of predictions that can be executed. Though, practical implementations are restricted by the computational requirements, which will impose a maximum number of reachable predictions [14].

In terms of the weighting factors for multi-objective functions, the method of finding the weighting factor is only empirical. Another approach for compensating the unit difference is normalizing each component in order to eliminate their unit effects. we will discuss in detail about this issue in Chapter 5.

4.4 A Longer Prediction Horizon

The direct power control (DPC) pursues to control a power converter by employing the active and reactive powers as the control variables. DPC has become a popular control strategy due to its simplicity, outstanding transient performance, and robustness. Although DPC directly selects the power switch states to follow the desired active and reactive powers, the resulting switching frequency is varying [15]. The block diagram of the MPC based DPC for an rL-sPh inverter is depicted in Fig. 4.1. The discrete-time mathematical model of the system is used to compute the predictions of the output until time $k + N$ for a given sequence of inverter voltage

vectors and measurements at time k. The optimal sequence of voltage vectors that minimize the objective function is selected and the first element of the resultant control sequence is applied based on the receding horizon control principle. This algorithm is repeated at each sampling time.

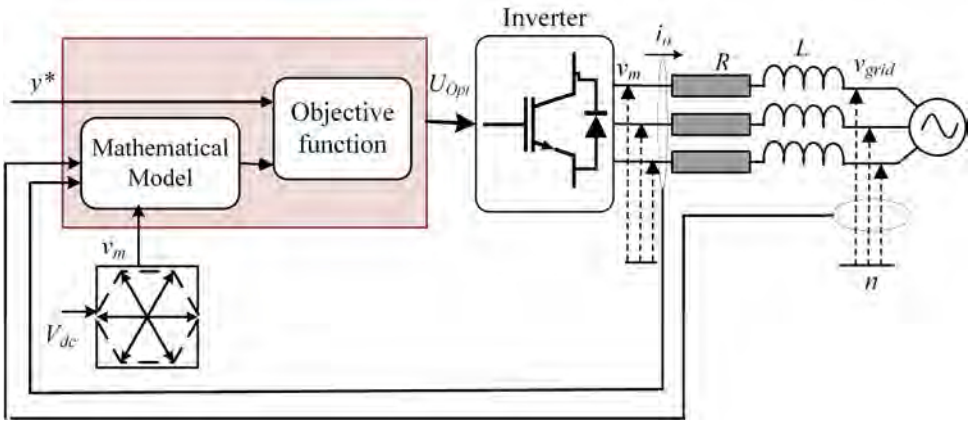

Figure 4.1: Block diagram of the grid-connected inverter with MPC controller

The control delay caused by the digital data processor is a crucial factor that needs to be reflected in the RTI of MPC schemes. The calculation time is considerable, and the delay between the measurements and actuation can impose some problems if not addressed. Furthermore, in distributed power generations, the lower the switching frequency is, the less the power loss will be.

As discussed, a key solution to compensate the time delay is to take into account the computation time and apply the selected switching state after the next sampling instant. In order to tackle these problems, a longer prediction horizon is required. Therefore, the continuous time state space of the system can be improved by

$$\begin{aligned} \frac{d\mathbf{x}}{dt} &= D\mathbf{x}(t) + F\mathbf{u}(t-\tau) \\ \mathbf{y}(t) &= G\mathbf{x}(t) \end{aligned} \tag{4.6}$$

where τ is the required time delay for the controller to minimize the objective function of the algorithm. If we assume that τ is equal to the sampling time and is long enough for exhaustive search of the optimal switching positions, a two-step prediction can be implemented.

With the one-step prediction in case of 2L-3Ph inverter, only eight voltage vectors are considered, $V_0, ..., V_7$. When two steps are considered for prediction, the total number of the voltage vectors will be $8^2 = 64$. It means, for optimal reference tracking, the objective function needs to be evaluated for 64 times. In fact, as the prediction horizon is enlarged, the number of decision variables is increased. Since the computational complexity grows, the experimental implementation of the algorithm will be difficult and almost impossible.

To simplify this approach, it is possible to eliminate the redundant voltage vectors in order to reduce the number of calculations [16]; i.e. in this case, if we look at the graphical representation of voltage vectors in Fig. 4.2, it can be seen

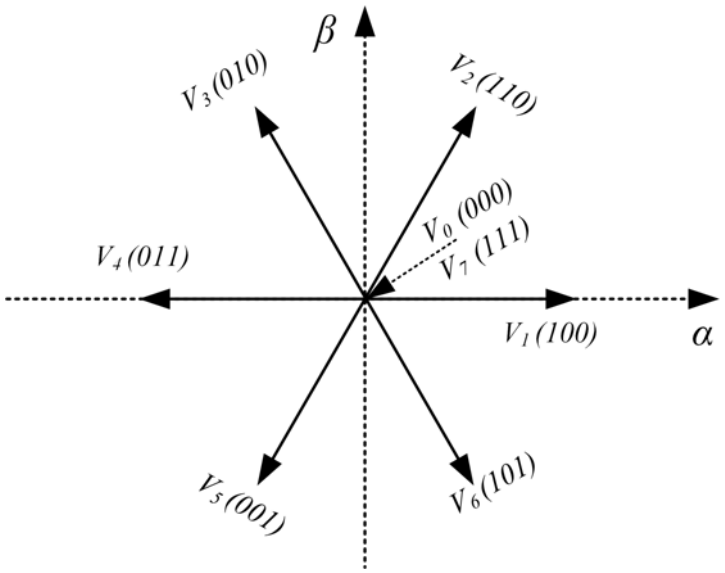

Figure 4.2: Graphical representation of voltage vectors generated by the 2L-3Ph inverter

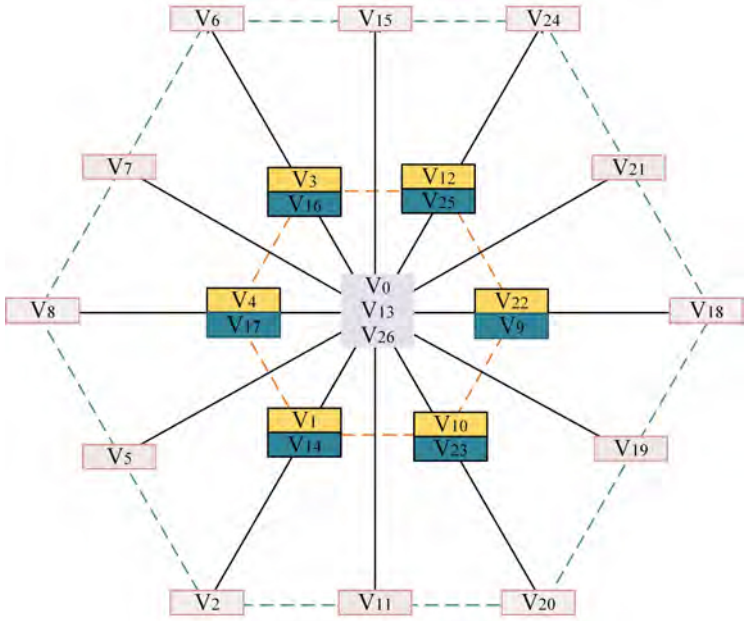

Figure 4.3: Graphical representation of voltage vectors generated by the 3L-3Ph inverter

V_0 and V_7 both represent zero vectors. Therefore, the total number of the voltage vectors will be decreased to $7^2 = 49$.

Eliminating the redundant voltage vectors is more effective in multi-level converters [17, 18]. In the 3L-3Ph neutral point clamped (NPC) inverter, the total number of the voltage vectors is $3^3 = 27$, as depicted in Fig. 4.3. With two-step prediction $(k + 2)$, the resultant possibilities is $27^2 = 729$. However, the redundant voltage vectors can be eliminated and the total possibilities will be reduced to $19^2 = 361$ for the two-step prediction.

Another approach is to utilize simplified two-step prediction. In case of 2L-3Ph inverter, instead of 49 possible trajectories, 7 voltage vectors can be utilized as illustrated in Fig. 4.4.

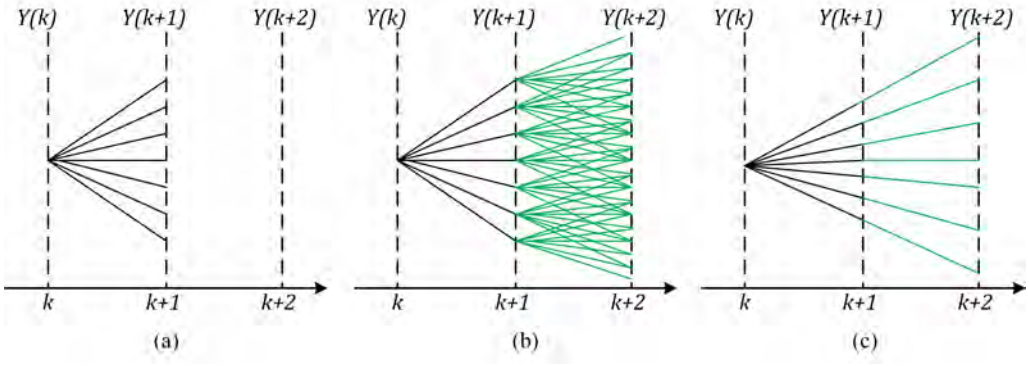

Figure 4.4: Prediction of the output voltage vectors considering different input sequences. a) One-step prediction b) Two-step prediction c) Simplified two-step prediction

4.5 Case Study: Three-level Three-phase Grid-connected Neutral Point Clamped Voltage Source Inverter

In this section, two scenarios for longer prediction in control of 3L-3Ph neutral point clamped voltage source inverter (NPC-VSI) is considered: scenario 1 where a simplified N-step prediction is considered and scenario 2 considering N-step prediction by eliminating the redundant voltage vectors.

A detailed study on 3L-3Ph NPC-VSI is conducted in Section 3.4. At each time-step k, the upper and lower DC-link capacitor voltages and the currents and grid voltages at each phase are measured. The upper and lower capacitor voltages determines $V_{DC}(k)$ and $V_n(k)$. As mentioned before, in this topology, the balance of voltage across the capacitors is one of the most important objectives to achieve high power quality. Therefore, the mathematical model for capacitor voltages and their prediction is an essential. In our modeling, we assume that the direction of power flow is from the inverter towards the grid. The total DC-link voltage is the sum of voltages across the capacitors $V_{DC} = V_{C1} + V_{C2}$. Under the balanced situations, the neutral point voltage V_n is zero and can be obtained as

$$V_n = \frac{V_{C2} - V_{C1}}{2} \tag{4.7}$$

Then, the measured currents and grid voltages are transformed from the natural frame (ABC) to the stationary frame ($\alpha\beta$). These measured values are used to calculate the active and reactive powers at the current time for the controller. The calculated value along with the references are given to the controller. The predictions are then evaluated in a way that the switching states, which minimize the cost function, will be applied to the 3L-3Ph NPC-VSI. The cost function is defined as

$$J = Err_{pwr}(k+N) + \lambda_1 Err_{V_n}(k+N) + \lambda_2 Err_{SW}(k+N1) \qquad \text{for} \quad m = 1, ..., 27 \tag{4.8}$$

where λ_1 and λ_2 are the weighting factors (tuned by heuristic methods), Err_{pwr}, Err_{V_n}, and Err_{SW} are given as

$$
\begin{aligned}
Err_{pwr}(k+N) &= [P^*(k+N) - P_m(k+N)]^2 + [Q^*(k+N) - Q_m(k+N)]^2 \\
Err_{V_n}(k+N) &= [V_n^*(k+N) - V_{nm}(k+N)]^2 \\
Err_{SW}(k+N) &= [u_m(k+N) - u_m(k+N-1)]^2
\end{aligned} \tag{4.9}
$$

4.5.1 Simulation and experimental results

Table 4.1: Parameters of the system

Filter resistance	R	0.3 Ω
Filter inductance	L	10 mH
DC-link capacitor	C	1800 μF
Grid voltage(L-n)	v_{grid}	110 V_{rms}
DC-link voltage	V_{DC}	340 V
Grid frequency	f	50 Hz

Simulation of a 3L-3Ph NPC-VSI with L filter is carried out using MATLAB/Simulink. The state-space model of the plant is discretized by selecting backward Euler method. The system parameters are listed in Table 4.1. The initial active and reactive power references both are set to zero. The active power reference is set to 700 W at 1s and increased from 700 to 1800 W at 2s . After that, the active power reference is kept to zero. The reactive power reference is altered to 350 and 800 Var at 3s and 4s , respectively.

Figs. 4.5 and 4.6 demonstrate the power flow tracking for scenarios 1 and 2, respectively. In scenario 1, $\lambda_1 = 0.8$ and $\lambda_2 = 0.03$ are set based on try and error approach for all the operating points, whereas in scenario 2, $\lambda_1 = 10$ and $\lambda_2 = 1.1$.

To validate the simulation results, a series of experiments have been conducted. The set-up is consists of three three-level Semikron IGBT power modules as the converter, a DC power supply, a three-phase L filter, and a variac for the main grid connection. To implement the control algorithm, a digital signal processor (DSP) through a dSPACE R&DS1104 control board and FPGA Digilent Cmod A7 is used. The voltages and currents are sampled through sensors and analogue to digital converter (ADC) of the CLP1104 using ControlDesk. The system parameters are kept the same as the simulation. The block diagram in Fig. 4.7 shows the RTI procedures.

Figs. 4.8 and 4.9 demonstrate the RTI performances of a 3L-3Ph NPC-VSI with two-step FCS-MPC in terms of the power flow control for scenarios 1 and 2. In scenario 1, $\lambda_1 = 0.899$ and $\lambda_2 = 0.0211$ are set based on try and error approach for all the operating points, whereas in scenario 2, $\lambda_1 = 12.2$ and $\lambda_2 = 1.001$.

A quantitative comparison of the scenarios is carried out. With the intention of obtaining a better comparison of the approaches for longer prediction in multi-objectives MPC, indices like the average switching frequency, total harmonic distortion (THD), power ripples, settling and calculation time are tabulated in Ta-

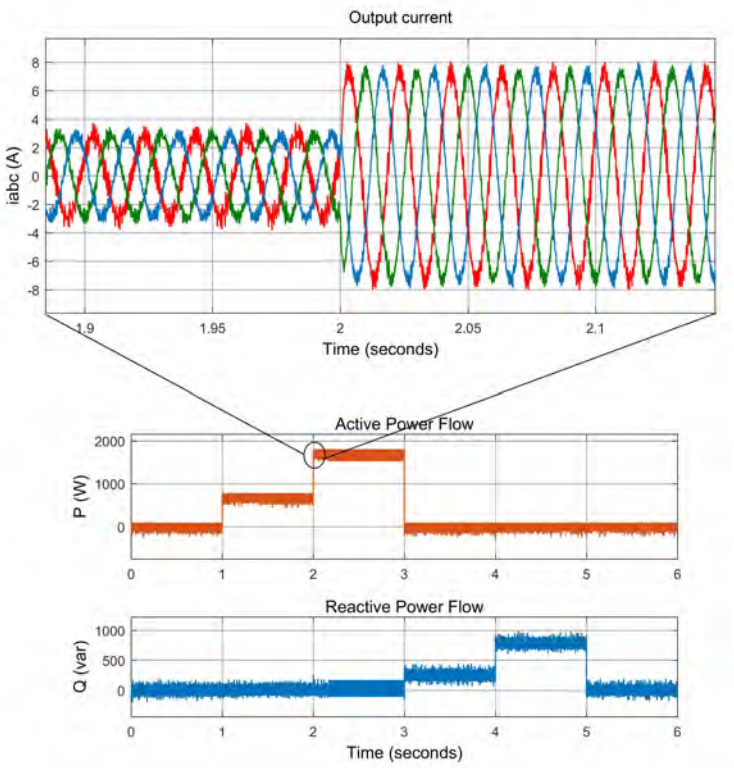

Figure 4.5: Power flow tracking via two-step prediction (simulation) for scenario 1

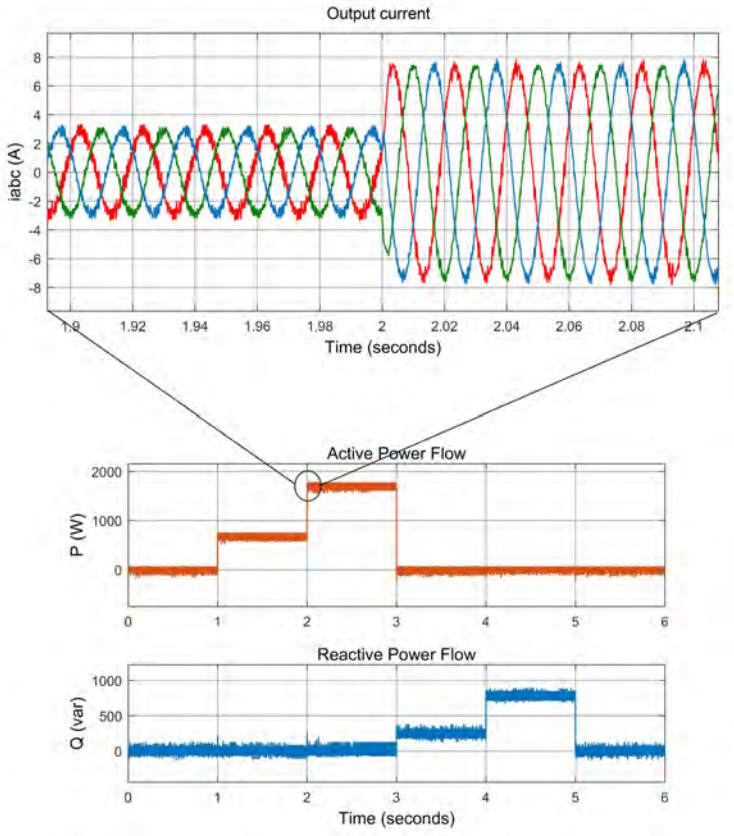

Figure 4.6: Power flow tracking via two-step prediction (simulation) for scenario 2

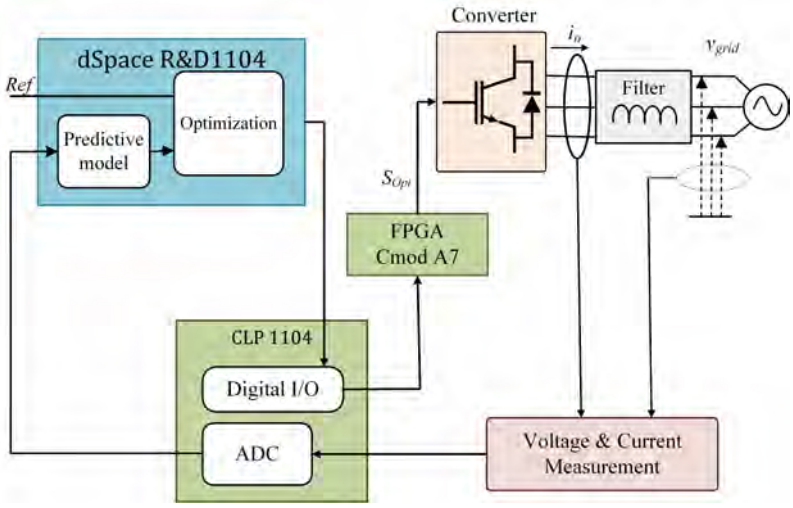

Figure 4.7: Block diagram of the experimental set-up

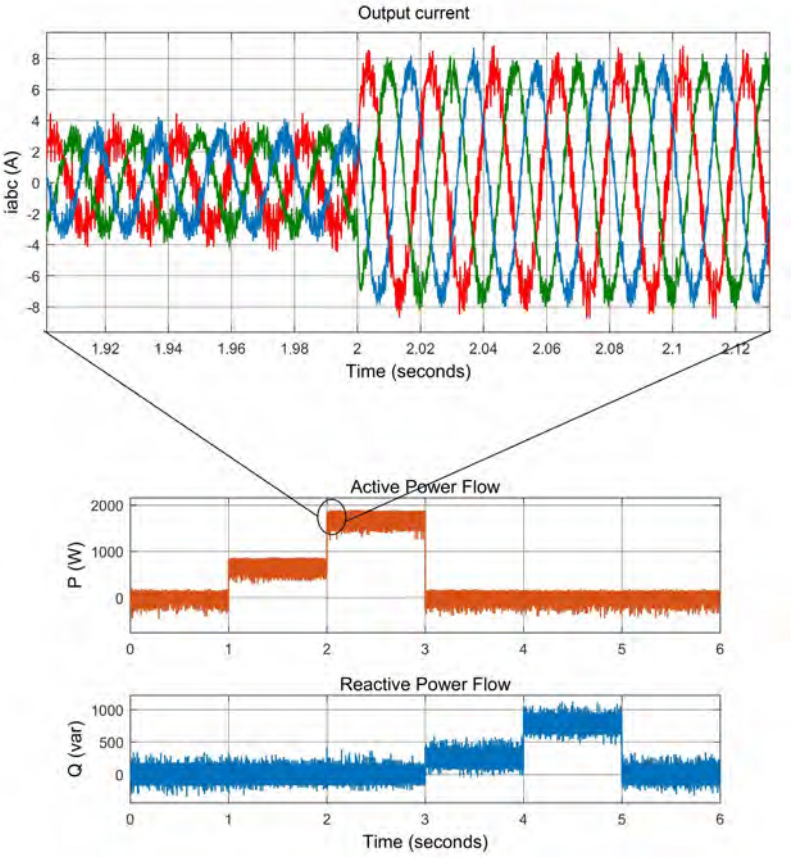

Figure 4.8: Power flow tracking via two-step prediction (experimental) for scenario 1

ble 4.2. The power ripple at the specific operating points can be obtained using the standard deviation approach in [19] as follows,

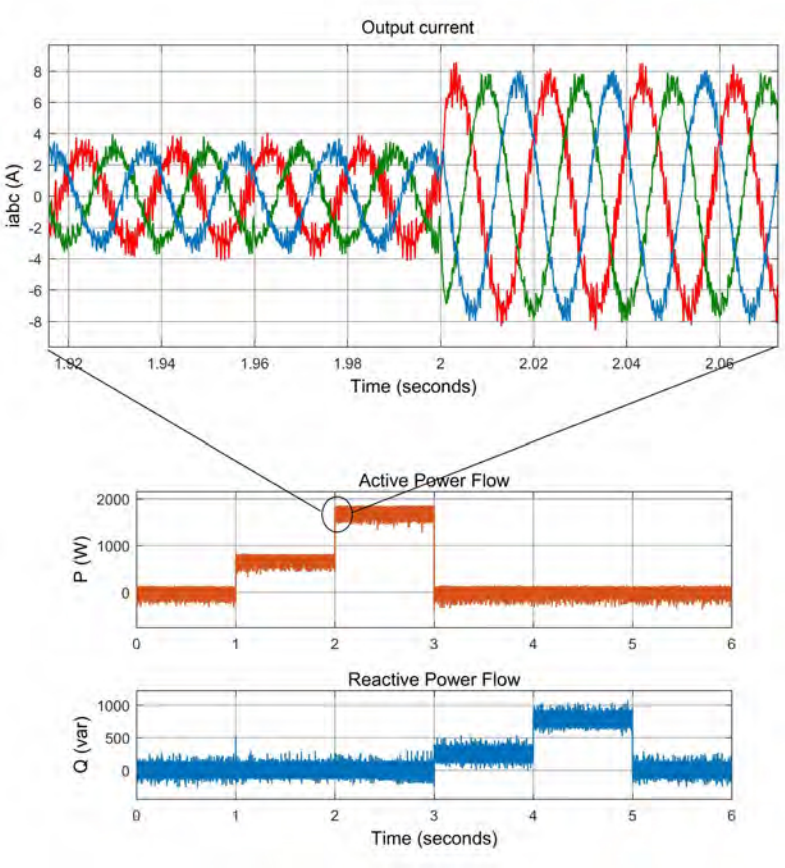

Figure 4.9: Power flow tracking via two-step prediction (experimental) for scenario 2

$$P_{rip} = \sqrt{\frac{1}{N_r}\sum_{\varsigma=1}^{N_r}(P_\varsigma - \frac{1}{N_r}\sum_{\varsigma=1}^{N_r}P_\varsigma)^2}$$
$$Q_{rip} = \sqrt{\frac{1}{N_r}\sum_{\varsigma=1}^{N_r}(Q_\varsigma - \frac{1}{N_r}\sum_{\varsigma=1}^{N_r}Q_\varsigma)^2} \tag{4.10}$$

where N_r is the sampling number in a period of $0.1s$. For more explicit quantitative comparison, the indices such as settling time, rise time, P_{rip} and Q_{rip} are normalized by the sampling time and the nominal values for active and reactive power, respectively.

It can be realized that by simplifying the computation burden, the power ripples are increased by almost 70%. However, the calculation time for simplified method is decreased by approximately 57% in comparison with two-step prediction scenario. Additionally, the simplifying method has a higher THD percentage which indicates a weaker performance of controller in tracking the reference in comparison with the second scenario. However, the average switching frequency is lower in the first scenario. In term of transient response, the both approaches have quite similar response time. By changing the sampling time to 10 kHz, both methods show almost same performance in terms of power ripples.

Table 4.2: Quantitative comparison of experimental results at the operating point of $P = 1100\,W$ and $Q = 0\,Var$

Indices	Scenario 1	Scenario 2
$f_s(kHz)$	50	50
$\overline{f_{sw}}(kHz)$	2.03	2.91
P_{rip}	0.73	0.414
Q_{rip}	0.871	0.589
$\text{THD}_{i_{oa}}(\%)$	10.1	6.78
Settling time	0.41	0.35

4.6 Summary

The MPC method can be effective for converter control in distributed power generations but requires a large amount of computation, leading to a considerable time delay in the actuation. If the delay is not reflected, the system performance could get worse. This chapter presents a two-step (horizon) prediction algorithm of MPC technique for grid-tied inverters used in distributed generation systems. The control objectives such as tracking the active and reactive power flow, balancing the neutral point and switching loss reduction are reflected in the objective function of the controller. The proposed MPC strategy is verified numerically by using MATLAB/Simulink and implemented in the laboratory experiments.

Bibliography

[1] M. Morari and J. H. Lee, "Model predictive control: past, present and future," *Computers & Chemical Engineering*, vol. 23, no. 4-5, pp. 667–682, 1999.

[2] V. Yaramasu, M. Rivera, M. Narimani, B. Wu, and J. Rodriguez, "Finite state model-based predictive current control with two-step horizon for four-leg npc converters," *Journal of Power Electronics*, vol. 14, no. 6, pp. 1178–1188, 2014.

[3] T. Geyer and D. E. Quevedo, "Multistep finite control set model predictive control for power electronics," *IEEE Transactions on power electronics*, vol. 29, no. 12, pp. 6836–6846, 2014.

[4] T. Dragičević, "Model predictive control of power converters for robust and fast operation of ac microgrids," *IEEE Transactions on Power Electronics*, vol. 33, no. 7, pp. 6304–6317, 2018.

[5] R. Baidya, R. P. Aguilera, P. Acuna, S. Vazquez, and H. du Toit Mouton, "Multistep model predictive control for cascaded h-bridge inverters: Formulation and analysis," *IEEE Transactions on Power Electronics*, vol. 33, no. 1, pp. 876–886, 2018.

[6] T. Geyer and D. E. Quevedo, "Performance of multistep finite control set model predictive control for power electronics," *IEEE Transactions on power electronics*, vol. 30, no. 3, pp. 1633–1644, 2015.

[7] P. Karamanakos, T. Geyer, and R. Kennel, "Reformulation of the long-horizon direct model predictive control problem to reduce the computational effort," in *Energy Conversion Congress and Exposition (ECCE), 2014 IEEE*. IEEE, 2014, pp. 3512–3519.

[8] P. KaraMaNaKOS, T. Geyer, N. Oikonomou, F. D. KIEFErNDOrF, and S. MaNIaS, "Direct model predictive control: A review of strategies that achieve long prediction intervals for power electronics," *IEEE Industrial Electronics Magazine*, vol. 8, no. 1, pp. 32–43, 2014.

[9] M. M. Aghdam, L. Li, and J. Zhu, "A model predictive power control method with longer prediction horizon for distributed power generations," in *Control, Automation, Robotics and Vision (ICARCV), 2016 14th International Conference on*. IEEE, 2016, pp. 1–6.

[10] P. Karamanakos, T. Geyer, and R. P. Aguilera, "Computationally efficient long-horizon direct model predictive control for transient operation," in *Energy Conversion Congress and Exposition (ECCE), 2017 IEEE*. IEEE, 2017, pp. 4642–4649.

[11] S. Vazquez, J. Rodriguez, M. Rivera, L. G. Franquelo, and M. Norambuena, "Model predictive control for power converters and drives: Advances and trends," *IEEE Transactions on Industrial Electronics*, vol. 64, no. 2, pp. 935–947, 2017.

[12] T. Geyer and S. Mastellone, "Model predictive direct torque control of a five-level anpc converter drive system," *IEEE transactions on Industry Applications*, vol. 48, no. 5, pp. 1565–1575, 2012.

[13] R. P. Aguilera, P. Lezana, and D. E. Quevedo, "Finite-control-set model predictive control with improved steady-state performance," *IEEE Transactions on Industrial Informatics*, vol. 9, no. 2, pp. 658–667, 2013.

[14] J. Rodriguez, M. P. Kazmierkowski, J. R. Espinoza, P. Zanchetta, H. Abu-Rub, H. A. Young, and C. A. Rojas, "State of the art of finite control set model predictive control in power electronics," *IEEE Transactions on Industrial Informatics*, vol. 9, no. 2, pp. 1003–1016, 2013.

[15] J. Hu, J. Zhu, and D. G. Dorrell, "In-depth study of direct power control strategies for power converters," *IET Power Electronics*, vol. 7, no. 7, pp. 1810–1820, 2014.

[16] ——, "Model predictive control of grid-connected inverters for pv systems with flexible power regulation and switching frequency reduction," *IEEE Transactions on Industry Applications*, vol. 51, no. 1, pp. 587–594, 2015.

[17] Z. Gong, P. Dai, X. Yuan, X. Wu, and G. Guo, "Design and experimental evaluation of fast model predictive control for modular multilevel converters," *IEEE Transactions on Industrial Electronics*, vol. 63, no. 6, pp. 3845–3856, 2016.

[18] J. D. Barros, J. F. A. Silva, and É. G. Jesus, "Fast-predictive optimal control of npc multilevel converters," *IEEE Transactions on Industrial Electronics*, vol. 60, no. 2, pp. 619–627, 2013.

[19] Y. Zhang, Y. Peng, and C. Qu, "Model predictive control and direct power control for pwm rectifiers with active power ripple minimization," *IEEE Transactions on Industry Applications*, vol. 52, no. 6, pp. 4909–4918, 2016.

[20] C. A. Rojas, J. Rodriguez, F. Villarroel, J. R. Espinoza, C. A. Silva, and M. Trincado, "Predictive torque and flux control without weighting factors," *IEEE Transactions on Industrial Electronics*, vol. 60, no. 2, pp. 681–690, 2013.

[21] M. Siami, H. K. Savadkoohi, A. Abbaszadeh, D. Khaburi, J. Rodriguez, and M. Rivera, "Predictive torque control of a permanent magnet synchronous motor fed by a matrix converter without weighting factor," in *Power Electronics and Drive Systems Technologies Conference (PEDSTC), 2016 7th.* IEEE, 2016, pp. 614–619.

Chapter 5

FCS-MPC OF POWER CONVERTERS: WEIGHTING FACTOR

5.1 Introduction

This chapter presents a self-tuning model predictive control (MPC) for power flow control and power quality improvement in grid-connected power converters. While MPC carries some benefits, the algorithm needs to be reformed for various purposes, mostly due to the variety of the plant characteristics that causes some challenges for the design. A multi-objective optimization problem can be formulated to take into account different requirements and constraints with corresponding weighting factors. Therefore, all the control necessities will be observed by the controller simultaneously. Nevertheless, the weighting factor adjustment is generally addressed by heuristic approaches for which there is not a detailed analytical study [1]. To overcome this challenge, the selection of weighting factors is avoided in some cases via a nontrivial process based on a ranking approach in [2, 3]. By using this method, multiple voltage vectors may have the same average ranking. Although priorities can be allocated for each objective to overcome this matter, it remains an open discussion in this approach. Furthermore, it also increases the computational burden up to three times more than the heuristic methods. In [15] the weighting factors are eliminated by converting the objectives to the same nature. Moreover, fuzzy decision making approach is utilized and developed in [4–7], where a membership function represents the degree of achievement of the target.

In this chapter, finite control set MPC (FCS-MPC) combining with a fuzzy logic control (FLC) approach with several objectives for grid-connected power converters is explored. This method uses an FLC scheme to regulate the fitting value of weighting factors online subject to the specific dynamic conditions, leading to improved power system performance. Based on the simulation results, it is shown that with the variable weighting factors, corresponding to each operating condition, better transient and steady state performance can be achieved.

5.2 State of the Art

Adding control objectives and constraints is a significant feature of FCS-MPC. These additional terms can be simply incorporated into the cost function with their specific weighting factors. Consequently, all the control necessities will be observed by the controller simultaneously. However, the weighting factor tuning is usually a heuristic process for which there is not a precise or analytical approach. In [2], the calculation of weighting factors is attained via a nontrivial process based on a ranking approach.

The main contribution of [8] is the exclusion of weighting factors in the multi-objective function. The algorithm is applied to a three-level one-phase (3L-1Ph) neutral point clamped (NPC) converter as an active power filter (APF) with three control objectives. A combination of a good current reference generator and choice of redundant switching states can be used to remove the weighting factors and DC capacitor currents. In [9–11], a two-vector based model predictive torque control is studied where the weighting factors are removed by normalizing all the terms in the objective function. An online fuzzy approach for tuning of weighting factors based on Sugeno technique is discussed in [4].

A well-defined analytic technique is proposed in [12] for the real-time adjustment of dynamic weighting factors, as well as a new objective function formulation. It provides a dynamic controller behavior, automatically adapted to distinct operating points, which ensures better steady-state performance in different conditions while improving simultaneously the dynamic response.

5.3 Proposed FCS-MPC Algorithm with Online Tuning of Weighting Factors

In a self-tuning MPC approach for power flow control and power quality improvement in grid-connected power converters, the FCS-MPC is combined with an FLC.

5.3.1 FCS-MPC for power converters

A block diagram of a gird-connected voltage source inverter (VSI) is depicted in Fig. 5.1. Aforementioned, in FCS-MPC, developing a precise dynamic model is essential [13]. Please refer to Section 3.3.1 for the mathematical model of a gird-connected VSI.

5.3.2 Fuzzy-based self-tunig FCS-MPC

A fuzzy logic system works on the principle of assigning a particular output depending on the probability of the state of the input. The FLC has been employed to adjust the weighting factor of the optimization problem for predicting the optimal switching pattern of the next sampling time. Every fuzzy inference system (FIS) is composed of three stages including fuzzification, fuzzy rules, and defuzzification as described in Fig. 5.2. The membership functions (MFs) are the essential part of FLC; they can be an arbitrary curve defined as a function that suits designers in

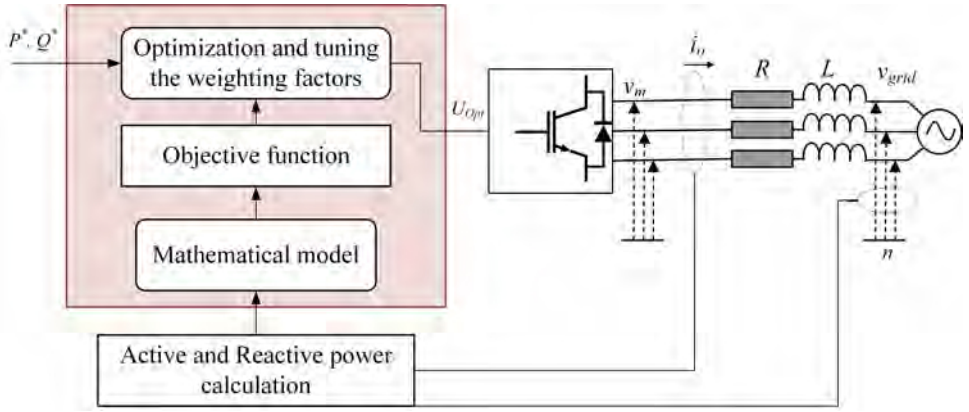

Figure 5.1: Block diagram for FCS-MPC of a grid-connected inverter

approaching simplicity and efficiency. A degree of membership is given to the inputs through MFs. In other words, we can say that membership function represents the degree of truth in fuzzy logic.

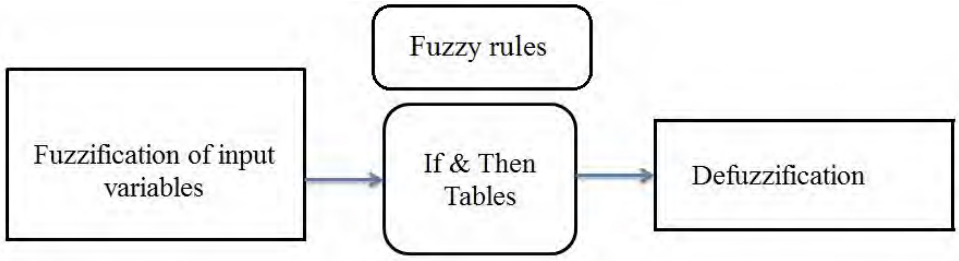

Figure 5.2: Fuzzy logic control technique

The flowchart of the proposed fuzzy-based self-tuning FCS-MPDPC is illustrated in Fig. 5.3. To evaluate and minimize the multi-objectives function, for each operating point, a specific weighting factor is required [17].

5.4 Case Study I: 2L-3Ph Grid-connected VSI

5.4.1 Mathematical model of 2L-3Ph grid-connected VSI

This topology is broadly used by industry applications and dominates the market at low voltage (LV). A block diagram of 2L-3Ph grid-connected inverter is represented in Fig. 5.4. It is formed by a complementary pair of power switches for each phase and linked to the utility grid through an RL filter.

There are a total number of eight possible output voltage vectors for this topology ($m = 2^3 = 8$) as follows,

$$v_m = \begin{cases} \frac{2}{3} e^{j(m-1)\frac{\pi}{3}} V_{DC}, & \text{if } m = 1, ..., 6 \\ 0 & \text{if } m = 0, 7 \end{cases} \tag{5.1}$$

By discretizing the state space model, the future value of output variables can be estimated. Backward Euler method has been used for discretizing the plant. In this way, the future value of the system inputs is used to predict the future value

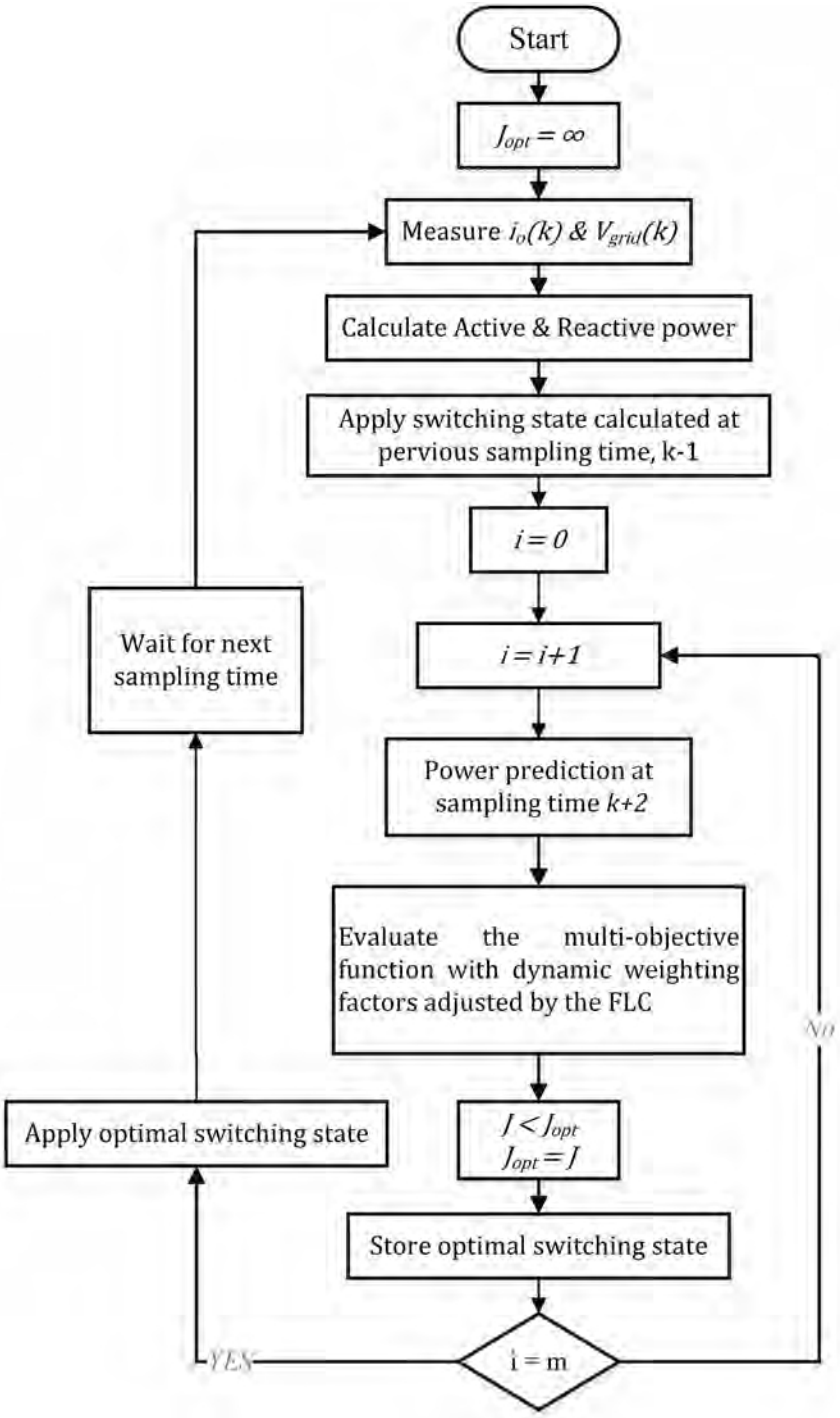

Figure 5.3: Flowchart of proposed method

of the controlled variables. Given the continuous model developed in (3.17), the following discrete time model can be obtained.

$$\mathbf{x}(k+1) = A\mathbf{x}(k) + B\mathbf{u}(k) \tag{5.2}$$

where A, and B are the discrete time matrices and can be calculated as

$$\begin{aligned} A &= e^{DT_s} \\ B &= \int_0^{T_s} e^{D\delta} F d\delta \end{aligned} \tag{5.3}$$

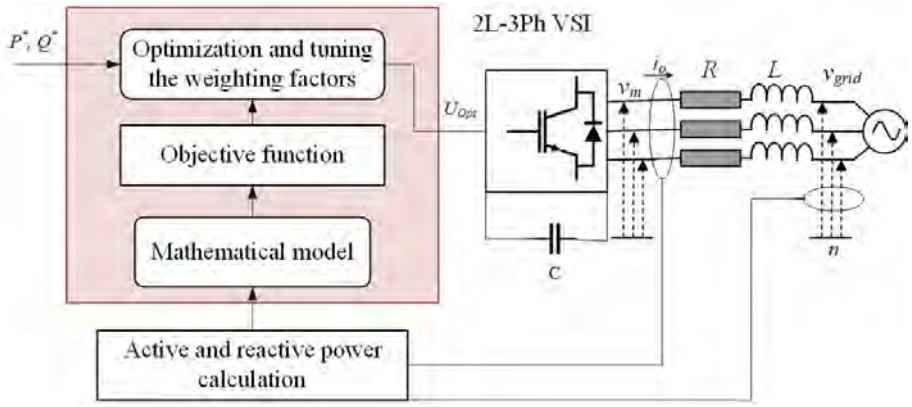

Figure 5.4: Block diagram of 2L-3Ph grid-tied inverter

where the matrices D and F are obtained according to mathematical model of the system in (3.18). Finally, the output vector contains the variables which are involved in the objectives of the controller. The control objective in this case can be defined as

$$J_m = Err_{PWR_m}(k+1) + \lambda Err_{SW_m}(k+1) \qquad \text{for} \quad m = 1, ..., 8 \tag{5.4}$$

where λ is the weighting factor coefficient; a larger value shows a higher priority for the second term. Err_{PWR} and Err_{SW} are given as

$$\begin{aligned} Err_{PWR_m}(k+1) &= [P^*(k+1) - P_m(k+1)]^2 + [Q^*(k+1) - Q_m(k+1)]^2 \\ Err_{SW_m}(k+1) &= \sum_h [u_m^h(k+1) - u_m^h(k)]^2 \qquad \text{for} \quad m = 1, ..., 8 \quad \text{and} \quad \text{for } h = a, b, c \end{aligned} \tag{5.5}$$

where $P^*(k+1)$ and $P_m(k+1)$ are the reference and predicted active power, $Q^*(k+1)$ and $Q_m(k+1)$ are the reference and predicted reactive power at $(k+1)T_S$. $u_m(k+1)$ and $u_m(k)$ are the sequence of power converter switch positions at next and current sampling interval, respectively. u_m can be either 0 or 1, where 0 means that the upper switch is off and the lower one is on, and 1 means the opposite. For example, supposing that $V_2(110)$ and $V_3(010)$ are applied at the current interval and next interval correspondingly, then the second term of the objective function can be determined as $Err_{SW} = [(0-1)^2 + (1-1)^2 + (0-0)^2] = 1$.

The valuation of the cost function with eight predictions $(i = 1, ..., 8)$ will lead to an eight different costs. Certainly, the control action will be chosen as the one which leads to the minimum cost. With the help of FLC, the weighting factor will be adjusted for optimal results in each operating point.

As mentioned, the proposed FIS is composed of three stages including fuzzification (input), fuzzy rules (processing), and defuzzification (output)as described in Fig. 5.5. The input variables in an FLC are mapped by sets of MFs. The process of converting a numerical input value to a fuzzy value is fuzzification. The most common shape of MF is triangular, however the number of curves and their position are more important than the shape [18].

The processing stage is a collection of IF-THEN statements. This stage checks each rule and generates a result for each, and then combines the results of the

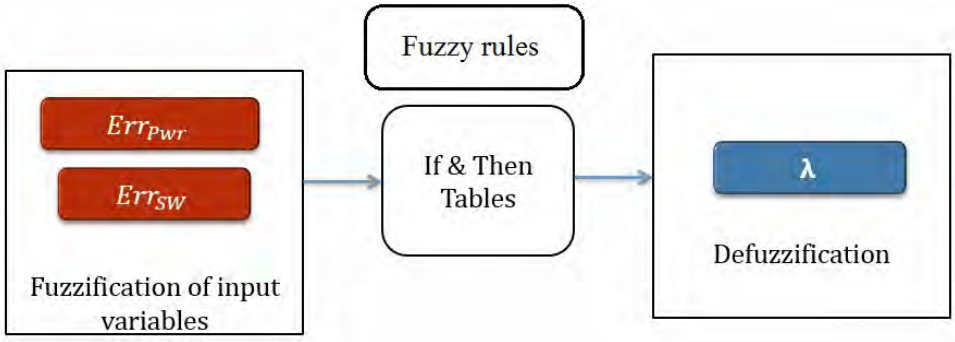

Figure 5.5: Fuzzy logic control technique

rules. The proposed rules are defined based on Fig. 5.6 for λ. The AND method simply uses the minimum weight for evaluating the rules, and centroid technique is applied for defuzzification to get the numerical values of the weighting factors. The input and output variables map into very small (VS), small (S), medium (M), big (B), and very big (VB) fuzzy set. The rules are defined base on these fuzzy sets, i.e. if Err_{PWR} is S and Err_{SW} is M, then λ is B. By changing the rules after gaining knowledge from behavior of the system, the controller performance can be improved. Finally, the output stage, defuzzification, converts the overall result back into a numeric output value.

λ		$Err_{PWR}(k+1)$				
		VS	S	M	B	VB
$Err_{SW}(k+1)$	VS	M	S	VS	VS	VS
	S	B	M	S	VS	VS
	M	VB	B	M	S	VS
	B	VB	VB	B	M	S
	VB	VB	VB	VB	B	M

Figure 5.6: Fuzzy rules for λ

5.4.2 Numerical results

In order to compare the proposed methods, the simulation and experimental validation of proposed FCS-MPC are presented. The system parameters are listed in Table 5.1.

5.4.2.1 Simulation results

Simulation of a 2L-3Ph VSI with L filter is carried out using MATLAB/Simulink. The state-space model of the plant is discretized by selecting backward Euler method. The initial active and reactive power references are both set to zero. The active power reference is increased to $-500\ W$ at $1s$ and decreased from -500 to $200\ W$ at $2s$. After that, the active power reference is kept to zero. The reactive power reference is altered to -200 and $400\ Var$ at $3s$ and $4s$, respectively. The results are

Table 5.1: Parameters of the system

Filter resistance	R	0.4 Ω
Filter inductance	L	4.6 mH
DC-link capacitor	C	680 μF
Grid voltage (L-n)	v_{grid}	65 V_{rms}
DC-link voltage	V_{DC}	180 V
Grid frequency	f	50 Hz

presented based on scenario 1, the weighting factors are considered fixed, and scenario 2, where FLC adjust the weighting factors for each operating point. Figs. 5.7 and 5.8 demonstrate the power flow control and the output currents in ABC-frame for scenarios 1 and 2.

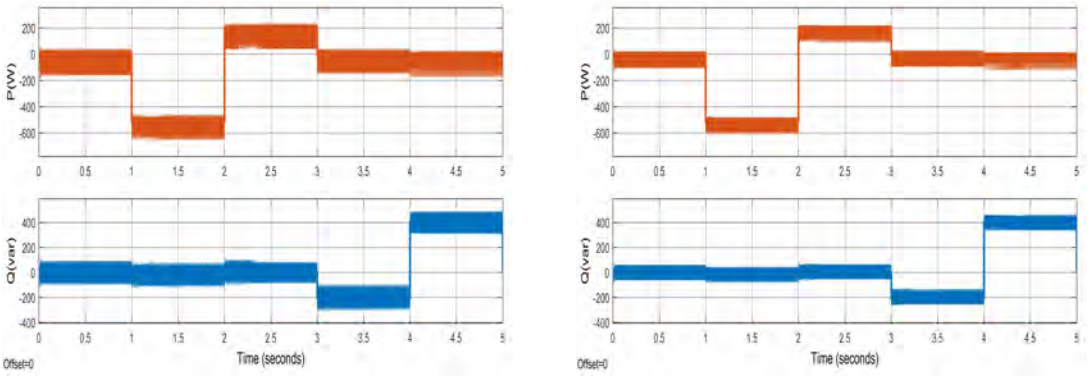

(a) (b)

Figure 5.7: Power flow control (simulation) (a) scenario 1 (b) scenario 2

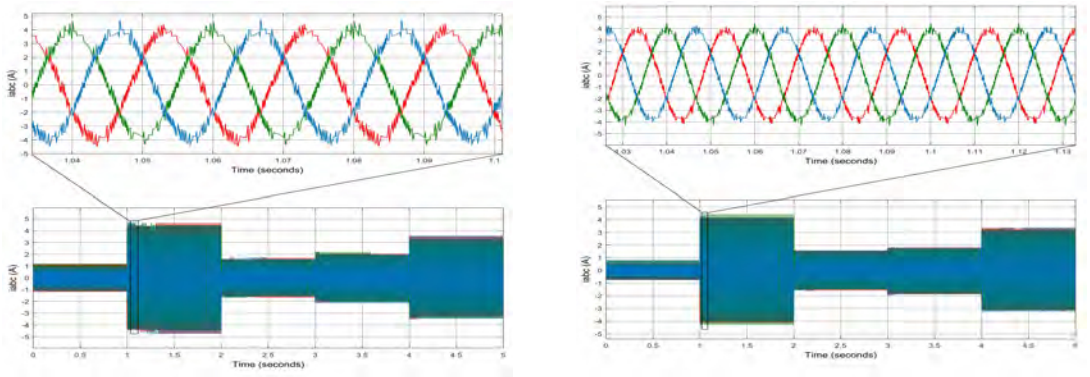

(a) (b)

Figure 5.8: Output currents in ABC-frame (simulation) (a) scenario 1 (b) scenario 2

Weighting factors surface curve and MF of Err_{PWR} are illustrated in Figs. 5.10 and 5.9. Each input and output has five MF which are of triangle function.

The number of rules would be 25 in total. As the number of MFs increases, the accuracy as well as complexity of the controller will increase.

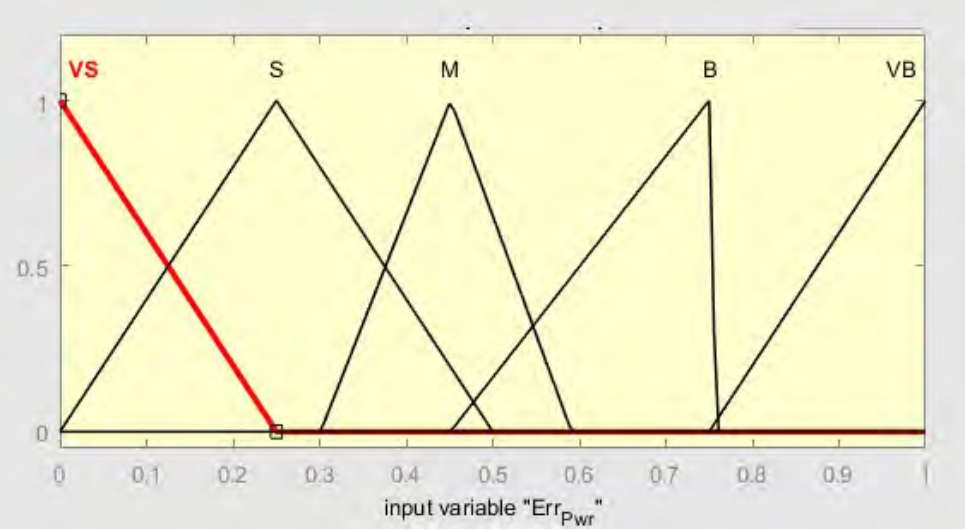

Figure 5.9: Membership function for Err_{PWR}

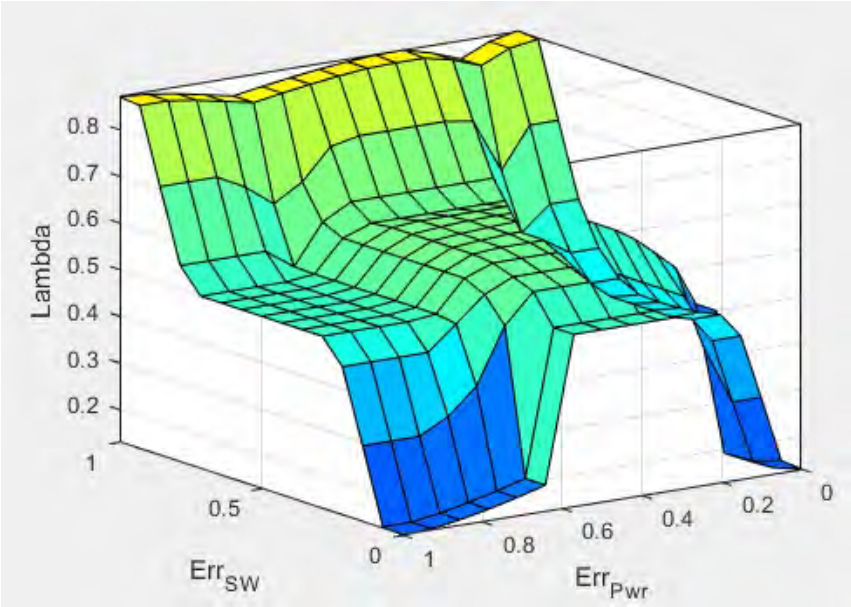

Figure 5.10: Weighting factors surface curve for λ

5.4.2.2 Experimental results

A real-time implementation (RTI) of the system is tested through the experimental set-up. The set-up is depicted in Fig. 3.11 which consists of three Semikron IGBT power modules as the inverter, a TDK-Lambda DC source, a three-phase L filter, and a variac for main grid connection. To implement the control algorithm, a digital signal processor (DSP) through a dSPACE R&DS1104 control board is used. The voltages and currents are sampled through sensors and converted to digital signal via analogue to digital converter (ADC) of the connector panel of dSpace

(CLP1104). The system parameters are kept same as the simulation. The power flow control and the output currents in ABC-frame are illustrated in Figs. 5.11 and 5.12.

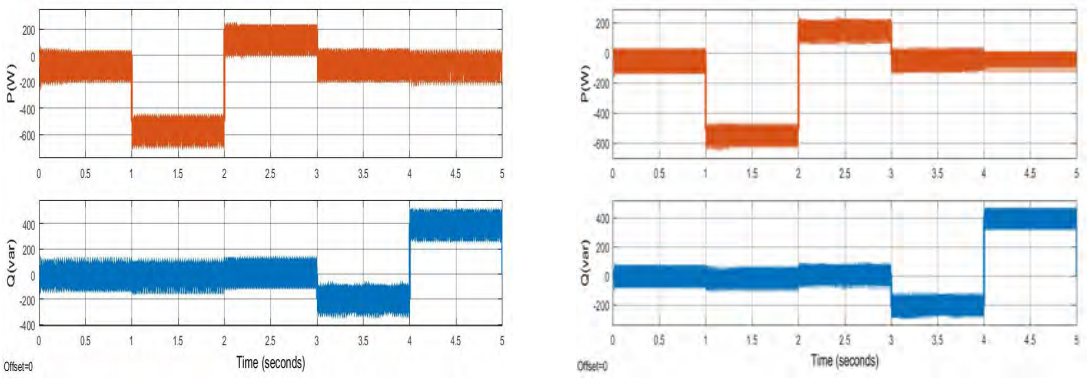

(a) (b)

Figure 5.11: Experimental power flow control (a) scenario 1 (b) scenario 2

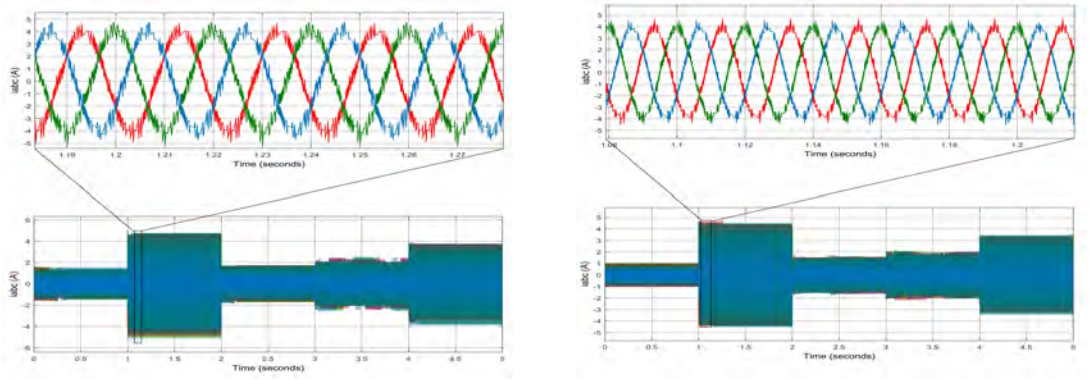

(a) (b)

Figure 5.12: Output currents in ABC-frame (a) scenario 1 (b) scenario 2

Fig. 5.11 shows the power flow for a 2L-3Ph grid-connected inverter with fixed and adaptive weighting factors. In Fig. 5.11a, scenario 1, the active and reactive power tracking is achieved through a fixed weighting factor, $\lambda = 0.013$, for all the operating points. The corresponding weighting factor for Err_{SW}, λ, is obtained based on the changes in Err_{pwr} and Err_{SW}. As can be seen, the power flow tracking shows the improvement in transient and steady state performance for scenario 2 than scenario 1. In order to get a better evaluation of the proposed control algorithm, quantitative comparison has been conducted.

5.4.3 Quantitative comparison and discussion

A quantitative comparison of tuning weighting factors for the FCS-MPDPC strategy in this case study is carried out. The fuzzy-based self-tuning method is compared with other mentioned approaches. With the intention of leading a better comparison of the approaches for tuning weighting factors in multi-objectives MPC, indices like the average switching frequency, total harmonic distortion (THD), power

ripples, overshoot, settling and calculation time are tabulated in Table 5.2. The quantities are measured through MATLAB tools.

P_{rip} and Q_{rip} are the active and reactive power ripples which are gained based on their standard deviation from the average one. The power ripple at the specific operating points can be obtained using the standard deviation approach in [19] as follows,

$$\begin{aligned} P_{rip} &= \sqrt{\frac{1}{N_r}\sum_{\varsigma=1}^{N_r}(P_\varsigma - \frac{1}{N_r}\sum_{\varsigma=1}^{N_r}P_\varsigma)^2} \\ Q_{rip} &= \sqrt{\frac{1}{N_r}\sum_{\varsigma=1}^{N_r}(Q_\varsigma - \frac{1}{N_r}\sum_{\varsigma=1}^{N_r}Q_\varsigma)^2} \end{aligned} \tag{5.6}$$

where N_r is the sampling number in a period of $0.1s$. For more explicit quantitative comparison, the indices such as settling time, rise time, P_{rip} and Q_{rip} are normalized with respect to sampling time and the nominal values for active and reactive power, respectively.

Table 5.2: Quantitative comparison of experimental results at the operating point of P = -500 W and $Q = 0\,Var$

Operating points	P = -500 W and $Q = 0\,Var$	
Indices	Senario 1	Senario 2
$f_s(kHz)$	20	20
$\overline{f_{sw}}(kHz)$	2.23	1.67
P_{rip}	0.651	0.384
Q_{rip}	0.786	0.445
$\text{THD}_{i_{oa}}(\%)$	17.2	12.1
Settling time	0.126	0.115
Rise time	0.174	0.161
Overshoot(%)	43.5	28.4

It can be realized that the by tuning weighting factors by FLC scheme, the power ripples have been reduced by almost 40.9 %. However, the calculation time for FLC-based method has increased, by approximately 36% in comparison with the heuristic approach. Additionally, the proposed method has shown a good performance in terms of the THD percentage, as depicted in Fig 5.13, and average switching frequency. In terms of the transient, the resulting performance of the proposed strategy with tuning weighting factors reserves the fast dynamic response compared with the conventional MPC.

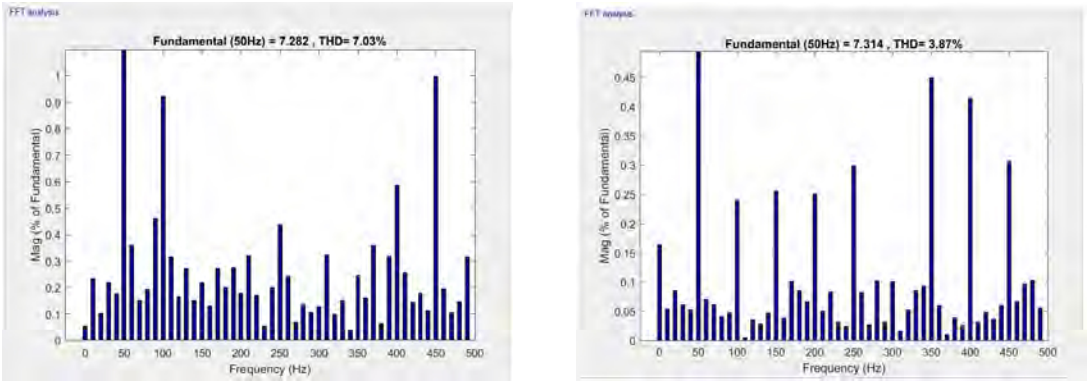

(a) (b)

Figure 5.13: FFT analysis (experimental) (a) scenario 1 (b) scenario 2

5.5 Case Study II: 3L-3Ph Grid-connected Neutral Point Clamped VSI

5.5.1 FCS-MPC for 3L-3Ph NPC-VSI

At the medium voltage (MV) level, there are a wide range of topologies which share the market. In fact, for high-power applications, like industrial MV drives, it is possible to employ direct converters (without DC-link) as well as indirect converters (with DC-link). Among the all, NPC-VSI is used widely for high-power industrial applications. The block diagram of a grid-connecteed 3L-3Ph NPC-VSI is represented in Fig. 5.14. The inverter consists of six complementary pairs of IGBTs. At the DC side, the inverter has two series-connected capacitors C_1 and C_2 ($C_1 = C_2 = C$) which divide the DC-link voltage into three levels of $\frac{V_{DC}}{2}$, 0, and $-\frac{V_{DC}}{2}$.

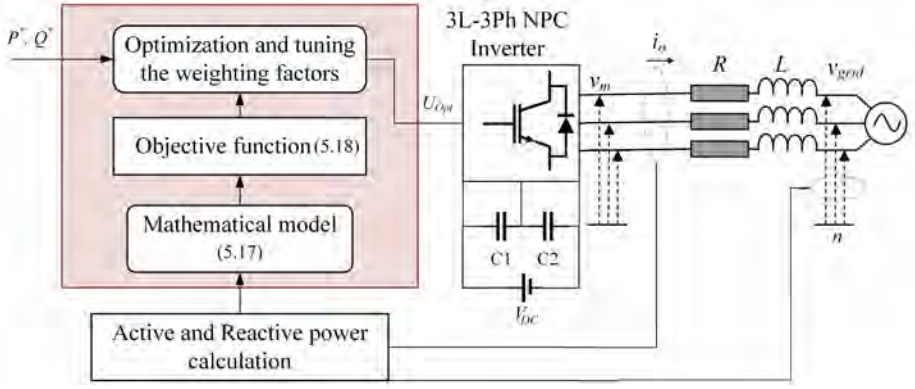

Figure 5.14: Block diagram of grid-connected 3L-3Ph NPC-VSI

The output voltage of 3L-3Ph NPC inverter can be obtained as follows,

$$V_m = \frac{2}{3}(V_{an} + aV_{bn} + a^2V_{cn}) \tag{5.7}$$

In NPC-VSI, the balance of voltage across the capacitors is one the most important objectives to achieve high power quality. Therefore, the mathematical

model for capacitor voltages and their prediction is an essential. In our modeling, we assume that the direction of power flow is from the inverter towards the grid. The total DC-link voltage is the sum of voltages across the capacitors, $V_{DC} = V_{C1} + V_{C2}$. Under the balanced situations, the neutral point voltage V_n is zero. To obtain the discrete time state space model, the dynamics of state vectors and neutral point voltage are discretized through forward Euler approach. Given the continuous model developed in (3.33), the following discrete time model can be obtained.

$$\mathbf{x}(k+2) = A\mathbf{x}(k+1) + B\mathbf{u}(k+1) \tag{5.8}$$

where A, and B are the discrete time matrices and can be calculated as

$$\begin{aligned} A &= e^{DT_s} \\ B &= \int_0^{T_s} e^{D\delta} F d\delta \end{aligned} \tag{5.9}$$

where the matrices D and F are obtained according to mathematical model of the system in (3.35). Finally, the output vector contains the variables which are involved in the objectives of the controller. The output vector is given by

$$\begin{aligned} Y &= \begin{bmatrix} P(k+2) & Q(k+2) & V_n(k+2) \end{bmatrix}^T \\ \begin{bmatrix} P(k+2) \\ Q(k+2) \end{bmatrix} &= \frac{3}{2} \begin{bmatrix} v_{grid}^{\alpha} & v_{grid}^{\beta} \\ -v_{grid}^{\beta} & v_{grid}^{\alpha} \end{bmatrix} \begin{bmatrix} i_o^{\alpha}(k+2) \\ i_o^{\beta}(k+2) \end{bmatrix} \\ V_n(k+2) &= \frac{T_s}{2C} [u_m(k+1)]^T i_o^{\alpha\beta}(k+1) + V_n(k+1) \end{aligned} \tag{5.10}$$

where $P(k+2)$, $Q(k+2)$ and $V_n(k+2)$ are the predicted active power, reactive power, and neutral point voltage at $(k+2)T_S$, respectively. $C_1 = C_2 = C$, $i_o^{\alpha\beta} = [\ i^{\alpha}\ i^{\beta}]^T$, and $u_m = [\ u_m^{\alpha}\ u_m^{\beta}]^{\ T}$, for $m = 0, ..., 27$.

At each time-step k, the upper and lower DC-link capacitor voltages, and the currents and grid voltages at each phase are measured. The upper and lower capacitor voltages determine $V_{DC}(k)$ and $V_n(k)$. Then, the measured currents and grid voltages are transformed from the natural ABC-frame to the stationary $\alpha\beta$-frame. These measured values are used to calculate the active and reactive powers at the current time for the controller. The calculated value along with the references are given to the controller. The switching sequence $[u_m(k)]$ is in $\alpha\beta$-frame using the Clarke transformation. The predictions are then evaluated in a way that the switching states, which minimize the cost function, will be applied to the 3L-3P NPC-VSI. The cost function is defined as

$$J = Err_{pwr}(k+2) + \lambda_1 Err_{V_n}(k+2) + \lambda_2 Err_{SW}(k+2) \qquad \text{for} \quad m = 1, ..., 27 \tag{5.11}$$

where λ_1 and λ_2 are the weighting factors, Err_{pwr}, Err_{V_n}, and Err_{SW} are given as

$$\begin{aligned} Err_{pwr}(k+2) &= [P^*(k+2) - P_m(k+2)]^2 + [Q^*(k+2) - Q_m(k+2)]^2 \\ Err_{V_n}(k+2) &= [V_n^*(k+2) - V_{nm}(k+2)]^2 \\ Err_{SW}(k+2) &= [u_m(k+2) - u_m(k+1)]^2 \qquad \text{for} \quad m = 1, ..., 27 \end{aligned} \tag{5.12}$$

The proposed FIS is composed of three stages including fuzzification, fuzzy rules, and defuzzification as described in Fig. 5.15. Rules are defined based on Fig. 5.16 for λ_1 and λ_2.

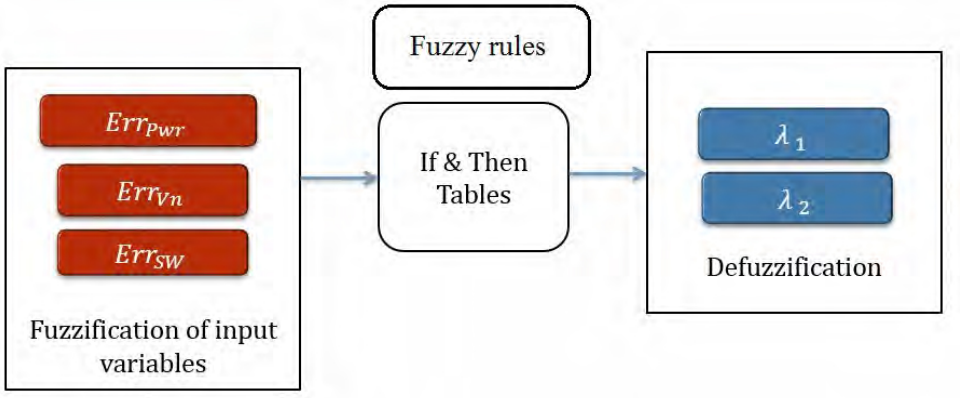

Figure 5.15: Fuzzy logic control technique

λ_1		$Err_{Pwr}(k+2)$				
		VS	S	M	B	VB
Err_{Vn} $(k+2)$	VS	VS	S	M	M	M
	S	S	M	M	M	M
	M	M	B	B	B	M
	B	B	B	B	B	VB
	VB	B	VB	VB	VB	VB

λ_2		$Err_{Pwr}(k+2)$				
		VS	S	M	B	VB
Err_{SW} $(k+2)$	VS	M	S	VS	VS	VS
	S	B	M	S	VS	S
	M	B	B	M	S	S
	B	VB	B	B	M	M
	VB	M	VB	M	B	M

Figure 5.16: Fuzzy rules for λ_1 and λ_2

5.5.2 Simulation and experimental results

The simulation and experimental validation are carried out to compare the proposed methods with the conventional FCS-MPC. The system parameters are listed in Table 5.3.

5.5.2.1 Simulation results

Simulation of a 3L-3Ph NPC-VSI with L filter is carried out using MATLAB/Simulink. The initial active and reactive power references both are set to

Table 5.3: Parameters of the system

Filter resistance	R	0.3 Ω
Filter inductance	L	10 mH
DC-link capacitor	C	1800 μF
Grid voltage (L-n)	v_{grid}	110 V_{rms}
DC-link voltage	V_{DC}	340 V
Grid frequency	f	50 Hz

zero. he active power reference is set to 700 W at 1s and increased from 700 to 1800 W at 2s . After that, the active power reference is kept to zero. The reactive power reference is altered to 350 and 800 Var at 3s and 4s, respectively. Figs. 5.17, 5.18 and 5.19 demonstrate the power flow control, the output currents in ABC-frame, and neutral voltage for two scenarios; in scenario 1, $\lambda_1 = 0.8$ and $\lambda_2 = 0.03$ for all the operating points, while in scenario 2, λ_1 and λ_2 are adaptively adjusted by the proposed FLC approach.

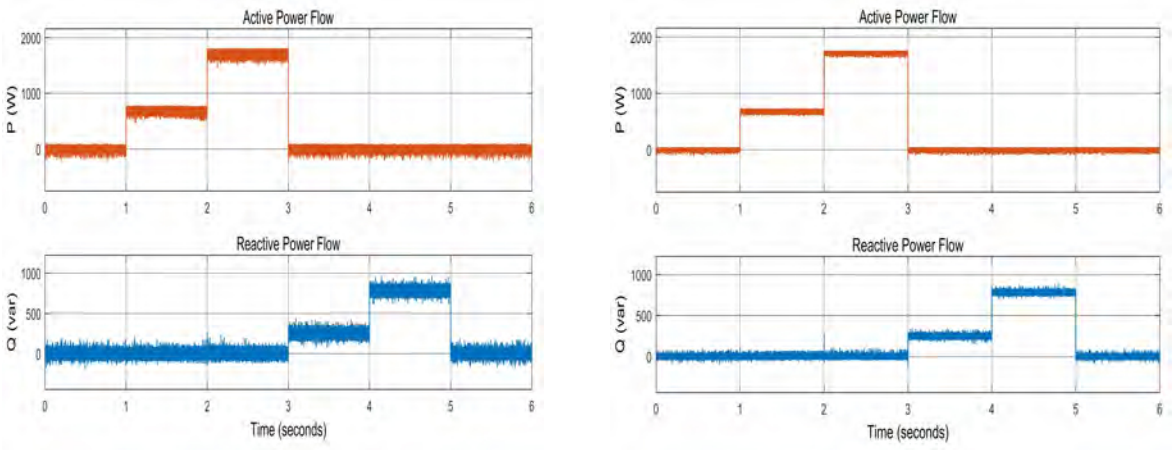

(a) (b)

Figure 5.17: Power flow control (simulation) (a) scenario 1 (b) scenario 2

Weighting factors surface curve for λ_1 and λ_2 are illustrated in Figs. 5.20 and 5.21, respectively. These curves shows how the weighting factors are distributed for different operating points. As mentioned, by gaining the knowledge about system behavior, these curves will change accordingly.

5.5.2.2 Experimental results

To validate the simulation results, a series of experiments have been conducted. The set-up is consists of three three-level Semikron IGBT power modules as the converter, a DC power supply, a three-phase L filter, and a variac for main grid connection as depicted in Fig. 5.22. To implement the control algorithm, a digital signal processor (DSP) through a dSPACE R&DS1104 control board and FPGA Digilent Cmod A7 is used. The voltages and currents are sampled through sensors and and

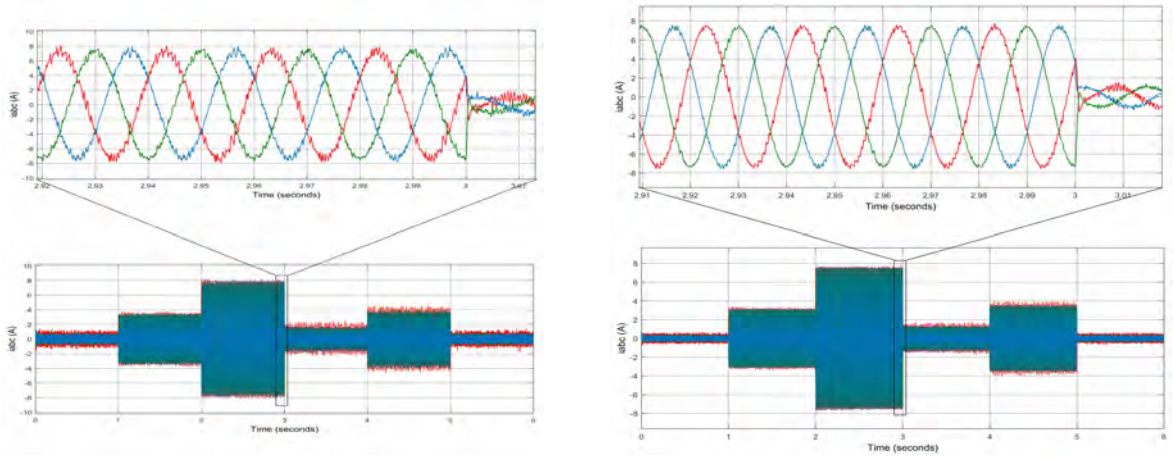

(a) (b)

Figure 5.18: Output current (simulation) (a) scenario 1 (b) scenario 2

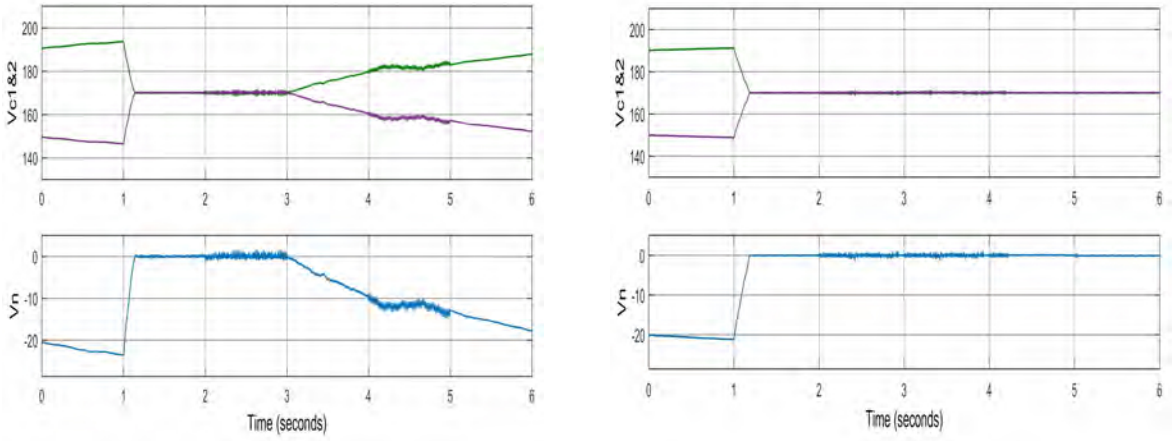

(a) (b)

Figure 5.19: Capacitor voltages and neutral point voltage (simulation) (a) scenario 1 (b) scenario 2

converted to digital signal via ADC of the connector panel of dSpace (CLP1104). The system parameters are kept the same as the simulation. The block diagram in Fig. 5.23 shows the RTI procedures.

Fig. 5.24 demonstrates a RTI performance of the 3L-3Ph NPC-VSI for the two scenarios with fixed and self-tuning weighting factors. Furthermore, the output currents in ABC-frame, capacitor voltages and neutral voltage are illustrated in Figs. 5.25 and 5.26.

Fig. 5.24 shows the power flow for the 3L-3Ph NPC grid-connected inverter with FCS-MPC strategy. In Fig. 5.24a (a), scenario 1, the active and reactive power tracking is achieved through the fixed weighting factors, $\lambda_1 = 0.753$ and $\lambda_2 = 0.01$, for all the operating points. The corresponding weighting factor for Err_{V_n}, λ_1, is obtained based on the changes in Err_{pwr} and Err_{V_n}. Similarly, λ_2 is adjusted based on the variations in Err_{pwr} and Err_{SW}. As can be seen, the power flow tracking shows the improvement in transient and steady state performance for scenario 2 compared to scenario 1. In order to get a better evaluation of the proposed control

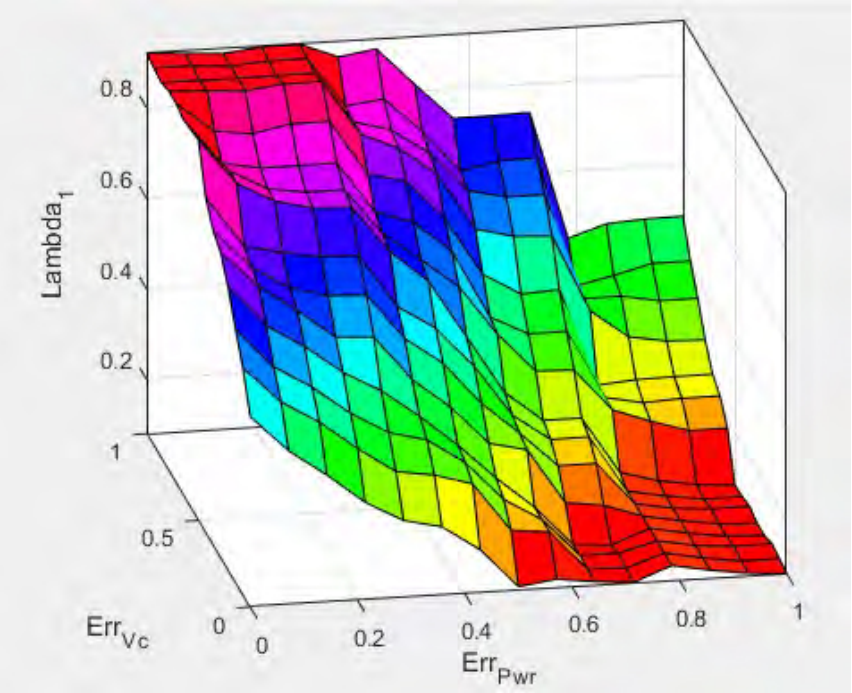

Figure 5.20: Weighting factor surface curve for λ_1

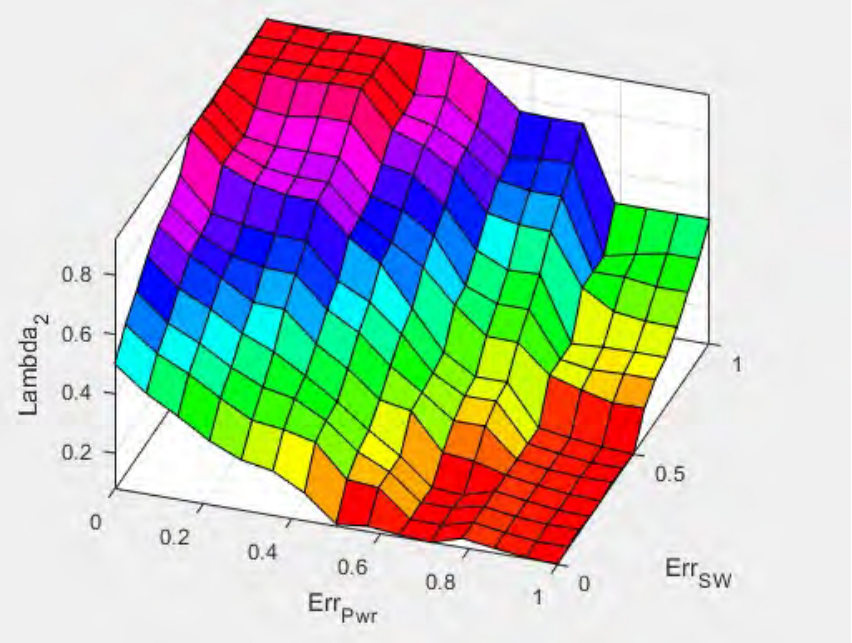

Figure 5.21: Weighting factor surface curve for λ_2

algorithm, quantitative comparison has been conducted.

5.5.3 Quantitative comparison and discussion

A quantitative comparison of tuning weighting factors for the FCS-MPC strategy in this case study is carried out. The fuzzy-based self-tuning method is compared with other mentioned approaches. With the intention of leading a better comparison of the approaches for tuning weighting factors in multi-objectives MPC, indices

Figure 5.22: Experimental set-up

like the average switching frequency, THD, power ripples, overshoot and settling are tabulated in Table 5.4. The quantities are measured through MATLAB tools. For clearer quantitative comparison, the indices such as settling time, rise time, P_{rip} and Q_{rip} are normalized with respect to sampling time and the nominal values for active and reactive power, respectively.

It can be realized that by tuning weighting factors by FLC scheme, the power ripples have been reduced by 37.16%. However, the calculation time for FLC-based method has increased, by approximately 41% and 13% in comparison with heuristic and ranked-based schemes [2, 3], respectively. Additionally, the proposed method has shown a good performance in terms of the THD percentage, as depicted in Fig 5.27, and average switching frequency. In term of transient response, the proposed FLC-based FCS-MPC obtains about 15% less settling time and overshoot.

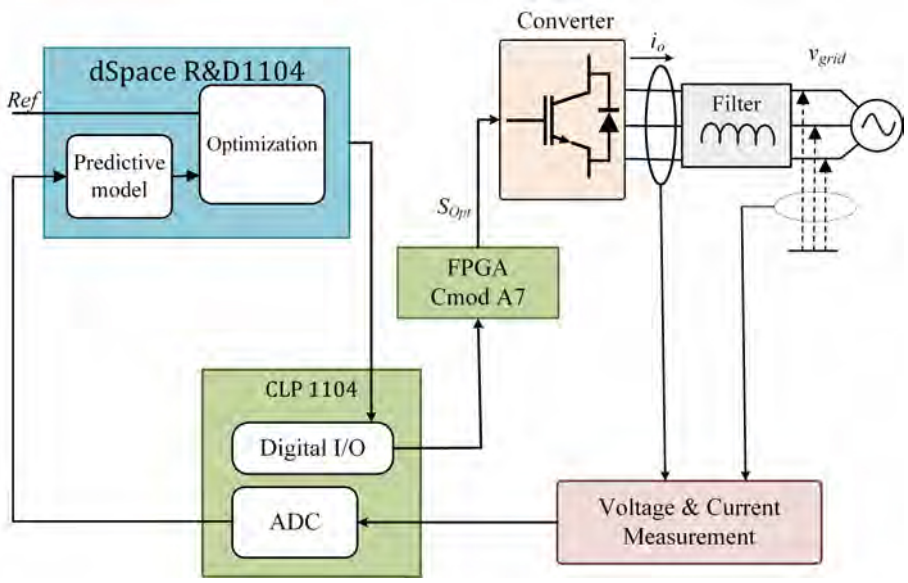

Figure 5.23: Block diagram of the experimental set-up

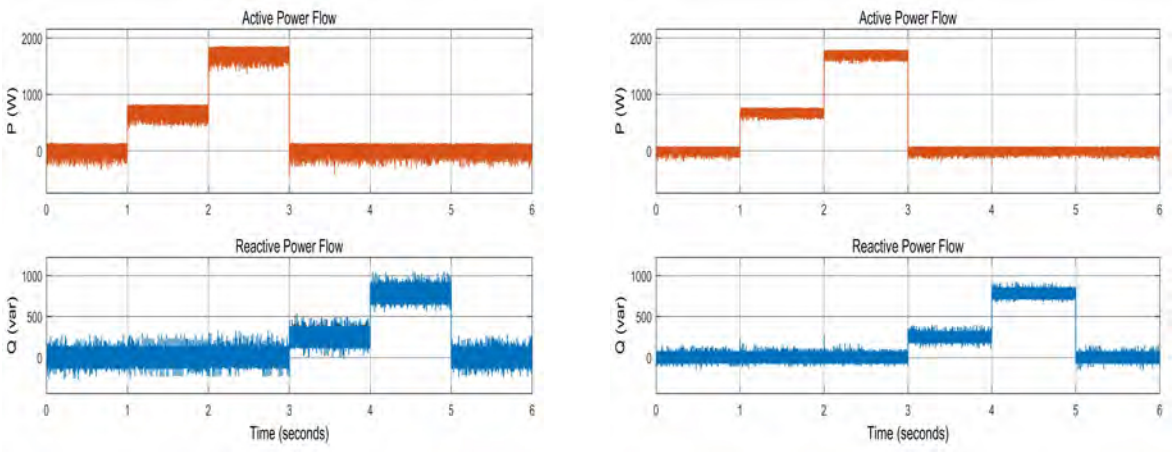

(a) (b)

Figure 5.24: Power flow control (experimental) (a) scenario 1 (b) scenario 2

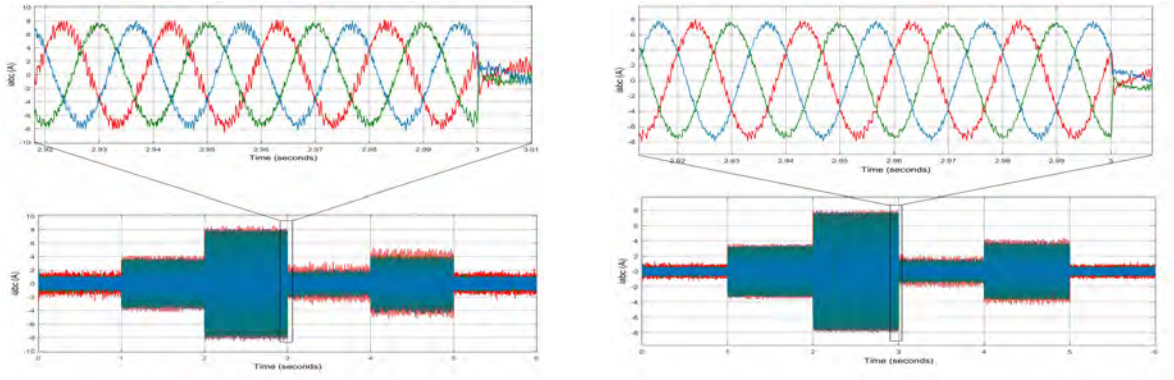

(a) (b)

Figure 5.25: Output current (experimental) (a) scenario 1 (b) scenario 2

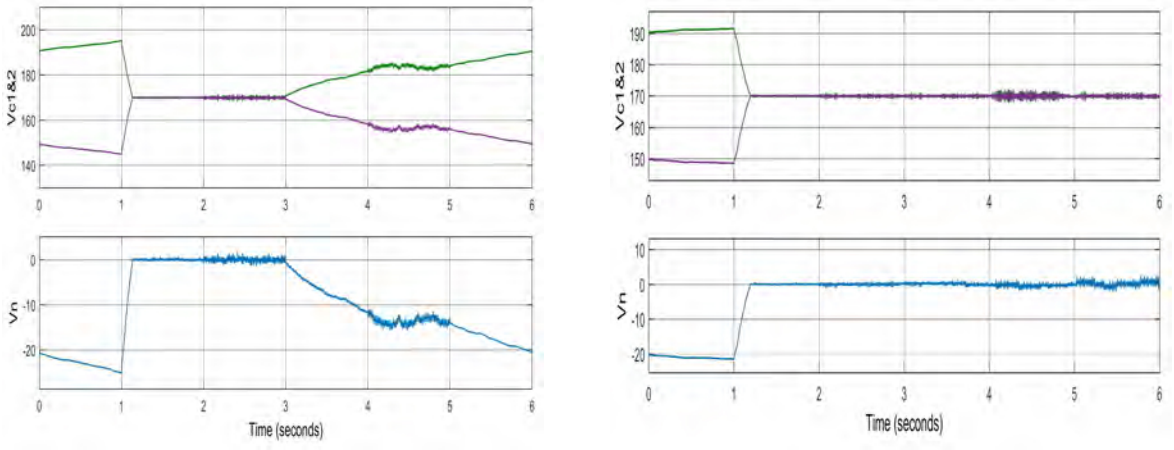

(a) (b)

Figure 5.26: Capacitor voltages and neutral point voltage (experimental) (a) scenario 1 (b) scenario 2

Table 5.4: Quantitative comparison of experimental results at the operating point of $P = 1500\,W$ and $Q = 0\,Var$

Operating points	$P = 1500\,W$ and $Q = 0\,Var$		
Indices	Heuristic	Ranked-based	FLC
$f_s(kHz)$	10	10	10
$\overline{f_{sw}}(kHz)$	3.23	2.1	1.9
P_{rip}	0.696	0.524	0.404
Q_{rip}	0.719	0.512	0.384
$\text{THD}_{i_{oa}}(\%)$	7.2	5.8	3.9
Settling time	0.26	0.25	0.234
Overshoot(%)	47.5	40.4	37.3
Weighting Factor(%)	Constant	Variable	Variable

5.6 Summary

This chapter proposes a self-tuning model predictive direct power control strategy for power flow control and power quality improvement in grid-connected power converters. At each sampling instant, an FLC is used to determine online the best weighting factor values for a given operating point. These values are then used to solve the multi-objective optimal control problem associated to the FCS-MPC. The optimal input (power switch state) that minimizes the multi-objective cost function is chosen. The proposed method is examined numerically via MATLAB SIMULINK for case studies and verified by an experimental set-up in the research laboratory.

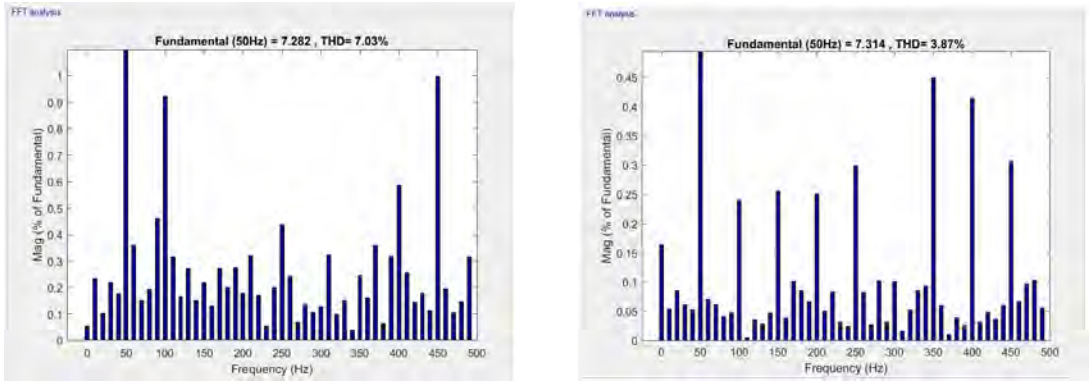

(a) (b)

Figure 5.27: FFT analysis (experimental) (a) scenario 1 (b) scenario 2

A comparative study is conducted to demonstrate the effective performance of this approach. As a result of the proposed weighting factor online tuning, an improved performance in terms of THD and average switching frequency is attained when compared with fixed weighting factors.

Bibliography

[1] P. Cortés, S. Kouro, B. L. Rocca, R. Vargas, J. Rodríguez, J. I. León Galván, S. Vázquez Pérez, and L. García Franquelo, "Guidelines for weighting factors design in model predictive control of power converters and drives," in *International Conference On Industrial Technology (ICIT), 1-7. Gippsland, Australia: IEEE.* IEEE, 2009.

[2] C. A. Rojas, J. Rodriguez, F. Villarroel, J. R. Espinoza, C. A. Silva, and M. Trincado, "Predictive torque and flux control without weighting factors," *IEEE Transactions on Industrial Electronics*, vol. 60, no. 2, pp. 681–690, 2013.

[3] M. Siami, H. K. Savadkoohi, A. Abbaszadeh, D. Khaburi, J. Rodriguez, and M. Rivera, "Predictive torque control of a permanent magnet synchronous motor fed by a matrix converter without weighting factor," in *Power Electronics and Drive Systems Technologies Conference (PEDSTC), 2016 7th.* IEEE, 2016, pp. 614–619.

[4] D. Zhou, J. Zhao, and Y. Liu, "Online tuning of weighting factors based on sugeno fuzzy method in predictive torque control of four-switch three-phase inverter-fed im," in *Power Electronics, Electrical Drives, Automation and Motion (SPEEDAM), 2016 International Symposium on.* IEEE, 2016, pp. 734–739.

[5] F. Villarroel, J. R. Espinoza, C. A. Rojas, J. Rodriguez, M. Rivera, and D. Sbarbaro, "Multiobjective switching state selector for finite-states model predictive control based on fuzzy decision making in a matrix converter," *IEEE Transactions on Industrial Electronics*, vol. 60, no. 2, pp. 589–599, 2013.

[6] A. M. Bozorgi, H. Gholami-Khesht, M. Farasat, S. Mehraeen, and M. Monfared, "Model predictive direct power control of three-phase grid-connected converters with fuzzy-based duty cycle modulation," *IEEE Transactions on Industry Applications*, 2018.

[7] C. A. Rojas, S. Kouro, M. Perez, and F. Villarroel, "Multiobjective fuzzy predictive torque control of an induction machine fed by a 3l-npc inverter," in *Predictive Control of Electrical Drives and Power Electronics (PRECEDE), 2015 IEEE International Symposium on.* IEEE, 2015, pp. 21–26.

[8] P. Acuna, L. Morán, M. Rivera, R. Aguilera, R. Burgos, and V. G. Agelidis, "A single-objective predictive control method for a multivariable single-phase three-level npc converter-based active power filter," *IEEE Transactions on Industrial Electronics*, vol. 62, no. 7, pp. 4598–4607, 2015.

[9] Y. Zhang and H. Yang, "Two-vector-based model predictive torque control without weighting factors for induction motor drives," *IEEE Transactions on Power Electronics*, vol. 31, no. 2, pp. 1381–1390, 2016.

[10] Y. Zhang, Y. Peng, and H. Yang, "Performance improvement of two-vectors-based model predictive control of pwm rectifier," *IEEE Transactions on Power Electronics*, vol. 31, no. 8, pp. 6016–6030, 2016.

[11] L. Guo, X. Zhang, S. Yang, Z. Xie, L. Wang, and R. Cao, "Simplified model predictive direct torque control method without weighting factors for permanent magnet synchronous generator-based wind power system," *IET Electric Power Applications*, vol. 11, no. 5, pp. 793–804, 2017.

[12] L. M. Caseiro, A. M. Mendes, and S. M. Cruz, "Dynamically weighted optimal switching vector model predictive control of power converters," *IEEE Transactions on Industrial Electronics*, vol. 66, no. 2, pp. 1235–1245, 2019.

[13] C. Bordons and C. Montero, "Basic principles of mpc for power converters: Bridging the gap between theory and practice," *IEEE Industrial Electronics Magazine*, vol. 9, no. 3, pp. 31–43, 2015.

[14] J. Hu, J. Zhu, and D. G. Dorrell, "Model predictive control of inverters for both islanded and grid-connected operations in renewable power generations," *IET Renewable Power Generation*, vol. 8, no. 3, pp. 240–248, 2013.

[15] ——, "Model predictive control of grid-connected inverters for pv systems with flexible power regulation and switching frequency reduction," *IEEE Transactions on Industry Applications*, vol. 51, no. 1, pp. 587–594, 2015.

[16] ——, "In-depth study of direct power control strategies for power converters," *IET Power Electronics*, vol. 7, no. 7, pp. 1810–1820, 2014.

[17] M. M. Aghdam, R. P. Aguilera, L. Li, and J. Zhu, "Fuzzy-based self-tuning model predictive direct power control of grid-connected multilevel converters," in *Electrical Machines and Systems (ICEMS), 2017 20th International Conference on.* IEEE, 2017, pp. 1–6.

[18] M. Hannan, Z. A. Ghani, A. Mohamed, and M. N. Uddin, "Real-time testing of a fuzzy-logic-controller-based grid-connected photovoltaic inverter system," *IEEE Transactions on Industry Applications*, vol. 51, no. 6, pp. 4775–4784, 2015.

[19] Y. Zhang, Y. Peng, and C. Qu, "Model predictive control and direct power control for pwm rectifiers with active power ripple minimization," *IEEE Transactions on Industry Applications*, vol. 52, no. 6, pp. 4909–4918, 2016.

Chapter 6

MODEL PREDICTIVE CONTROL OF PARALLEL INVERTERS

6.1 Introduction

Nowadays, microgrid concept has been counted as an effective approach to incorporating distributed renewable resources in distribution networks. Distributed generation (DG) with flexible installation location and low-power transmission losses becomes a practical solution for expansion of the electrical power grid. DGs also present a higher degree of controllability and operability compared to the conventional generators [1], which will allow the grid to achieve high power quality, stability, and reliability.

Aforementioned, in microgrid, the hierarchical control structure is an essential to reduce the operation cost while maximizing the controllability and effectiveness. In hierarchy control, the primary control is in charge of the stability of voltage and frequency [2–7]. The droop control is applied in this level to achieve the active and reactive power sharing without using communication channels. To control the power sharing among DGs, communication-based control approaches such as centralized control, master-slave [8], average load sharing are not the best practice, as the DGs and load are distributed. The droop control method [9] is a conventional control scheme for controlling the parallel inverters in different applications, for example DGs and microgrids [10, 11]. The droop regulation method is applied on grid-supporting inverters (in parallel) to regulate the exchange of the power with the grid [12–15]. In order to ensure stability and economical operation of microgrid, the active and reactive powers of the DGs should be shared simultaneously [1]. This distinguished control method comprises measuring active and reactive powers, regulating locally the output voltage magnitude of each inverter and frequency so as to track the reference power values of a system. However, the droop control methods have the inherent weakness of the slow transient response and poor voltage regulation due to the instantaneous power calculation and the restraint of low-pass filter [16].

From the viewpoint of the microgrid, the inverters ought to be supervised to provide real power to meet the demand and export the surplus to the grid. From the grid point of view, the interfaces would also be capable of providing reactive power,

to refine the power quality and improve the stability. Due to this fact, advanced control methods of the microgrid for power flow optimization are anticipated [17].

This chapter focuses on a predictive power flow control in parallel inverters of microgrids, which can improve the transient of the power flow in microgrids [18]. The microgrid under this case study operates in the grid-tied mode with appropriate power sharing capability among parallel distributed generations and the main grid.

6.2 Parallel Grid-tied Inverters

The general architecture of the microgrid is discussed in [5, 19–21]. When grid-supporting inverters are connected to the grid, the DGs provide required power to the loads together with the grid. If the generated power of DGs is less than the load consumption, the grid will inject the required power to the load. Alternatively, if the generated power of DGs is more than the load demand, the surplus power from DGs will be fed back to the grid.

Several grid-connected inverters can be linked in parallel to the grid in a way that the sum of each output current of the grid-tied inverter at the point of common coupling (PCC) is equal to the grid current plus the load current as illustrated in Fig. 6.1. This system configuration appears in microgrids when several distributed energy resources (DERs) are connected to the main grid through a common AC bus.

The system topology selected for the study involves two parallel inverters. Each of them can perform in the grid-tied mode. The voltage source inverter (VSI) has been chosen for each DG. The DC link can be provided by the output of the DER converters or from energy storage units.

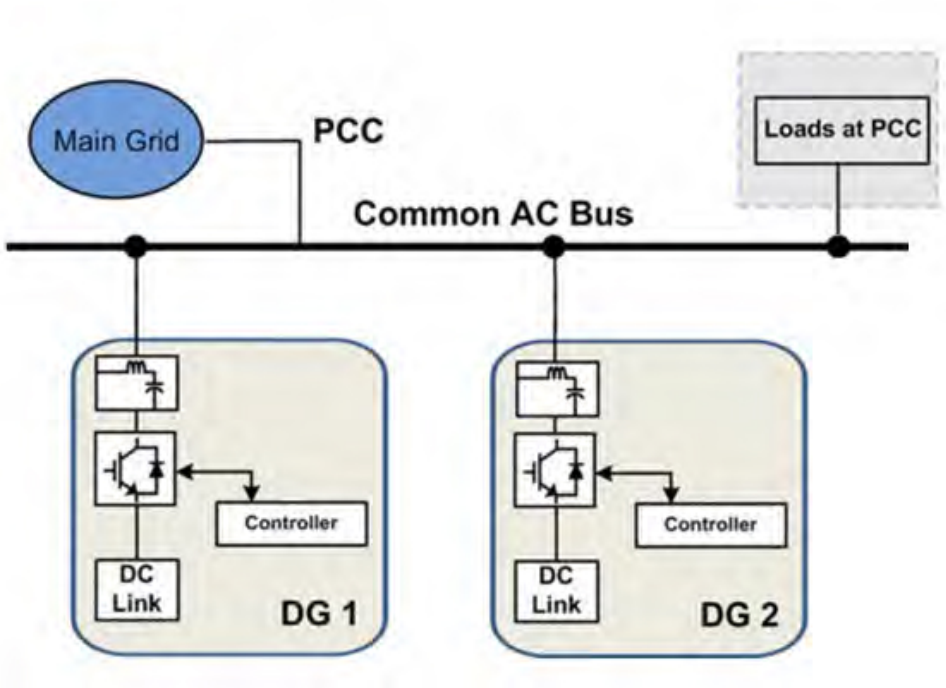

Figure 6.1: Parallel inverters in microgrids

6.3 Load Sharing

The equivalent circuit of this case is described in Fig. 6.2. The complex power flow, $S_n = P_n + jQ_n$ for $n = 1, 2$, between the grid-supporting inverter and the AC bus can be designated as

$$\begin{aligned} P_n &= \frac{(|V_n|^2 cos(\delta_n) - |V_n||E|cos(\delta_n + \Theta_{Z_n}))}{|Z_n|} \\ Q_n &= \frac{(|V_n|^2 sin(\delta_n) - |V_n||E|sin(\delta_n + \Theta_{Z_n}))}{|Z_n|} \end{aligned} \tag{6.1}$$

where $V_n = |V_n|\angle\theta_{V_n}$ and $E = |E|\angle\theta_E$ are the voltage vector of the n-th inverter output and common AC bus, $Z_n = R_n + jX_n = |Z_n|\angle\theta_{Z_n}$ is the line impedance, and the power angle $\delta_n = \theta_{V_n} - \theta_E$. The line impedance plays a significant role in the active and reactive power delivery to the AC bus.

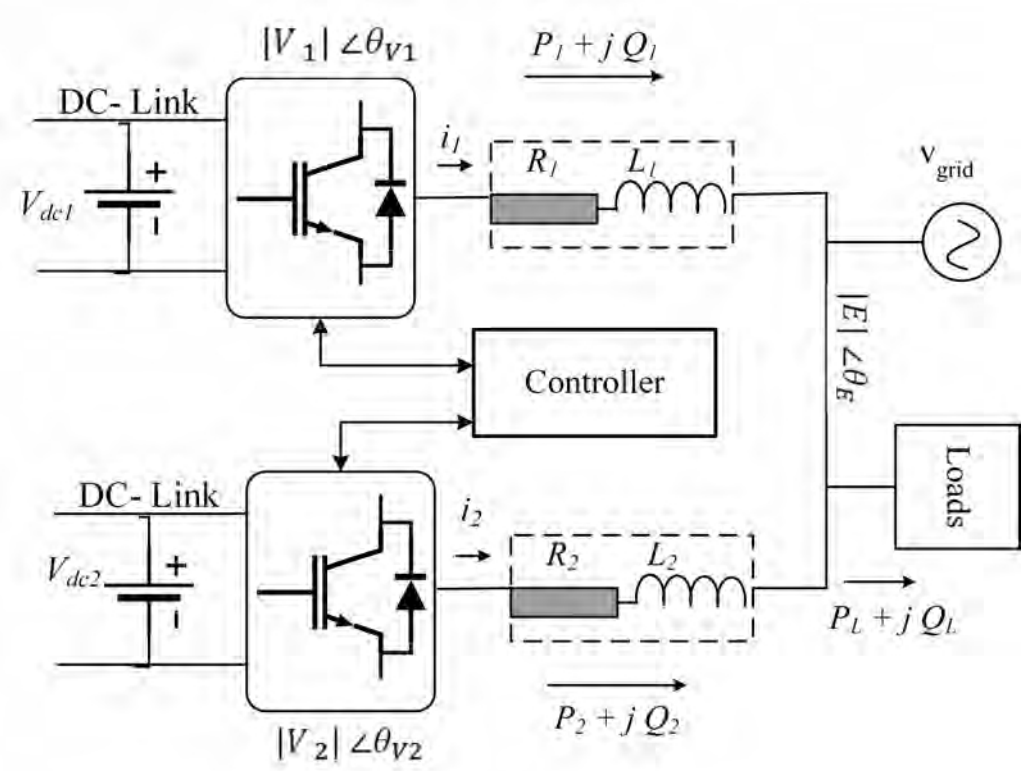

Figure 6.2: Equivalent diagram of parallel grid-tied inverters

In HV and MV networks, the inductive component of the line impedance is much higher than the resistive part [12]. Hence, the resistive part can be neglected. Furthermore, considering that δ_n is generally small, we can adopt $sin(\delta_n) \approx \delta_n$ and $cos(\delta_n) \approx 1$, and therefore (6.1) is expressed as,

$$\begin{aligned} P_n &= \frac{|V_n||E|sin(\delta_n)}{|X_n|} \approx \frac{|V_n||E|\delta_n}{|X_n|} \\ Q_n &= \frac{|V_n|^2 - |V_n||E|cos(\delta_n)}{|X_n|} \approx \frac{|V_n|(|V_n| - |E|)}{|X_n|} \end{aligned} \tag{6.2}$$

Therefore, the active and reactive power flow are dependent on the angle and change in voltage amplitude, respectively. These relationships permit tuning the grid frequency and voltage at the PCC by controlling P_n and Q_n delivered to the grid.

In LV networks, the resistive component of the line impedance is much higher than the inductive part. Hence, the inductive part can be neglected. Considering that δ_n is generally small, (6.1) can be approximated as follows,

$$\begin{aligned} P_n &= \frac{|V_n|(|V_n| - |E|cos(\delta_n))}{|R_n|} \approx \frac{|V_n|(|V_n| - |E|)}{|R_n|} \\ Q_n &= -\frac{(|V_n||E|sin(\delta_n))}{|R_n|} \approx -\frac{|V_n||E|\delta_n}{|R_n|} \end{aligned} \tag{6.3}$$

Consequently, the voltage amplitude and frequency in LV systems are mainly controlled by regulating the active and reactive power flow, respectively.

6.3.1 Droop-based active and reactive power flow control

Generally, the droop control is used as the conventional control method of parallel inverters for regulating active power and reactive power in microgrids [10]. In this scheme, frequency droop and voltage curves are determined, and the active and reactive power of the DGs can be managed by two PI controllers to regulate the frequency and voltage, correspondingly, based on the pre-defined characteristics. Consequently, the new demands are supported by the DGs which are controlled through the two droop controllers [22]. This approach is based on the power system theory, for example, when the load increases, the frequency is reduced. To this end, the frequency and voltage droop characteristics in HV and MV network are expressed as

$$\begin{aligned} \omega_m - \omega_{ref} &= -g(P_n - P_{ref}) \\ V_n - V_{ref} &= -h(Q_n - Q_{ref}) \end{aligned} \tag{6.4}$$

while for LV network the frequency and voltage droop characteristics are as follow,

$$\begin{aligned} V_n - V_{ref} &= -h(P_n - P_{ref}) \\ \omega_m - \omega_{ref} &= -g(Q_n - Q_{ref}) \end{aligned} \tag{6.5}$$

where P_{ref} and Q_{ref} are the set point for active and reactive power, ω_{ref} and V_{ref} the set point for frequency and inverter voltage magnitude, and g and h the droop curve slopes. Figs. 6.3 and 6.4 illustrate the frequency and voltage droop characteristics for girds with dominant inductive and resistive lines, respectively.

To control the parallel inverters, the instantaneous active and reactive powers are calculated based on the PCC voltage and output current of inverters. The measured powers are then fed to a droop regulator to attain the appropriate power sharing among DGs. In the grid-tied mode, the steady state frequency of the system is set to the grid frequency.

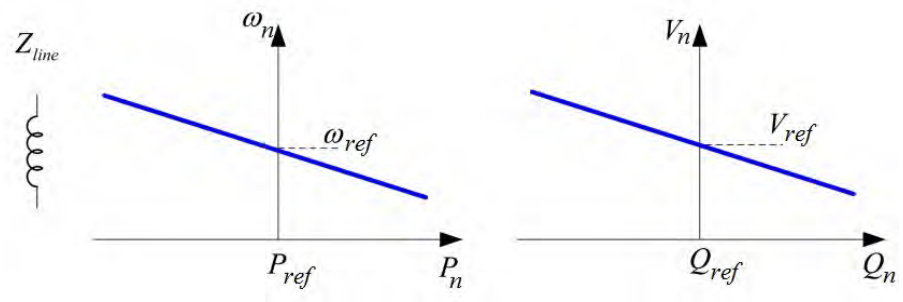

Figure 6.3: Droop characteristics in inductive grids

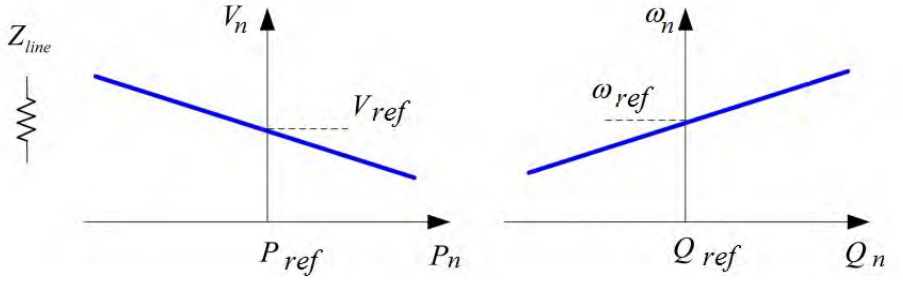

Figure 6.4: Droop characteristics in resistive grids

6.3.2 MPC-based direct power control

To help improve the power quality and enhance the system stability, adaptable active and reactive power regulation has to be gained. Hence, the FCS-MPC is recommended to regulate the active/reactive power flow. The MPC chooses the optimal voltage vector sequence for each inverter to meet the load demand and in the meantime maintain the power flow at a pre-determined level between the microgrid and main grid. The FCS-MPC takes benefits of the discrete characteristic of power converters in the MPC calculations with reduced computation time. As there are finite numbers of switching states in each inverter, the prediction procedure will be conducted through minimizing the cost function.

6.3.2.1 Mathematical model of system

This strategy, direct power control (DPC), involves a predictive model of the instantaneous power evolution. In the stationary $\alpha - \beta$ reference frame and for a symmetrical three-phase power system, instantaneous active and reactive powers by grid-tied inverters can be derived as follows,

$$i_n^{\alpha\beta}(k+1) = i_n^{\alpha\beta}(k) + \frac{T_S}{L_n}[(V_n)_m^{\alpha\beta}(k) - E^{\alpha\beta}(k) - R_n i_n^{\alpha\beta}(k)] \tag{6.6}$$

where i_n, V_n and E are the current, voltage vector of the n-th inverter output and common AC bus respectively. T_S is the sampling time, $Z_n = R_n + j\omega L_n = |Z_n|\angle\theta_{Z_n}$ is the line impedance. $n = 1, 2$ is the index of inverters connected in parallel to the common bus, and m denotes the possible switching state of the n-th inverter. Note that, for an r-level s-phase (rL-sPh) converter, the total number of potential switching positions is $m = r^s$. The estimation of the cost function with the m possibilities will lead to m different costs. The predicted current to the grid can be

expressed as

$$i_o^{\alpha\beta}(k+1) = (i_1)_m{}^{\alpha\beta}(k+1) + (i_2)_m{}^{\alpha\beta}(k+1) + i_L^{\alpha\beta}(k+1) \tag{6.7}$$

The active power P and the reactive power Q to the grid are derived in $\alpha\beta$-stationary frame as

$$\begin{aligned} P &= \frac{3}{2}(v_{grid}^{\alpha}\, i_o^{\alpha} + v_{grid}^{\beta}\, i_o^{\beta}) \\ Q &= \frac{3}{2}(v_{grid}^{\beta}\, i_o^{\alpha} - v_{grid}^{\alpha}\, i_o^{\beta}) \end{aligned} \tag{6.8}$$

6.3.2.2 Cost function

Denote the power generated by the grid-connected DG systems as P_{DG}, and the power demand by loads as P_{demand}. The net power to the main grid can be obtained by

$$\begin{aligned} P_{net} &= P_{DG} - P_{demand} \\ P_{DG} &= P_1 + P_2 \end{aligned} \tag{6.9}$$

Thus, the predicted power to the grid can be gained as the following

$$\begin{aligned} P_{net} &= \frac{3}{2}(v_{grid}^{\alpha} i_o^{\alpha} + v_{grid}^{\beta} i_o^{\beta}) \\ Q_{net} &= \frac{3}{2}(v_{grid}^{\beta} i_o^{\alpha} - v_{grid}^{\alpha} i_o^{\beta}) \end{aligned} \tag{6.10}$$

The current and voltage available to the grid are measured at the current sampling time and applied to compute P_{net} and Q_{net} at the next sampling time for all switching states of each inverter [11, 17, 19]. The cost function is defined as follows,

$$J_m = [P^*(k+1) - P_{net}(k+1)]^2 + [Q^*(k+1) - Q_{net}(k+1)]^2 \quad \text{for}\, m = 1, ..., r^s \tag{6.11}$$

The minimization of the cost function leads to an optimal power flow of two DGs for the transmitted power to the grid at the scheduled reference level. The scheme diagram of the suggested algorithm is illustrated in Fig. 6.5.

6.4 Simulation

In this section, a predictive power flow control method for parallel inverters is investigated using Matlab/Simulink simulation platform. Two scenarios are is defined based on the topology of the grid-supporting inverters.

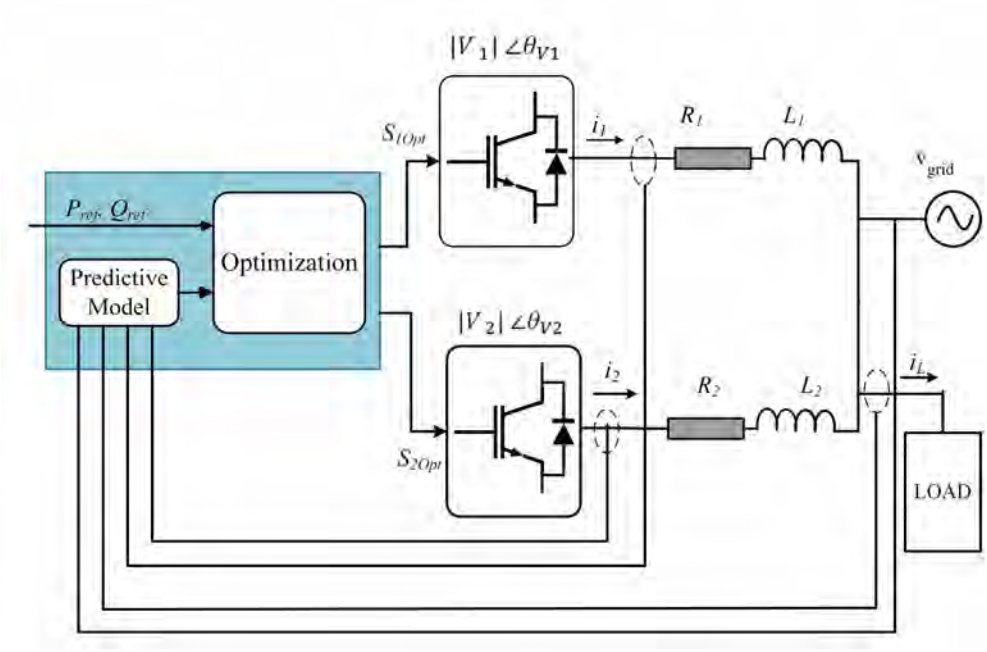

Figure 6.5: Schematic of the parallel inverter with MPC controller

6.4.1 Case Study I

A block diagram of two parallel 2L-3Ph inverters in the grid-tied mode of operation in a microgrid shown in Fig. 6.2 is executed by using the MATLAB/Simulink. Table 6.1 indicates the system parameters for this case study.

To help understand the performance of MPC, a simulation with $P - f$ droop control is conducted. The droop characteristics is illustrated in Fig. 6.6 and the flow chart of droop characteristic is depicted in Fig. 6.7. In Fig. 6.8, the performance of this approach for power flow control is depicted.

Table 6.1: System Parameters of Case Study I

Grid voltage	v_{grid}	100 V
Load active power	P_L	3 kW
Voltage frequency	f	50 Hz
Resistance	R_1	0.51 Ω
Inductance	L_1	4.8 mH
DC source voltage	V_{dc_1}	250 V
Resistance	R_2	1 Ω
Inductance	L_2	10 mH
DC source voltage	V_{dc_2}	400 V
Sampling time	T_s	50 μs

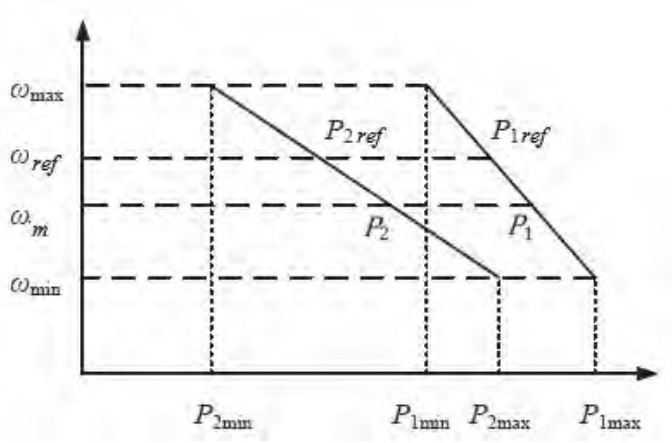

Figure 6.6: Frequency and active power droop characteristic

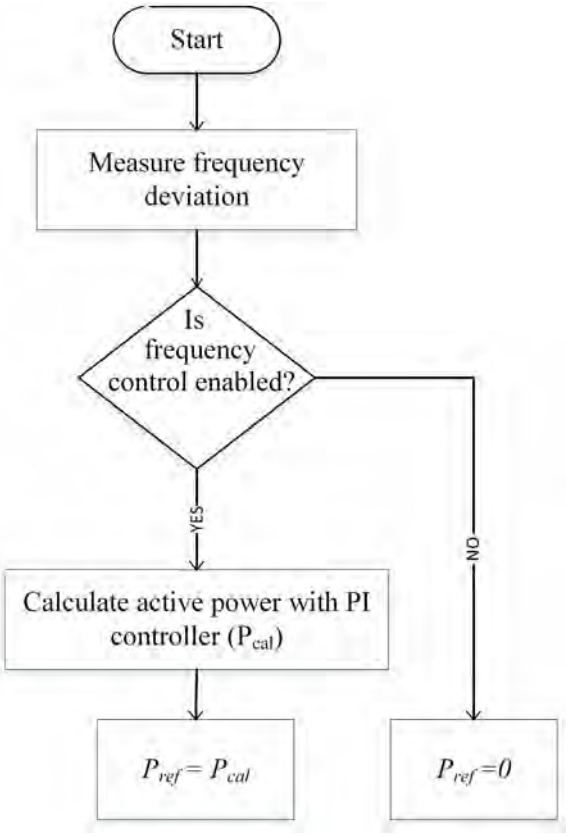

Figure 6.7: Flow chart for $P - f$ droop characteristic

The active and reactive powers are both initially set to zero. The active power reference is changed from 0 to $-4kW$ at $0.05s$, $0W$ at $0.06s$, $3kW$ at $0.07s$, and $0W$ at $0.08s$, and stays at $0kW$, whereas the reactive power reference is altered from 0 to -3, 0, and $1kVar$ at $0.02s$, $0.04s$, and $0.09s$, respectively.

Each inverter has eight voltage vector possibilities at a time, which gives the controller 64 possible switching patterns in total. Figs. 6.9 and 6.10 illustrate the performance of MPC controller in the cases of individual DG and parallel DGs respectively. It is shown that the suggested FCS-MPC method presents much better power flow tracking. The current and voltage of the common bus are demonstrated

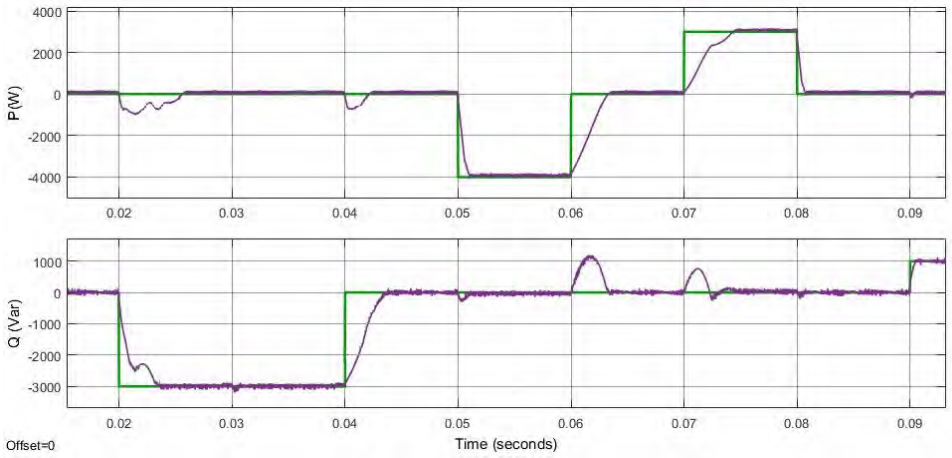

Figure 6.8: Active and reactive power flow - Droop control

in Fig. 6.11. As observed, the voltage and current are sinusoidal, so the system performance is stable.

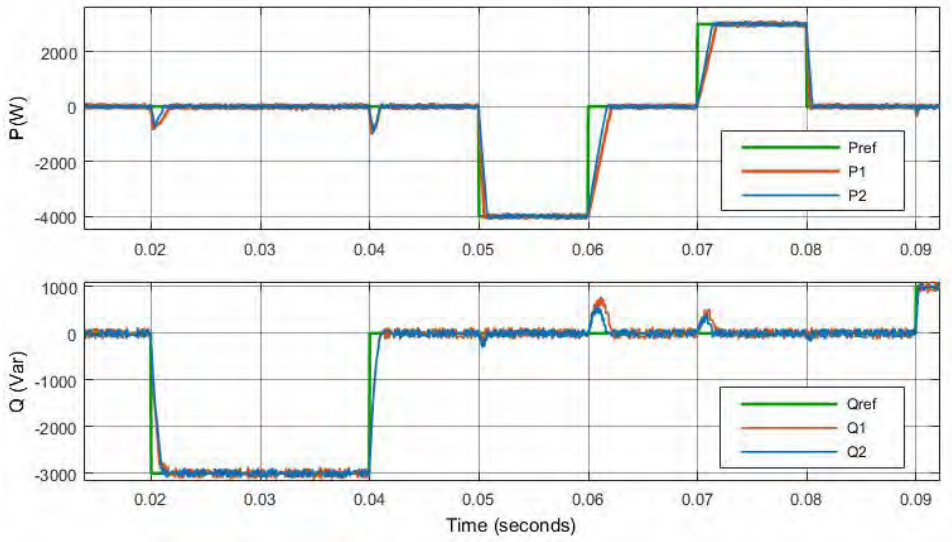

Figure 6.9: Power flow control for individual DG - MPC

6.4.2 Case Study II

In this case, a 2L-3Ph VSI with a total of 8 voltage possibilities and a 3L-3Ph neutral point clamped VSI with a total of 27 voltage vectors are connected in parallel to the PCC. Simulation of this case is executed by using the MATLAB/Simulink. Table 6.2 shows the system parameters for this case study. The set points are kept as same as Case Study I.

Figs. 6.12 and 6.13 illustrate the performance of MPC controller in the cases of individual DG and parallel DGs respectively.

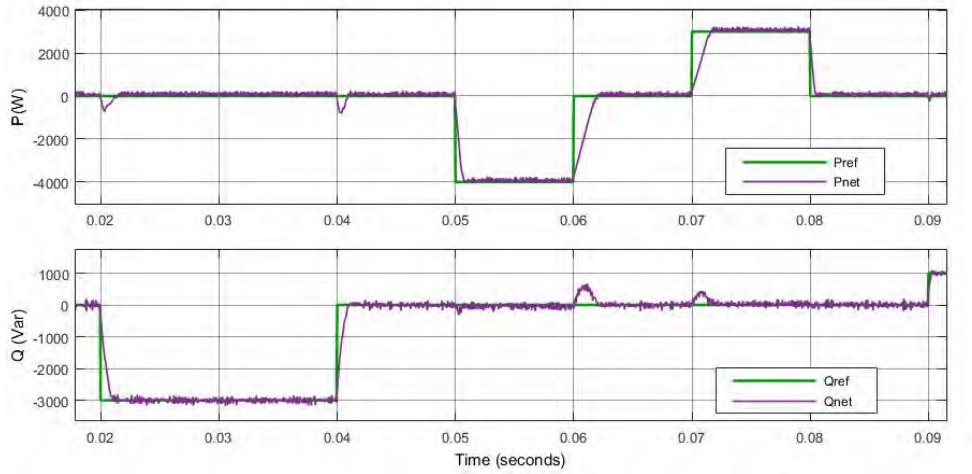

Figure 6.10: Power flow control for net power to the grid - MPC

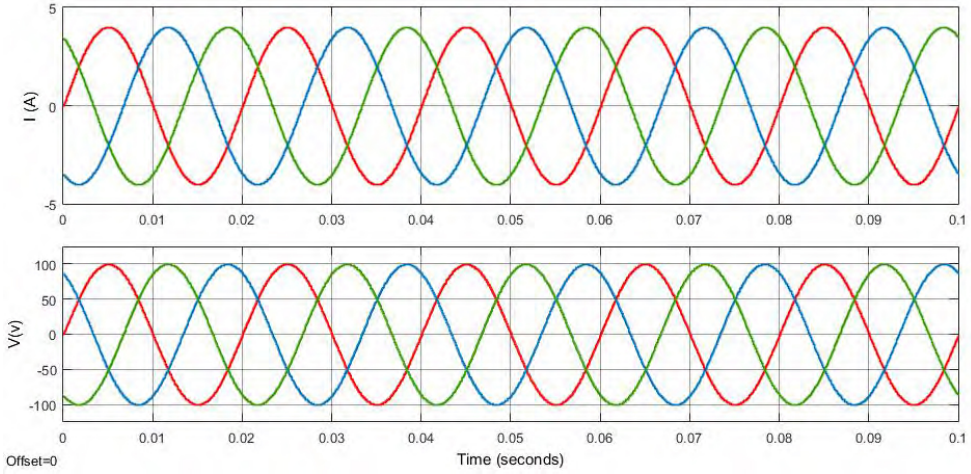

Figure 6.11: The current and voltage of the AC common bus - MPC

Table 6.2: System Parameters of Case Study II

Grid voltage	v_{grid}	100 V
Load active power	P_L	5 kW
Voltage frequency	f	50 Hz
Sampling time	T_s	100 μs
Resistance	R_1	0.51 Ω
Inductance	L_1	4.8 mH
DC source voltage	V_{dc_1}	250 V
Resistance	R_2	1 Ω
Inductance	L_2	10 mH
DC source voltage	V_{dc_2}	600 V

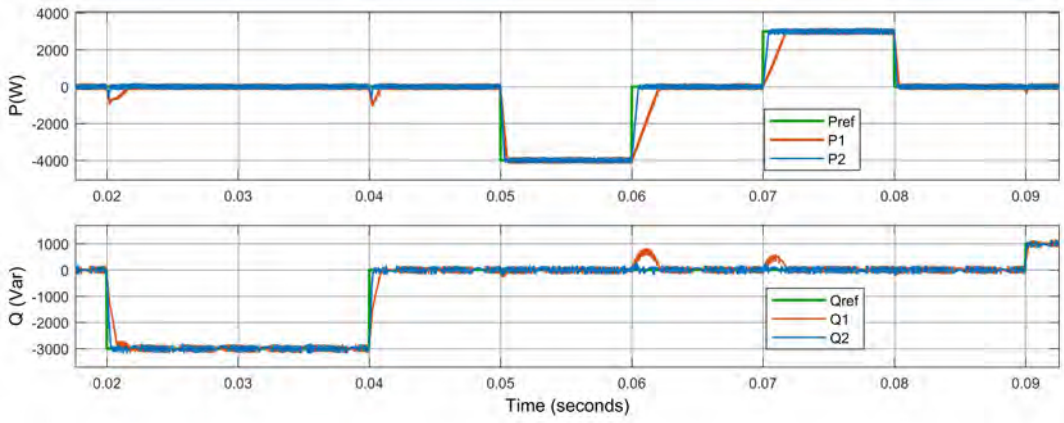

Figure 6.12: Power flow control for individual DG - MPC

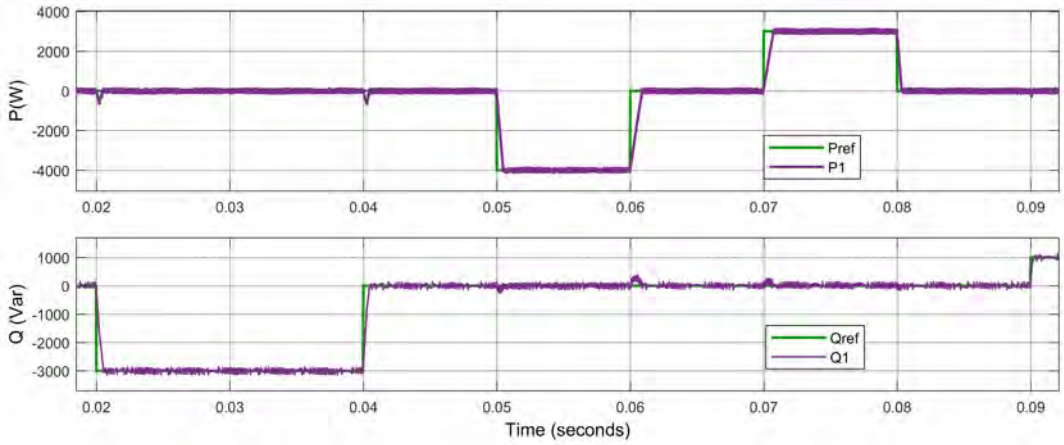

Figure 6.13: Power flow control for net power to the grid - MPC

6.4.3 Comparison and discussion

The DGs that are connected in parallel can take the appropriate actions in response of changes of the load demand. The controller tracks the load demand to maintain the net active/reactive power flow into the main grid at the scheduled level.

As can be seen in Figs. 6.9 and 6.10, the MPC approach shows a great performance and power flow tracking, in comparison to the droop control scheme. As aforementioned, the droop control as a conventional method for power sharing between parallel connected DERs has an inherent flaw of slow transient response due to the powers calculation and the restraint of low pass filter. Table 6.3 tabulates a quantitative comparison of indicators, including the frequency, power ripples, rise time, and settling time, between the droop control and the MPC methods by simulation in MATLAB/Simulink.

It can be seen in Figs. 6.8 and 6.10 that the MPC algorithm shows much better performance than the droop control in term of power sharing between two parallel grid-connected inverters. The measurements show that although the active and reactive power ripples have not been compensated much by the MPC approach, the rise time and settling time are reduced considerably. As a result, the MPC scheme provides a better transient dynamics than the droop control scheme.

In Figs. 6.9 and 6.12, the measurements show that the active and reactive

power ripples are compensated much by the DG_2 in Case Study II. The main reason behind is that the inverter of DG_2 uses three levels of DC voltage. The THD percentage in 3L-3Ph neutral point clamped VSI is much lower than that of 2L-3Ph VSI, which leads to less active and reactive power ripples.

Table 6.3: Quantitative Comparison

Power Sharing	$f_s(Hz)$	P_{rip}	Q_{rip}	Rise time	Settling time
V/f droop	20k	N/A	N/A	0.41	0.42
Case I-MPC (DG2)	20k	0.44	0.57	0.35	0.37
Case II-MPC (DG2)	10k	0.33	0.38	0.23	0.19
Case I-MPC (net)	20k	0.46	0.51	0.33	0.29
Case II-MPC(net)	10k	0.35	0.41	0.28	0.21

6.5 Summary

In this work, an MPC scheme is employed for the power sharing problem of parallel DGs in a microgrid. The equivalent microgrid model is established and the associated cost function is formulated. The case studies have been considered and the results show that the MPC technique attains better performance on the power flow control than the conventional droop control scheme. Furthermore, the DGs can respond appropriately to the load changes such that the power flow to the main grid is maintained at the scheduled level. The MPC approach is compared with the conventional frequency and voltage droop control approach in the case studies. For the future work, improving power quality and enhancing the system stability for both the islanded mode and gird-connected mode will be investigated. Moreover, seamless switching between two modes is an important concern that needs to be considered in the controller design to achieve power sharing without producing undesirable impacts on the grid and critical loads.

Bibliography

[1] L. Lei, M. A. Elgendy, N. Wade, S. Ethni, and H. M. Hasanien, "Power sharing between parallel inverters in microgrid by improved droop control," in *2018 53rd International Universities Power Engineering Conference (UPEC)*. IEEE, 2018, pp. 1–6.

[2] S. Parhizi, H. Lotfi, A. Khodaei, and S. Bahramirad, "State of the art in research on microgrids: A review," *IEEE Access*, vol. 3, pp. 890–925, 2015.

[3] Y. A.-R. I. Mohamed and A. A. Radwan, "Hierarchical control system for robust microgrid operation and seamless mode transfer in active distribution systems," *IEEE Transactions on Smart Grid*, vol. 2, no. 2, pp. 352–362, 2011.

[4] Y. A.-R. I. Mohamed and A. Radwan, "Hierarchical control system for robust microgrid operation and seamless mode transfer in active distribution systems," *Smart Grid, IEEE Transactions on*, vol. 2, no. 2, pp. 352–362, 2011.

[5] O. Palizban and K. Kauhaniemi, "Hierarchical control structure in microgrids with distributed generation: Island and grid-connected mode," *Renewable and Sustainable Energy Reviews*, vol. 44, pp. 797–813, 2015.

[6] A. Bidram and A. Davoudi, "Hierarchical structure of microgrids control system," *IEEE Transactions on Smart Grid*, vol. 3, no. 4, pp. 1963–1976, 2012.

[7] Y. Han, H. Li, P. Shen, E. A. A. Coelho, and J. M. Guerrero, "Review of active and reactive power sharing strategies in hierarchical controlled microgrids," *IEEE Transactions on Power Electronics*, vol. 32, no. 3, pp. 2427–2451, 2017.

[8] J. C. Vasquez, J. M. Guerrero, A. Luna, P. Rodríguez, and R. Teodorescu, "Adaptive droop control applied to voltage-source inverters operating in grid-connected and islanded modes," *IEEE Transactions on Industrial Electronics*, vol. 56, no. 10, pp. 4088–4096, 2009.

[9] D. C. Raj and D. Gaonkar, "Frequency and voltage droop control of parallel inverters in microgrid," in *Control, Instrumentation, Energy & Communication (CIEC), 2016 2nd International Conference on*. IEEE, 2016, pp. 407–411.

[10] V. Nasirian, Q. Shafiee, J. M. Guerrero, F. L. Lewis, and A. Davoudi, "Droop-free distributed control for ac microgrids," *Power Electronics, IEEE Transactions on*, vol. 31, no. 2, pp. 1600–1617, 2016.

[11] J. He and Y. W. Li, "An enhanced microgrid load demand sharing strategy," *IEEE Transactions on Power Electronics*, vol. 27, no. 9, pp. 3984–3995, 2012.

[12] J. Rocabert, A. Luna, F. Blaabjerg, and P. Rodriguez, "Control of power converters in ac microgrids," *Power Electronics, IEEE Transactions on*, vol. 27, no. 11, pp. 4734–4749, 2012.

[13] A. Ketabi, S. S. Rajamand, and M. Shahidehpour, "Power sharing in parallel inverters with different types of loads," *IET Generation, Transmission & Distribution*, vol. 11, no. 10, pp. 2438–2447, 2017.

[14] B. Fani, F. Zandi, and A. Karami-Horestani, "An enhanced decentralized reactive power sharing strategy for inverter-based microgrid," *International Journal of Electrical Power & Energy Systems*, vol. 98, pp. 531–542, 2018.

[15] M. Yazdanian and A. Mehrizi-Sani, "Distributed control techniques in microgrids," *IEEE Transactions on Smart Grid*, vol. 5, no. 6, pp. 2901–2909, 2014.

[16] F. Iraji, V. Azarm, E. Farjah, and T. Ghanbari, "A suitable power sharing control of parallel-connected inverters in microgrids," in *Control, Instrumentation, and Automation (ICCIA), 2017 5th International Conference on.* IEEE, 2017, pp. 313–318.

[17] J. Hu, J. Zhu, and J. M. Guerrero, "Model predictive control in next microgrid control architectures," in *IEEE 17th International Conference on Electrical Machines and Systems (ICEMS)*, 2014, pp. 2815–2820.

[18] C. H. Young and A. Bastias, "Finite-control-set predictive voltage control of paralleled inverters in an islanded microgrid," in *2018 IEEE 27th International Symposium on Industrial Electronics (ISIE).* IEEE, 2018, pp. 395–400.

[19] H. Han, X. Hou, J. Yang, J. Wu, M. Su, and J. M. Guerrero, "Review of power sharing control strategies for islanding operation of ac microgrids," *IEEE Transactions on Smart Grid*, vol. 7, no. 1, pp. 200–215, 2016.

[20] K. Rajesh, S. Dash, R. Rajagopal, and R. Sridhar, "A review on control of ac microgrid," *Renewable and Sustainable Energy Reviews*, 2017.

[21] D. E. Olivares, A. Mehrizi-Sani, A. H. Etemadi, C. A. Cañizares, R. Iravani, M. Kazerani, A. H. Hajimiragha, O. Gomis-Bellmunt, M. Saeedifard, R. Palma-Behnke *et al.*, "Trends in microgrid control," *IEEE Transactions on smart grid*, vol. 5, no. 4, pp. 1905–1919, 2014.

[22] J. C. Vasquez, J. M. Guerrero, M. Savaghebi, J. Eloy-Garcia, and R. Teodorescu, "Modeling, analysis, and design of stationary-reference-frame droop-controlled parallel three-phase voltage source inverters," *IEEE Transactions on Industrial Electronics*, vol. 60, no. 4, pp. 1271–1280, 2013.

Chapter 7

CONCLUSION and FUTURE RESEARCH

In general, it can be concluded that model predictive control (MPC) is a flexible and powerful scheme for control of power converters in different applications. In particular, for reliable operation of microgrids, the widespread implementation of MPC in future will be an essential key. MPC has demonstrated to be a powerful and reasonable alternative to the traditional control methods for power converter control in microgrids as discussed in Chapter 2. Moreover, the flexibility of the MPC technique has driven solutions for practical and real-time implementation (RTI) issues in this area.

The proposed time-delayed finite control set MPC (FCS-MPC), in Chapter 3, can compensate the delay time associated with RTI for different applications as delay time differs. This approach shows a better transient and steady state performance while reducing the power ripples significantly for power converters in distributed generation (DG) units. The proposed method compensates the delay time resulting from DSPs' computation and implementation of the controlled input to the converter. The delay time, in this work, is estimated through trial and error, which in the future research can be estimated by some algorithm.

The longer prediction horizon can reduce the power ripples considerably. In Chapter 4, the introduced method leads to a good performance of the power tracking ability in both transient and steady state, which can be used as a general control approach for DG units. Eliminating the redundant voltage vectors is not always the best approach to reduce the computation burden. Before considering the elimination of redundant voltage vectors, the topology of converter and the direction of the currents should be investigated. As the longer prediction horizon can reduce the power ripples, finding the optimal length of the prediction horizon is a key. For the future work, the study will focus on the algorithm to find or estimate the optimal length of the prediction horizon.

Chapter 5 explores a self-tuning MPC based on direct power control strategy for power flow control and power quality improvement in grid-connected power converters. The proposed method shows a better controllability on different objectives in the cost function. At each sampling instant, a fuzzy logic controller (FLC) is used to determine online the best weighting factor values at the given operating point. FLC checks the errors at each operating point and defines the priority of each objective. The FLC is a flexible and adjustable method which has the ability

to learn from the system performance. The rules of the FLC can be updated based on the system behavior to improve the overall performance. Two case studies are performed to compare the proposed self tuning approach with the fixed weighting factors approach. As a result, an improved performance in terms of THD and average switching frequency are attained. For the future work, the proposed method can be investigated further in different topologies of the converters. Moreover, as the weighting factors are adjusted online, the computational burden will be increased, and therefore combining with the longer prediction horizon algorithm will be beneficial.

An MPC scheme, in Chapter 6, is employed for the power sharing of parallel DG units in a microgrid. The equivalent microgrid model is established and the associated cost function is formulated. A case study is considered and the results show that the MPC technique attains better performance on the power flow control than the conventional droop control scheme. Furthermore, the DGs can respond appropriately to the load changes such that the power flow to the main grid is maintained at the scheduled level. For the future work, improving power quality and enhancing the system stability for both the islanded mode and gird-connected mode will be investigated. Moreover, seamless switching between two modes is an important concern that needs to be considered in the controller design to achieve power sharing without producing undesirable impacts on the grid and critical loads.

Nevertheless, industrial approval of MPC in power converters and drives has yet to come. In [1], the authors assessed the technology readiness of MPC with conclusion that MPC will perform a pivotal key for the next generation of power converters and electrical drives to operate in a more reliable, stable, and efficient way.

Bibliography

[1] G. A. Papafotiou, G. D. Demetriades, and V. G. Agelidis, "Technology readiness assessment of model predictive control in medium-and high-voltage power electronics," *IEEE Transactions on Industrial Electronics*, vol. 63, no. 9, pp. 5807–5815, 2016.

Chapter 8

APPENDIX A:PUBLICATIONS BASED ON THE THESIS WORK

8.1 Published papers

Aghdam, M.M., Li, L., Zhu, J., He, T. and Zhang, J., 2017, October. Time-delayed model predictive direct power control for vehicle to grid and grid to vehicle applications. In Industrial Electronics Society, IECON 2017-43rd Annual Conference of the IEEE (pp. 4662-4667). IEEE.

Aghdam, M.M., Aguilera, R.P., Li, L. and Zhu, J., 2017, August. Fuzzy-based self-tuning model predictive direct power control of grid-connected multilevel converters. In Electrical Machines and Systems (ICEMS), 2017 20th International Conference on (pp. 1-6). IEEE.

Aghdam, M.M., Li, L. and Zhu, J., 2016, November. A model predictive power control method with longer prediction horizon for distributed power generations. In Control, Automation, Robotics and Vision (ICARCV), 2016 14th International Conference on (pp. 1-6). IEEE.

Mahdavi Aghdam, M., Li, L. and Zhu, J., 2016, September. A Model Predictive Control of Parallel Inverters for Distributed Generations in Microgrids. In International IEEE Conference on Power Systems Technology (POWERCON).

Aghdam, M.M., Li, L., Zhu, J. and Palizban, O., 2016, June. Finite control set model predictive control-a powerful control algorithm for grid-connected power converters. In Industrial Electronics and Applications (ICIEA), 2016 IEEE 11th Conference on (pp. 2350-2355). IEEE.

Mahdavi, M., Li, L., Zhu, J. and Mekhilef, S., 2015, November. An adaptive Neuro-Fuzzy controller for maximum power point tracking of photovoltaic systems. In TENCON 2015-2015 IEEE Region 10 Conference (pp. 1-6). IEEE.

8.2 Published papers: Collaborations

Zhang, J., Li, L., He, T., Aghdam, M.M. and Dorrell, D.G., 2017, October. Investigation of direct matrix converter working as a versatile converter (AC/AC, AC/DC, DC/AC, DC/DC conversion) with predictive control. In Industrial Electronics Society, IECON 2017-43rd Annual Conference of the IEEE (pp. 4644-4649). IEEE.

He, T., Zhu, J., Lu, D.D.C., Zheng, L., Aghdam, M.M. and Zhang, J., 2017, October. Comparison study of electric vehicles charging stations with AC and DC buses for bidirectional power flow in smart car parks. In Industrial Electronics Society, IECON 2017-43rd Annual Conference of the IEEE (pp. 4609-4614). IEEE.

Beiranvand, A., Aghdam, M.M., Li, L., Zhu, S. and Zheng, J., 2016, September. Finding the optimal place and size of an energy storage system for the daily operation of microgrids considering both operation modes simultaneously. In Power System Technology (POWERCON), 2016 IEEE International Conference on (pp. 1-6). IEEE.

8.3 Submitted papers

Mahdavi Aghdam, M., Li, L. and Zhu, J., A Comprehensive Study of Finite Control Set Model Predictive Control Algorithms for Power Converter Control in Microgrids. Submitted to IET Smart Grid.